Establishment of surface functionalization methods for spore-based biosensors and implementation into sensor technologies for aseptic food processing

Dissertation

Zur

Erlangung des Doktorgrades

der Naturwissenschaften

(Dr. rer. nat.)

dem

Fachbereich Pharmazie

der Philipps-Universität Marburg

vorgelegt von

Julio César Arreola Becerra

aus Monterrey

Marburg/Lahn 2020

Gutachter: Prof. Dr. M.J. Schöning

Gutachter: Prof. Dr. M. Keusgen

Eingereicht am: 11.02.2020

Tag der mündlichen Prüfung am 21.04.2020

Hochschulkennziffer: 1180

Erklärung

Ich versichere, dass ich meine Dissertation:

"Establishment of surface functionalization methods for spore-based biosensors and implementation into sensor technologies for aseptic food processing"

selbständig ohne unerlaubte Hilfe angefertigt und mich dabei keiner anderen als der von mir ausdrücklich bezeichneten Quellen bedient habe. Alle vollständig oder sinngemäß übernommenen Zitate sind als solche gekennzeichnet.

Die Dissertation wurde in der jetzigen oder einer ähnlichen Form noch bei keiner anderen Hochschule eingereicht und hat noch keinen sonstigen Prüfungszwecken gedient.

Marburg, den 11.02.2020 _____

Julio César Arreola Becerra

Abstract

Aseptic processing has become a popular technology to increase the shelf-life of packaged products and to provide non-contaminated goods to the consumers. In 2017, the global aseptic market was evaluated to be about 39.5 billion USD. Many liquid food products, like juice or milk, are delivered to customers every day by employing aseptic filling machines. They can operate around 12,000 ready-packaged products per hour (e.g., Pure-Pak® Aseptic Filling Line E-PS120A). However, they need to be routinely validated to guarantee contamination-free goods. The state-of-the-art methods to validate such machines are by means of microbiological analyses, where bacterial spores are used as test organisms because of their high resistance against several sterilants (e.g., gaseous hydrogen peroxide). The main disadvantage of the aforementioned tests is time: it takes at least 36-48 hours to get the results, i.e., the products cannot be delivered to customers without the validation certificate. Just in this example, in 36 hours, 432,000 products would be on hold for dispatchment; if more machines are evaluated, this number would linearly grow and at the end, the costs (only for waiting for the results) would be considerably high. For this reason, it is very valuable to develop new sensor technologies to overcome this issue. Therefore, the main focus of this thesis is on the further development of a spore-based biosensor; this sensor can determine the viability of spores after being sterilized with hydrogen peroxide. However, the immobilization strategy as well as its implementation on sensing elements and a more detailed investigation regarding its operating principle are missing.

In this thesis, an immobilization strategy is developed to withstand harsh conditions (high temperatures, oxidizing environment) for spore-based biosensors applied in aseptic processing. A systematic investigation of the surface functionalization's effect (e.g., hydroxylation) on sensors (e.g., electrolyte-insulator semiconductor (EIS) chips) is presented. Later on, organosilanes are analyzed for the immobilization of bacterial spores on different sensor surfaces. The electrical properties of the immobilization layer are studied as well as its resistance to a sterilization process with gaseous hydrogen peroxide. In addition, a sensor array consisting of a calorimetric gas sensor and a spore-based biosensor to measure hydrogen peroxide concentrations and the spores' viability at the same time is proposed to evaluate the efficacy of sterilization processes.

Abstract (Deutsch)

Die aseptische Prozesstechnik hat sich zu einer beliebten Technologie entwickelt, um die Haltbarkeit von verpackten Produkten zu verlängern und den Verbrauchern nicht kontaminierte Waren zur Verfügung zu stellen. Im Jahr 2017 wurde der globale Aseptikmarkt auf rund 39,5 Mrd. USD geschätzt. Viele flüssige Lebensmittelprodukte, wie Saft oder Milch, werden täglich mit aseptischen Abfüllmaschinen produziert und an die Kunden geliefert. Moderne Abfüllanlagen können ungefähr 12.000 fertig verpackte Produkte pro Stunde befüllen (z. B. Pure-Pak® Aseptic Filling Line E-PS120A). Sie müssen jedoch routinemäßig validiert werden, um eine kontaminationsfreie Ware zu gewährleisten. Die Verfahren zur Validierung derartiger Maschinen erfolgen häufig mittels mikrobiologischer Analysen, wobei bakterielle Sporen als Testorganismen wegen ihrer hohen Beständigkeit gegenüber verschiedenen Sterilisationsmittels (z.B. gasförmiges Wasserstoffperoxid) verwendet werden. Der Hauptnachteil der vorgenannten Tests ist deren Läufe: Es dauert mindestens 36-48 Stunden, um die Ergebnisse zu erhalten, d.h. die Produkte können nicht ohne das Validierungszertifikat an den Kunden geliefert werden. Nur in diesem Beispiel würden in 36 Stunden ca. 432.000 Produkte für den Versand zurückgestellt. Beim parallelen Betreib mehrerer Maschinen würde diese Zahl linear ansteigen und am Ende wären die Kosten (nur für das Warten auf die Ergebnisse) beträchtlich hoch. Aus diesem Grund ist es sinnvoll, neue Sensortechnologien zu entwickeln, um dieses Problem zu lösen. Daher liegt der Schwerpunkt dieser Arbeit auf der Weiterentwicklung eines sporenbasierten Biosensors; dieser Sensor kann die Lebensfähigkeit von Sporen nach der Sterilisation mit Wasserstoffperoxid bestimmen. Es fehlen jedoch eine reproduzierbare Immobilisierungsstrategie sowie deren Implementierung auf Sensorelementen, sowie eine detailliertere Untersuchung hinsichtlich ihres Funktionsprinzips.

In dieser Arbeit wird eine Immobilisierungsstrategie für sporenbasierte Biosensoren entwickelt, um rauen Bedingungen (hohe Temperaturen, oxidierende Umgebung) standzuhalten, wo sie in der aseptischen Verpackung eingesetzt werden. Eine systematische Untersuchung der Wirkung der Oberflächenfunktionalisierung (z.B. Hydroxylierung) auf Sensoren (z.B. Elektrolyt-Isolator-Halbleiter- (EIS-) Chips) wird vorgestellt. Im Anschluss werden Organosilane bezüglich der Immobilisierung von Bakteriensporen auf verschiedenen Sensoroberflächen charakterisiert. Die elektrischen Eigenschaften der

Immobilisierungsschicht sowie ihre Beständigkeit gegenüber einem Sterilisationsprozess mit gasförmigem Wasserstoffperoxid werden validiert. Zusätzlich wird ein Sensorarray bestehend aus einem kalorimetrischen Gassensor und einem sporenbasierten Biosensor zur gleichzeitigen Messung der Wasserstoffperoxidkonzentration und der Lebensfähigkeit der Sporen vorgeschlagen, um die Wirksamkeit von Sterilisationsprozessen zu bewerten.

Table of contents

Abstract ..... **v**

Abstract (Deutsch) ..... **vi**

Acronyms ..... **xv**

1 Introduction **1**

1.1 Aseptic processing technology 1

1.2 State-of-the art methods to validate the H_2O_2 sterilization process 1

1.2.1 Count-reduction test 2

1.2.2 End-point test 3

1.3 Sensor technologies to monitor gaseous hydrogen peroxide 4

1.4 Cell-based biosensors 6

1.4.1 Spore-based biosensors 6

1.4.2 Sensor technologies for the determination of spore viability 8

1.5 Spore immobilization 10

1.5.1 Physical confinement 10

1.5.2 Gel entrapment 10

1.5.3 Hydrophobic forces 11

1.5.4 Electrostatic interactions 11

1.5.5 Biospecific binding system 12

1.6 Objectives and contents of this contribution 15

References 17

2 Theoretical aspects **25**

2.1 Sensing principles 25

2.1.1 Resistance temperature detectors (RTDs) and wire configurations 25

2.1.2 Calorimetric H_2O_2 sensing principle 28

2.1.3 Impedimetric sensing principle 31

2.2 Surface functionalization 34

2.2.1 Organosilanes 34

2.3 Characterization methods for surface functionalization and spore immobilization 37

2.3.1 Electrolyte-insulator-semiconductor (EIS) sensors 37

2.3.2 Contact angle measurement 38

2.3.3 Atomic force microscopy (AFM) 39

2.3.4 Scanning electron microscopy (SEM) 40
2.3.5 Microbiological methods 42
References 42
3 Effect of O_2 plasma on properties of electrolyte-insulator-semiconductor structures (Physica Status Solidi (a) – applications and materials science, 214, 9 (2017), 1700025 (1-6)) **48**
Abstract **48**
3.1 Introduction 50
3.2 Experimental 51
3.2.1 Fabrication of the EIS sensor 51
3.2.2 Experimental setup 51
3.2.3 Hydroxylation 52
3.2.4 Annealing 52
3.2.5 Contact angle measurements 52
3.3 Results and discussion 53
3.3.1 Effect of O_2 plasma on the EIS sensor 53
3.3.2 Annealing effect on the EIS sensor 54
3.3.3 Contact angle measurements 57
3.4 Conclusions 59
Acknowledgements 60
References 60
4 Optimization of the immobilization of bacterial spores on glass substrates with organosilanes (Physica Status Solidi (a) – applications and materials science, 213, 6 (2016), 1463-1470) **63**
Abstract **63**
4.1 Introduction 65
4.2 Experimental 67
4.2.1 Materials 67
4.2.2 Surface functionalization 68
4.2.3 Contact angle measurement (CA) 69
4.2.4 Atomic force microscopy (AFM) 69
4.2.5 Bacterial culture, sporulation and spore purification 70
4.2.6 Microbiological evaluation of the immobilization of the spores 70

4.3 Results and discussion 71
4.3.1 Optimization of the liquid-phase silanization 71
4.3.2 Nature of the solvent 72
4.3.3 Concentration of the silane 74
4.3.4 Silanization time 74
4.3.5 Curing process 75
4.3.6 Temperature 75
4.3.7 Contact angle measurements 76
4.3.8 Atomic force microscopy 77
4.4 Conclusions 78
5 Surface functionalization for spore-based biosensors with organosilanes (Electrochimica Acta, 241 (2017), 237-243) **83**
Abstract **83**
5.1 Introduction 85
5.2. Experimental 87
5.2.1 Materials 87
5.2.2 Fabrication of the silicon oxide (SiO_2), platinum (Pt) substrates and sensors 87
5.2.2.1 SiO_2 substrates 87
5.2.2.2 Pt substrates 87
5.2.2.3 Sensor fabrication 88
5.2.3 Surface functionalization 88
5.2.3.1 Hydroxylation 89
5.2.3.2 APTES 89
5.2.4 Physical characterizations of the SiO_2- and Pt substrates 89
5.2.4.1 Contact angle measurements 89
5.2.4.2 Atomic force microscopy 89
5.2.4.3 Scanning electron microscopy 90
5.2.4.4 Ellipsometry 90
5.2.5 Microbiological methods 90
5.2.5.1 Bacterial culture, sporulation and spore purification 90
5.2.5.2 Microbiological evaluation 90
5.2.6 Electrical characterization of the sensors 91
5.3. Results and discussion 91

5.3.1 Physical characterizations of APTES on SiO_2- and Pt substrates 91
5.3.1.1 Contact angle measurements 91
5.3.1.2 Atomic force microscopy and ellipsometry 92
5.3.2 Microbiological evaluation of the SiO_2-, Pt substrates and sensors 93
5.3.3 Impedance measurements of the sensors with APTES 96
5.4. Conclusions 97
Acknowledgements 98
References 98
6 Toward an immobilization method for spore-based biosensors in oxidative environment (Electrochimica Acta, 302 (2019), 394-401) 102
Abstract 102
6.1 Introduction 104
6.2 Materials and methods 106
6.2.1 Materials 107
6.2.2 Sensor fabrication 108
6.2.2.1 Si/SiO_2 substrates 108
6.2.2.2 Spore-based biosensor 108
6.2.3 Silanization 108
6.2.3.1 Hydroxylation 109
6.2.3.2 APTES 109
6.2.4 Physical and impedimetric characterizations 109
6.2.4.1 Contact angle measurements (CA) 109
6.2.4.2 Ellipsometry 109
6.2.4.3 Atomic force microscopy (AFM) 110
6.2.4.4 Impedimetric characterization 110
6.2.5 Microbiological approaches 111
6.2.5.1 Bacterial culture, sporulation and spore purification 111
6.2.5.2 Microbiological method for the evaluation of the APTES efficiency 111
6.2.6 Sterilization process 111
6.3. Results and discussion 112
6.3.1 Physical characterization of the APTES layer on Si/SiO_2 substrates after sterilization 112
6.3.1.1 Contact angle measurements (CA) 112

6.3.1.2 Ellipsometry 113
6.3.1.3 Atomic force microscopy (AFM) 114
6.3.2 APTES efficiency for the immobilization of spores on sensors 115
6.3.3 Effect of gaseous hydrogen peroxide on APTES-funtionalized spore-based biosensors 116
6.4 Conclusions 120
Acknowledgements 121
References 121
7 Combined calorimetric gas- and spore-based biosensor array for online monitoring and sterility assurance of gaseous hydrogen peroxide in aseptic filling machines (Biosensors & Bioelectronics, 143 (2019), 111628 (1-8)) **125**
Abstract **125**
7.1 Introduction 127
7.2. Materials and methods 129
7.2.1 Sensor fabrication: calorimetric gas- and spore-based biosensor array 129
7.2.2 Spore production 131
7.2.3 Sterilization with vaporized H_2O_2 131
7.2.4 Physical and electrical characterizations 132
7.2.4.1 Calorimetric H_2O_2 sensor 132
7.2.4.2 Spore-based biosensor 132
7.2.4.3 Scanning electron microscopy (SEM) 133
7.2.4.4 Atomic force microscopy (AFM) 133
7.3. Results and discussion 134
7.3.1 Calorimetric H_2O_2 sensor 134
7.3.2 Effect of gaseous H_2O_2 on the morphology of spores 134
7.3.2.1 SEM measurements 134
7.3.2.2 AFM measurements 137
7.3.3 Spore-based biosensor 140
7.4. Conclusions 142
Acknowledgements 144
References 144
Supplementary information 148
7. S1 Sensor fabrication: calorimetric gas- and spore-based biosensor array 148

7.S1.1 H_2O_2 response time and calibration curve 148
References 149
8 Conclusions and remarks **150**
References 159
Zusammenfassung **161**
List of publications **164**
Acknowledgments **167**
Curriculum Vitae **168**

Acronyms

4-AAP:	4-Aminoantipyrine
AC:	Alternate current
AFM:	Atomic force microscopy
Al:	Aluminum
Al_2O_3:	Aluminum oxide
APTES:	3-(Aminopropyl)triethoxysilane
Ca:	Calcium
CA:	Contact angle
CdTe:	Cadmium telluride
CFU/ml:	Colony forming units per milliliter
CLE:	Cortex-lytic enzyme
ConCap:	Constant capacitance
C-V:	Capacitance-voltage
DNA:	Deoxyribonucleic acid
DC:	Direct current
DI water:	Deionized water
DIN:	Deutsches Institut für Normung
DPA:	Dipicolinic acid
DSM:	Deutsche Sammlung von Mikroorganismen
EDC:	1-Ethyl-3-(3-dimethylaminopropyl)carbodiimide
EIS:	Electrolyte-insulator-semiconductor
GPTMS:	3-(glycidyloxypropyl)trimethoxysilane
H_2O_2:	Hydrogen peroxide
IC:	Initial count

IDE: Interdigitated electrode

MAL: Muramic-δ-lactam

MIS: Metal-insulator-semiconductor

MLCR: Mean logarithmic count reduction

MnO_2: Manganese dioxide

mRNA: Messenger ribonucleic acid

NA: Numerical aperture

NAM: N-Acetylmuramic acid

NHS: N-Hydroxysuccinimide

O_2: Oxygen

PAH: Poly(allylamine hydrochloride)

PCA: Plate count agar

PFA: Perfluoralkoxy

PFDTES: 1H,1H,2H,2H-Perfluorodecyltriethoxysilane

pH: *potentia Hydrogenii*

PI: Proportional-integral

PLL: Poly-l-lysine

PSPD: Position-sensitive photo diode

Pt: Platinum

RH: Relative humidity

RTD: Resistance temperature detector

SAM: Self-assembled monolayer

SASP: Small-acid soluble protein

SC: Mean survivor count

SEM: Scanning electron microscopy

Si:	Silicon
SiH_4:	Silane
SiO_2:	Silicon dioxide
SU-8:	Photoresist (8 epoxy groups)
Sulfo-NHS-LC-Biotin:	Biotin labeling reagents
Ti:	Titanium
UV:	Ultraviolet
ZnS:	Zinc sulfide

1 Introduction

1.1 Aseptic processing technology

Aseptic processing technology is broadly employed in biomedical, pharmaceutical and food industry to provide sterilized (liquid) products. Different modules are integrated in these machines including the sterilization of the packaging material, the filling and the sealing of the products. An important element to consider is producing sterile aseptic packaging to guarantee the shelf life and safety of the goods. Several sterilization methods are available to fulfill this task such as sterilization by heat, plasma radiation, UV or hydrogen peroxide [1].

Chemical techniques utilizing gases are widely applied, for instance, ethylene oxide, formalaldehyde, peracetic acid or gaseous hydrogen peroxide (H_2O_2). Despite of the fact that all of them have been used to sterilize packaging materials, not all are advisable for aseptic processing because of health hazards; in case of ethylene oxide and formaldehyde, both of them are carcinogenic [2]. In addition, it is important that the sterilant is as much as residue-free as it can, since it might otherwise affect the taste of the goods. In regard to peracetic acid, upon decomposition, it forms acetic acid and water. Because its vapor is very pungent and irritating, residuals may cause unwanted flavors in some food products [3]. Moreover, H_2O_2 has become a popular choice as a sterilant for aseptic filling machines. H_2O_2 has the best safety profile in comparison to other sterilization gases [4], mainly because it breaks down into water and oxygen, leaving virtually no residues and therefore being eco-friendly [5]. In addition, its strong oxidation properties are capable of killing an extensive number of microorganisms, for example, viruses, bacteria, spores and fungi [6–9]; the effectiveness of H_2O_2 is primarily affected by its exposure time, temperature and concentration.

1.2 State-of-the art methods to validate the H_2O_2 sterilization process

Microbiological tests are the state-of-the-art methods to validate the sterilization process with gaseous hydrogen peroxide, where microorganisms with a high resistance (e.g., endospores) against the sterilization process are used as probes. Standardized procedures are applied in food industry to validate aseptic filling machines, such as those stipulated by

the Association of German Machinery and Plant Constructors (Verband Deutscher Maschinen- und Anlagenbau e.V.) and the Industry Association for Food Processing Machines and Packaging (Fachverband Nahrungsmittelmaschinen und Verpackungsmaschinen) [10]. Two procedures can be performed to evaluate this, namely the count-reduction test and the end-point test [10][11].

1.2.1 Count-reduction test

In the count-reduction test, the packaging material is artificially infected (inoculated) with the test organism (endospores, in short form hereafter spores) and passed through the aseptic plant. Then, the number of viable spores is determined before and after the sterilization process and the mean logarithmic count reduction (killing rate) is obtained from the difference of both values. This process is described in detail as follows:

For a single-line aseptic filling machine, at least 25 packing units must be inoculated under the same conditions; for multiline aseptic filling machines, the number of packages was to be increased accordingly; each package must contain an initial microorganism count of at least 10^5 spores. Then, from the 25 packages, 5 of them are taken as a reference and the initial count (IC) must be determined. To recover the spores from the inner surface of the containers, the packages are rinsed with a test medium; on sheet packaging, the microorganisms are recovered by swabs in accordance to DIN 10113-2. Furthermore, the remaining 20 inoculated packages are submitted to the sterilization process; critical parameters (e.g., hydrogen peroxide concentration and temperature) should be set prior to the test run. In addition, if possible, the packaging units should be filled during the test run (after sterilization) to 25% of the nominal filling with sterile skimmed milk cooled down to room temperature or a sterile, pipettable or filterable liquid and the packaging units should be cooled down immediately after filling. If the packages are not filled with a test medium, the sterilized packages must be taken as quickly as possible after the test run for microbiological analysis in order to avoid falsification of the results (contamination). Finally, the mean logarithmic count reduction (kill rate) is determined from the mean survivor count (SC) of the 20 packages and the mean initial count (IC) of the 5 packages taken as a reference as it is shown in Equation 1.1. The test yields a positive result when at least a mean logarithmic count reduction (MLCR) of 4 is achieved, i.e., at least four log cycles of the spores have to be inactivated during the sterilization process.

$$MLCR_{CR}(mean\ logarithmic\ count\ reduction) = \log\left[\left(\frac{1}{5}\right) \times \sum IC_j\right] - \log\left[\left(\frac{1}{20}\right) \times \sum SC_i\right] \quad \text{(Equation 1.1)}$$

$\left(\frac{1}{5}\right) \times \sum IC_j : mean\ initial\ count$

$\left(\frac{1}{20}\right) \times \sum SC_i : mean\ survivor\ count$

$i = 1, \dots, 20$

$j = 1, \dots, 5$

1.2.2 End-point test

In the end-point test the packaging material is also inoculated in a similar manner as in the count-reduction test. However, in this case three different, graduated infection stages are used, each being greater by a power of ten than the one before (e.g., 10^4, 10^3 and 10^2 spores).

The major difference with respect to the count-reduction test is that in the end-point test, the inoculated packages are filled with a sterile culture medium matched to the test microorganism. After an incubation phase, only the number of unsterile packaging units is determined, i.e., in the count-reduction test, the spores are removed from the packages and evaluated, whereas in the end-point test, they remain inside of them and so they are further processed. Furthermore, besides the effectiveness of the packaging material sterilization, the end-point test provides information about the entire process from supplying the product and filling through recontamination-free sealing of the packages.

A typical end-point procedure is further specified in detail: For the test, 100 packaging units must be selected for each level of contamination, which must contain an initial microorganism count of 10^2, 10^3, and 10^4 spores, respectively. The packaging units should be uniformly distributed over the packing lines in the case of multiline filling machines and critical sterilization parameters (e.g., hydrogen peroxide concentration and temperature) should be specified prior the test run. Afterwards, the 300 packaging units (100 packages for each contamination level: 10^4, 10^3 and 10^2 spores) are passed through the sterilization process and later, they are filled using a test medium (e.g., sterile skimmed milk or a culture medium matched to the test microorganism). The enclosed packages are then incubated for at least one week at 30 °C or 55 °C, depending on the spore strain. At the end, the number of unsterile

packages is determined (unsterile packages have to be investigated in regard to possible contamination) and the mean logarithmic count reduction for each of the three levels of contamination can be obtained from Equation 1.2. In a similar case as in the count-reduction test, the test yields a positive result when at least an MLCR of 4 is achieved for each test series.

$$MLCR_{EP}(mean\ logarithmic\ count\ reduction) = \log(initial\ count\ per\ package) - \log\left[\ln\left(\frac{number\ of\ packages\ tested}{number\ of\ sterile\ packages}\right)\right] \quad \text{(Equation 1.2)}$$

Despite of the fact that these methods (count-reduction test, end-point test) are reliable and well-standardized, they lack of rapid responses since the results can be obtained at the earliest of 36-48 hours. These machines deliver around 12,000 ready-packaged products per hour (e.g., Pure-Pak® Aseptic Filling Line E-PS120A), i.e., around 430,000 packages cannot be delivered to the customers without a certified verification. Therefore, the validation time is a decisive parameter besides the trained staff and labor-intensive procedures. As a result, more sophisticated methods should be developed by the integration of sensor technologies.

1.3 Sensor technologies to monitor gaseous hydrogen peroxide

In recent years, novel sensor technologies have emerged to validate the efficacy of sterilization processes with gaseous hydrogen peroxide. Several detection mechanisms of gaseous H_2O_2 detection have been presented in literature by means of acoustic- [11], calorimetric- [12], conductometric- [13], colorimetric- [14] or electrochemical measurements [15]. A few of them are not adequate for online- and inline monitoring in aseptic filling machines (electrochemical, colorimetric), because of portability deficiency of the measuring equipment or complicated sample preparation (e.g., solution-based). Other methods have high response times (>30 s) in comparison to standard industrial H_2O_2 exposure times (<2 s) or may not be able to handle high temperatures (up to 300 °C). Moreover, calorimetric gas sensors have been earlier suggested [12, 16, 17] to overcome these limitations for applications in aseptic food industry. An exemplary H_2O_2 sensor is shown in Figure 1.1. It consists of a differential setup of two temperature-sensitive meander structures, which are passivated by an inert polymer layer (e.g., perfluoralkoxy). One of them functions as a reference, whereas the other one is additionally catalytically activated by manganese oxide (MnO_2). When gaseous H_2O_2 is in contact with the sensor surface, hydrogen peroxide is split

into oxygen and water at the catalytically activated side of the sensor, and the other part of the sensor remains inert. As a result, an exothermic reaction follows and an increase of temperature (specifically on the active side of the sensor) can be measured. Finally, the temperature difference can be quantitatively correlated to the H_2O_2 concentration. Further details regarding the principle of the calorimetric sensors can be found in chapter 2.

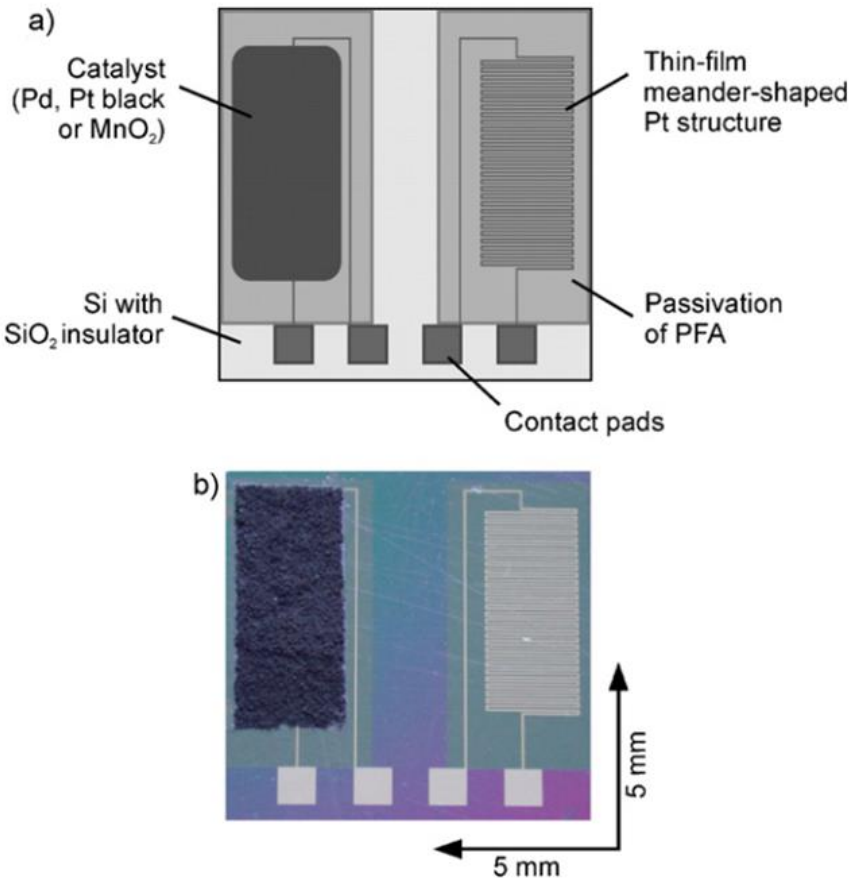

Figure 1.1 a) Schematic representation of the calorimetric H_2O_2 gas sensor and b) photograph of a fabricated H_2O_2 sensor with two Pt meander structures passivated with perfluoralkoxy (PFA): the left structure is catalytically activated with MnO_2, whereas the right structure is used as a reference (figure from [12] with permission from Elsevier).

However, the measurement of H_2O_2 concentrations alone cannot substitute the need of the microbiological methods by itself. Therefore, it is preferable to incorporate an additional measurement method of the spore viability by means of cell-based biosensors.

1.4 Cell-based biosensors

Cell-based biosensors are analytical devices able to detect biochemicals signals directly by the use of living cells and transform them into readable signals (e.g., electrical) by sensors or transducers [18]. They include a great number of applications in several fields, for instance, in the pharmaceutical, environmental, medical, defense or food industry [19, 20]. Eukaryotic or prokaryotic cells are commonly used as recognition elements since their native receptors and pathways can respond to specific analytes in a physiological way. These may involve different types of mammalian cells such as neuronal, endothelial or cancer cells [21–23], diverse bacterial species, e.g., *Escherichia coli*, *Bacillus subtilis* or *Clostridium butyricum* [24–26] or fungal cells, like yeasts or molds [27, 28]. Among them, the use of spores as sensing units offer several advantages in comparison to bacterial cells (or living cells) including robustness (withstand harsh conditions), ease of production and long-term preservation and storage [29, 30].

1.4.1 Spore-based biosensors

Certain bacteria, mostly (but not all) *Bacillus* and *Clostridium*, undergo under unfavorable environmental conditions (e.g., pH, temperature, starvation) endospore formation as a survival strategy; they transform from bacteria to spores. In this form, they are dormant, have not detectable metabolism, and can endure rough scenarios, for example, high temperatures, high pH, desiccation, radiation and several oxidizing chemicals [31]. These extraordinary resistances are mainly due to their unique architecture and components as shown in Figure 1.2. The most distant layer of the spores are the coats, except for some *Bacillus* species (e.g., *Bacillus anthracis*) that display an exosporium. The coats are the initial protective layers against chemical and mechanical stresses [32]. The outer membrane envelops the cortex and could serve as permeability barrier or might remain only as a vestigial structure [33]. The cortex and the germ cell wall have similar peptidoglycan structures. However, the cortex possesses particular properties, for example, muramic-δ-lactam (MAL) seems to be the recognition component for cortex-lytic enzymes (CLEs) that hydrolyze the cortex but not the germ cell wall during germination [34]. Protecting the core is the inner membrane, in which lipids are predominantly immobile. It has low permeability to small molecules (including water) and this may shield the spore core from DNA (deoxyribonucleic

acid)-damaging chemicals [34]. Finally, the innermost layer of the spore is the core, where its DNA, ribosomes and enzymes are contained. The core has a low water content (25-50% of wet weight), great amount (25% of core dry weight) of Ca-dipicolinic acid (DPA) and saturation of DNA with α/β-type small acid-soluble proteins (SASPs); these properties of the core contribute to its resistance to wet/dry heat and different oxidizing agents [34, 35]. As a result, the spores are flexible and tough microorganisms. They are able to stay dormant and still capable of sensing their environment, which makes them very convenient as sensing units for spore-based biosensors. For instance, bacterial spores have been used in microbial cell surface display technologies as biocatalysts, biosorbents and vaccines [36]. In addition, due to their high resistance, they are employed as biological indicators to validate sterilization processes [1].

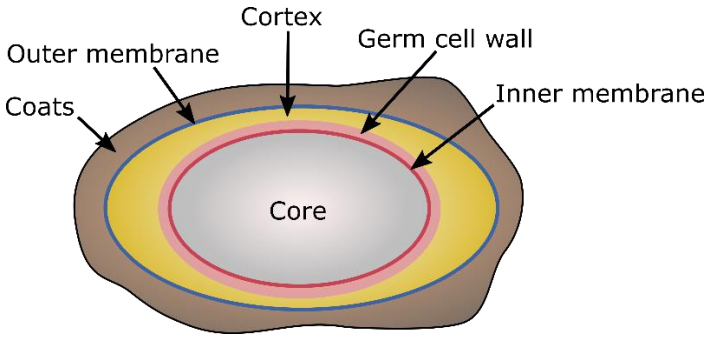

Figure 1.2. Schematic representation of a *Bacillus atrophaeus* spore. The different layers are not drawn to scale and some *Bacillus* species have an extra layer called exosporium. Adapted from [37] with permission from Elsevier.

Spore-based biosensors can be basically differentiated in two categories: genetically engineered and non-genetically engineered spores. The principle of the genetically engineered spore-based biosensors is to modify plasmids from vegetative cells to contain a sensing and a reporting element. Then, the vegetative cells are sporulated to form spores and can be stored under nearly any conditions prior to use. As they are needed, the spores are twice incubated to induce germination and as vegetative cells with the target analyte; optimally, these two steps may occur simultaneously. At the end, after a proper incubation period, the signal (e.g., fluorescence) produced by the reporting element (reporter gene) can be evaluated [38]. Furthermore, non-genetically engineered spore-based biosensors exploit the innate physiology of spores such as coats, receptors, channels and enzymes that are sensitive to different analytes or physical conditions. The spores can be immobilized on

sensor substrates together with transducing elements or be independent to a certain extent from them. Nevertheless, at the end, the read-out and evaluation of the signal can be accomplished. The focus of this work is on non-genetically engineered spore-based biosensors, and from now on for convenience just called spore-based biosensors. The reader is referred to [38] for further information regarding the genetically-engineered ones.

Several examples are given in literature for spore-based biosensors. For instance, spores have been utilized as quantum dots nanocomposites to function as a pH sensor [39]; quantum dots (CdTe/ZnS) were immobilized on to the surface of decoated spores and as a whole the fluorescence intensity was measured and correlated to pH changes. In another case, the spore surface was used as a catalyst for phenol detection [40]. A standard approach to determine phenols concentrations in water is based on the reaction of 4-Aminoantipyrine (4-AAP) with phenols; starting from this, 4-APP was mixed with a solution containing phenol and then, the spores were added to the solution to catalyze the coupling reaction of 4-APP with phenol. The spores were subsequently removed to avoid interference and the total concentration was quantified by a colorimetric method. A further example employs the hydroscopic properties of the spores to be used as a humidity sensor and an actuator [41]; spores were immobilized on a rubber sheet and submitted to different relative humidities (RHs). Depending on the RH, the rubber sheet with spores went from a contracted form (low RH) to an expanded one (high RH) and by this, the mechanical strain was able to be correlated to the RH. In addition, spores confined onto glass substrates with interdigitated electrodes have been applied to validate the sterilization with gaseous hydrogen peroxide [42]; as the concentration of hydrogen peroxide increased an impedimetric change at the sensor surface was observed. This was then suggested to be due to the change of morphology of the spores.

1.4.2 Sensor technologies for the determination of spore viability

Different methods have been proposed to measure the viability of spores such as with optical- [43, 44], potentiometric- [45], piezoelectric- [46] or impedimetric sensors [47]. The determination of the spore viability generally employs additional unique biomarkers from the spore coat or byproducts from germination, for example, mRNA (messenger ribonucleic acid) [48], dipicolinic acid (DPA) or calcium ions (Ca^{2+}) [49]. Therefore, specific (bio-) chemical transducers must be adapted. Nevertheless, most of these methods are solution-based,

having high response times (>20 min) and are not convenient to perform under a dry gaseous environment.

Recently, a novel impedimetric sensor was suggested at our institute to monitor the microbiological efficacy of gaseous H_2O_2 during sterilization processes [42]. This sensor (Figure 1.3) measures the variation of the spore morphology by means of impedance changes in regard to the hydrogen peroxide concentration. It consists of a differential setup of two interdigitated electrode arrangements: on one part, microbiological spores (i.e., *Bacillus atrophaeus*) are immobilized and the other one functions as a reference. The impedance of the spores is measured before and after the sterilization process and the spore viability can be determined due to the correlation between the H_2O_2 concentration and the impedance change. However, the principle of this sensor is still under ongoing research and is further addressed in this work (chapter 7).

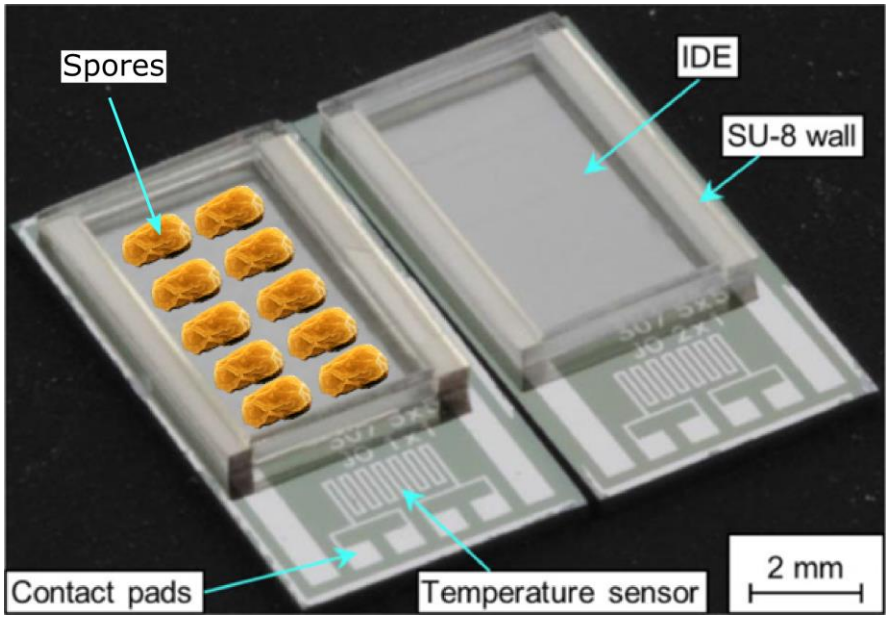

Figure 1.3 Spore-based biosensor adapted from [42] (with permission from Elsevier) consisting of interdigitated electrodes (IDEs), where the spores are immobilized within an SU-8 wall on one part of the setup (left), temperature sensors and contact pads.

Moreover, depending on the measurement setup of the spore-based biosensor, the spores may need to be immobilized on solid substrates. In this case, the coupling between the spores and the sensor substrates is an important task to enhance the performance of the sensor in terms of sensitivity, reproducibility and specificity.

1.5 Spore immobilization

The precise localization of spores onto sensor platforms can be achieved in different forms as shown in Figure 1.4: only immobilization methods are described in the following sections, which do not compromise the viability of the spores.

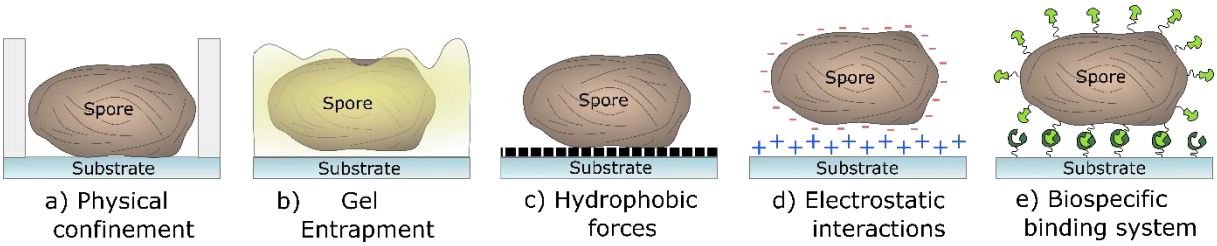

Figure 1.4 Immobilization methods to localize spores on solid substrates.

1.5.1 Physical confinement

The first immobilization method (Figure 1.4 a) is performed by physical confinement. Here, the spores are mechanically trapped inside a compartment (e.g., polycarbonate membrane). This can be easily carried out by pipetting a drop of a spore suspension on top of a membrane and let it dry in air. The spores will eventually fall into the membrane being completely restricted. The advantages of this method include the ease of use, efficiency, and no harmful chemicals (that can compromise the spore structure or viability) are needed. However, this method may not be suitable in some cases, for example, if the membrane affects transducer elements or the spore surface is needed for further investigations, since the membrane partially shields the spore.

1.5.2 Gel entrapment

The spores can also be immobilized inside a gel matrix (Figure 1.4 b). The gel consists of a polymer (e.g., agarose) and when it solidifies, it forms a porous three-dimensional structure; the melting and gelling temperatures can be tailored depending on the application. The immobilization is commonly performed by mixing the spore suspension together with the liquid gel. After this, the spore-gel mixture can be spread out onto a substrate and let it solidify. This method provides a finely controlled spore localization, since no washing steps are needed. However, it is limited for applications requiring high temperatures, since the gel may melt, freeing the spores during the process.

1.5.3 Hydrophobic forces

Bacterial spores are naturally hydrophobic [50]; as a result, the hydrophobic behavior of the spores can be exploited to immobilize them onto hydrophobic surfaces (Figure 1.4 c). This physical adsorption and non-covalent mechanism can be carried out in different ways. Some of them modify the surface physically, for example, patterning silicon nanowires on it [51], or chemically, like by the use of self-assembled monolayers (SAMs) [52]. After the substrate has been turned hydrophobic, it is incubated (e.g., 30 min) with spores. At the end, the substrate is carefully rinsed to remove loosely attached spores and then dried. This method provides a native and feasible way for the attachment of spores. However, care has to be taken into account while choosing the spore strain, since the spore hydrophobicity varies between different species [53].

1.5.4 Electrostatic interactions

Under physiological conditions, the spore surface is negatively charged [54]. This can be used to immobilize negatively charged spores onto positively charged surfaces (e.g., amine-terminated) by means of electrostatic interactions (Figure 1.4 d); two common approaches to achieve this are by the use of self-assembled monolayers (SAMs) or polyelectrolytes.

SAMs can be grafted onto a substrate by a liquid-phase- or a gas-phase deposition. One part of the self-assembled molecule is autonomously and uniformly attached onto the substrate, whereas the other part is terminated with a positively charged molecule, for instance, an amine. Later, the spores can be incubated for a certain time (e.g., 30-60 min) with the SAMs-substrate and then carefully washed to discard the weakly-bounded spores. One of the main advantages of this method is the very high stability of the SAMs: depending on the SAM, they can be stable at high temperatures (460 °C [55] or up to 720 °C [56]) and stable against several chemicals [56]. One of the main drawbacks, however, is the difficulty to achieve high-quality SAMs in terms of uniform monolayer formation and correct orientation of the reactive groups [57].

Moreover, polyelectrolytes can be utilized as well to reach a positively charged surface. It can be performed by immersing the substrate into a cationic polyelectrolyte (positively charged polymer) solution for a certain period and then the substrate is rinsed and dried. Afterwards, the spores can be incubated and washed in a similar manner as previously described with the

SAMs. One advantage of this technique is that the thickness of the immobilization layer can be easily adjusted by layering different polyelectrolytes (one cationic and one ionic) with high resolution (<1 nm) [58]. A main drawback is that the pH may influence drastically the performance of the polyelectrolyte [59], compromising the coupling between the spores and the immobilization layer.

1.5.5 Biospecific binding system

The last immobilization method is by binding high-specific biomolecules, ligands or bacterial viruses between the substrate and the spore surface (Figure 1.5 e). In this fashion, four different biospecific binding systems can be distinguished, namely antibody-antigen, biotin-avidin, peptide ligands and bacteriophages (bacterial viruses) [60–67].

The antibody-antigen binding system consists of a native immune reaction of anti-spore antibodies immobilized onto a substrate that specifically recognize and bind antigens from the spore surface. Generally, the substrate is modified with different steps of coupling reactions to be able to bind the anti-spore antibodies to the surface; for instance, SAMs formation onto the surface may be needed to facilitate the coupling of other molecules (e.g., 1-Ethyl-3-(3-dimethylaminopropyl)carbodiimide (EDC)/ N-Hydroxysuccinimide (NHS) coupling), which enables a covalent bond between them and the anti-spore antibodies. After this, the anti-spore antibodies are incubated with the modified substrate for a certain period of time and then the non-specifically bound antibodies are washed away. Finally, the spores can be incubated with the anti-spore-antibody-modified substrate and the rest non-specifically bound spores are removed. This method provides high sensitivity and selectivity to bind a specific strain of spores, since the anti-spore antibodies can be produced for a particular strain. Nevertheless, this immobilization technique may not be suitable for harsh conditions (e.g., high temperatures), since the immune complex may be denatured [63].

In addition, other non-native spore mechanisms can be implemented to localize the spores onto substrates, for example, by modifying the spore surface with biotin and the substrate with avidin. Avidin is a protein found in egg whites and it has an extraordinary high affinity to the vitamin B biotin. Due to its high degree of nonspecific adsorption induced by its basic isoelectric point (10) and carbohydrates groups [68], streptavidin (homologous protein of avidin produced from the bacteria species of *Streptomyces*) is often preferred over avidin. The

immobilization process can be realized in different manners; the spore surface and the substrates may need to be modified to attach streptavidin at the substrate and biotin at the surface of the spore. Here, the spore coat can be modified with antibodies to anchor biotin to the surface [60] or by the use of biotin-labeling reagents (e.g., Sulfo-NHS-LC-Biotin) [61]. In both cases, the spore coat is modified to contain a biotin-rich surface. Furthermore, the substrate is then modified in several steps (with SAMs and other reagents) to immobilize biotin as well on the surface. Then, the substrate is incubated with streptavidin, resulting in a streptavidin-modified surface. Streptavidin has four binding sites for biotin [68], two of them are used to immobilize it to the substrate and the other two are used to attach the biotin-modified spores onto the substrates. The biotin-(strept) avidin complex is considered the strongest non-covalent and biological interaction known [69], because of this, the immobilization is quite firm, specific and reliable. The bond is stable under a wide range of pH and temperatures and under certain circumstances it can be reversible [69]. However, the main drawback of this technique is that it cannot be implemented in applications where the spores cannot be chemically modified (e.g., spore recognition).

The spores can also be immobilized by means of ligands, which can naturally recognize and bind proteins from the spore coat. These ligands can be particularly constructed to match a certain spore strain. The substrates may need to be modified stepwise by SAMs and other coupling reagents to attach the ligands to the surface. After that, the attachment of the spores to the surface can be performed by incubation of the ligand-modified substrate with the spores for a stipulated time and then removing the nonbound spores. This method allows a certain degree of high selectivity regarding the binding of a specific spore strain, because, when different spore strains are simultaneously used, closely related species may also bind [70]. Nevertheless, it is a reliable and robust method to immobilize spores since the ligands are more stable than antibodies or proteins (their complex form make them prone to denaturation [63]).

Lastly, bacteriophages can also be employed as coupling elements for spores. They are bacterial viruses that can have different forms and dimensions; for example, the phage Ff has a filamentous architecture, 800-900 nm long with a diameter of 6.5 nm [71]. Their surface can be modified with phage ligands that precisely bind unique spore strains. The immobilization process can be fairly simple; for instance, the substrate can be incubated with the phages for

an interval of time and then washed away. Then, the same process can be performed for the spores with the phage-modified substrate. This immobilization technique has several advantages in comparison to antibody-antigen interactions: it can provide several binding sites, therefore a stronger attachment of the spores is possible; bacteriophages are robust with a resistance to heat (up to 80 °C), organic solvents, urea, acids, bases and they can be stored for long periods of time with minimal decrease in binding activity [62]. However, some drawbacks have been also observed, like partial phage inactivation because of the immobilization methods and in some cases, the binding efficiency was less than that of antibodies [72].

In summary, one can conclude that all these immobilization strategies to couple spores onto sensor substrates (e.g., by physical confinement, gel entrapment, hydrophobic forces, electrostatic interactions and biospecific binding systems) have advantages and suffer from drawbacks. The appropriate method has to be chosen according to its application; examples of the mentioned immobilization techniques are summarized in Table 1.1. In addition, surface functionalization is often required depending on the immobilization strategy to localize spores onto sensor substrates. SAMs such as organosilanes for hydroxylated surfaces (e.g., glass, Si/SiO_2) are widely used as coupling reagents. They can be applied in the liquid or gas phase, providing reactive moieties onto substrates for further immobilization procedures. It is worthy to note that functionalization steps (e.g., hydroxylation, cleaning practices) may also influence the performance of the sensor by themselves, for example, by etching the sensor surface or damaging the transducer elements. Therefore, it is advisable to review the chemical and physical limitations of the spore-based biosensor before choosing any immobilization method.

In the case of the spore-based biosensor in aseptic processing, the immobilization layer has to withstand high temperatures (up to 240 °C) and an oxidative environment (gaseous hydrogen peroxide). Therefore, organosilanes were chosen as immobilization strategy because of their robustness as previously mentioned in section 1.5.4.

Table 1.1 Immobilization methods of spores for spore-based biosensors.

Immobilization nature	Technique	Spores	Substrate	Reference
Physical confinement	Isopore membrane	*Bacillus anthracis*, *Clostridium tyrobutyricum*	Polycarbonate	[73], [74]
Gel entrapment	Gel	*Clostridium acetobutylicum*, *Bacillus sphaericus*	Silica, agarose	[75], [76]
Hydrophobic forces	SAMs, Si nanowires	*Bacillus mycoides*, *Bacillus cereus*	Glass, Si	[51], [52]
Electrostatic interactions (amino-terminated surfaces)	SAMs (APTES)	*Bacillus subtilis*, *Geobacillus spores D4*	Glass, Si_3N_4	[77], [78], [79]
	Polyelectrolytes (PLL, PAH)	*Bacillus subtilis*, *Bacillus anthracis*	Glass, silica	[77], [80], [81], [82]
Biospecific binding system	Antibody-antigen	*Bacillus subtilis*	Gold	[64], [65]
	Biotin-streptavidin	*Bacillus thuringiensis*, *Bacillus subtilis*	Glass, PDMS	[60], [61]
	Peptide ligands	*Bacillus subtilis*, *Bacillus anthracis*	Glass, gold	[63], [66]
	Bacteriophages	*Bacillus anthracis*	Gold	[62], [67]

1.6 Objectives and contents of this contribution

The main focus of this thesis is to develop an immobilization strategy (for the immobilization of spores on sensor substrates) that can withstand the harsh conditions (high temperatures, oxidizing environment) of a sterilization process with gaseous hydrogen peroxide. In addition, as part of the immobilization strategy, the effect of surface modification techniques (e.g., hydroxylation) on sensor surfaces was studied. Finally, the implementation of a sensor

array consisting of a calorimetric gas sensor and a spore-based biosensor for online monitoring and sterility assurance of gaseous hydrogen peroxide in aseptic filling machines is introduced.

The objectives of each chapter are listed below.

Chapter 3: Effect of O_2 plasma on properties of electrolyte-insulator-semiconductor structures

- → The hydroxylation effect of O_2 plasma is investigated on SiO_2/Si EIS structures by means of electrochemical and contact angle measurements.
- → Annealing on EIS chips is studied as well for further improvement of the sensor performance.

Chapter 4: Optimization of the immobilization of bacterial spores on glass substrates with organosilanes

- → Two organosilanes, namely (3-(Aminopropyl)triethoxysilane (APTES) and (3-(glycidyloxypropyl)trimethoxysilane (GPTMS)) are used to immobilize spores on glass substrates.
- → Another organosilane (1H,1H,2H,2H-Perfluorodecyltriethoxysilane (PFDTES)) is applied to hinder the immobilization of spores on glass substrates.
- → Several parameters influencing the silanization process are investigated such as nature of the solvent used, concentration of the silane, silanization time, silanization temperature and curing process.

Chapter 5: Surface functionalization for spore-based biosensors with organosilanes

- → APTES-functionalized biosensor substrates (SiO_2, Pt) are characterized by means of atomic force microscopy, contact angle measurements and microbiological evaluation tests to immobilize spores.
- → The electrical characteristics of the APTES layer are investigated by means of impedance spectroscopy measurements.
- → The impedance spectroscopy measurements were performed by Jan Oberländer.

Chapter 6: Toward an immobilization method for spore-based biosensors in oxidative environment

→ The influence of hydrogen peroxide on APTES-functionalized spore-based biosensors is studied.

→ Different parameters of the immobilization, like the solvent of APTES (toluene, ethanol) and the spore suspension (water, ethanol), are investigated and characterized by impedimetric- and contact angle measurements, microbiological evaluation tests for the spore immobilization, ellipsometric- and atomic force microscopic measurements.

Chapter 7: Calorimetric gas- and spore-based biosensor array for online monitoring and sterility assurance of gaseous hydrogen peroxide in aseptic filling machines

→ A sensor array that can measure simultaneously gaseous hydrogen peroxide concentrations and the spore viability is presented.

→ The effect of hydrogen peroxide on different spore strain is investigated by impedimetric-, atomic force microscopic-, scanning electron microscopic- and microbiological measurements.

Chapter 8: Conclusions and outlook

→ The conclusions and outlook of this thesis are summarized.

References

[1] I.A. Ansari and A.K. Datta, "An overview of sterilization methods for packaging materials used in aseptic packaging systems", *Food Bioprod. Process.* 81 (1), 57–65 (2003).

[2] S. Koda, S. Kumagai, and H. Ohara, "Environmental monitoring and assessment of short-term exposures to hazardous chemicals of a sterilization process in hospital working environments", *Acta Med. Okayama* 53 (5), 217–223 (1999).

[3] R.T. Toledo, "Overview of sterilization methods for aseptic packaging materials", in *Food and Packaging Interactions: Developed from a Symposium Sponsored by the Division of Agricultural and Food Chemistry at the 193rd Meeting of the American Chemical Society, Denver, Colorado, April 5-10, 1987*, American Chemical Society, Washington, DC, USA 1988.

[4] M.D. Johnston, S. Lawson, and J.A. Otter, "Evaluation of hydrogen peroxide vapour as a method for the decontamination of surfaces contaminated with *Clostridium botulinum* spores", *J. Microbiol. Meth.* 60 (3), 403–411 (2005).

[5] G. McDonnell, "The use of hydrogen peroxide for disinfection and sterilization applications", in *Patai's chemistry of functional groups*, John Wiley and Sons, 1-34 (2009).

[6] R.A. Heckert, M. Best, L.T. Jordan, G.C. Dulac, D.L. Eddington, and W.G. Sterrit, "Efficacy of vaporized H_2O_2 against exotic animal viruses", *Appl. Environ. Microb.* 63 (10), 3916–3918 (1997).

[7] N. Kitancharoen, A. Yamamoto, and K. Hatai, "Fungicidal effect of hydrogen peroxide on fungal infection of rainbow trout eggs", *Mycoscience* 38 (4), 375–378 (1997).

[8] J.A. Otter and G.L. French, "Survival of nosocomial bacteria and spores on surfaces and inactivation by hydrogen peroxide vapor", *J. Clin. Microbiol.* 47 (1), 205–207 (2009).

[9] P. Swartling and B. Lindgren, "The sterilizing effect against *Bacillus subtilis* spores of hydrogen peroxide at different temperatures and concentrations", *J. Dairy Res.* 35 (03), 423–428 (1968).

[10] Verband Deutscher Maschinen- und Anlagenbau e.V. (VDMA), "Code of practice: filling machines of VDMA hygiene class V: testing the effectiveness of packaging sterilization devices", *VDMA-Fachverbandsschriften* 6, 1–16 (2008).

[11] S. Liu, H. Sun, R. Nagarajan, J. Kumar, Z. Gu, J. Cho, and P. Kurup, "Dynamic chemical vapor sensing with nanofibrous film based surface acoustic wave sensors", *Sensor Actuat. A-Phys.* 167 (1), 8–13 (2011).

[12] P. Kirchner, B. Li, H. Spelthahn, H. Henkel, A. Schneider, P. Friedrich, J. Kolstad, M. Keusgen, and M.J. Schöning, "Thin-film calorimetric H_2O_2 gas sensor for the validation of germicidal effectivity in aseptic filling processes", *Sensor Actuat. B-Chem.* 154 (2), 257–263 (2011).

[13] A.L. Verma, S. Saxena, G.S.S. Saini, V. Gaur, and V.K. Jain, "Hydrogen peroxide vapor sensor using metal-phthalocyanine functionalized carbon nanotubes", *Thin Solid Films* 519 (22), 8144–8148 (2011).

[14] M. Xu, B.R. Bunes, and L. Zang, "Paper-based vapor detection of hydrogen peroxide: colorimetric sensing with tunable interface", *ACS Appl. Mater. Inter.* 3 (3), 642–647 (2011).

[15] J. Kulys, "Flow-through amperometric sensor for hydrogen peroxide monitoring in gaseous media", *Sensor Actuat. B-Chem.* 9 (2), 143–147 (1992).

[16] N. Näther, H. Henkel, A. Schneider, and M.J. Schöning, "Investigation of different catalytically active and passive materials for realizing a hydrogen peroxide gas sensor", *Phys. Status Solidi A* 206 (3), 449–454 (2009).

[17] J. Oberländer, P. Kirchner, H.-G. Boyen, and M.J. Schöning, "Detection of hydrogen peroxide vapor by use of manganese(IV) oxide as catalyst for calorimetric gas sensors", *Phys. Status Solidi A* 211 (6), 1372–1376 (2014).

[18] Q. Liu, C. Wu, H. Cai, N. Hu, J. Zhou, and P. Wang, "Cell-based biosensors and their application in biomedicine", *Chem. Rev.* 114 (12), 6423–6461 (2014).

[19] J.J. Pancrazio, J.P. Whelan, D.A. Borkholder, W. Ma, and D.A. Stenger, "Development and application of cell-based biosensors", *Ann. Biomed. Eng.* 27 (6), 697–711 (1999).

[20] Q. Gui, T. Lawson, S. Shan, L. Yan, and Y. Liu, "The application of whole cell-based biosensors for use in environmental analysis and in medical diagnostics", *Sensors* 17 (7), 1623 (1-17) (2017).

[21] Y. Nam, J. C. Chang, B. C. Wheeler, and G. J. Brewer, "Gold-coated microelectrode array with thiol linked self-assembled monolayers for engineering neuronal cultures", *IEEE T. Bio-Med. Eng.* 51 (1), 158–165 (2004).

[22] T.M. Curtis, M.W. Widder, L.M. Brennan, S.J. Schwager, W.H. van der Schalie, J. Fey, and N. Salazar, "A portable cell-based impedance sensor for toxicity testing of drinking water", *Lab Chip* 9 (15), 2176–2183 (2009).

[23] T. A. Nguyen, T. Yin, and G. Urban, Eds., "A cell impedance sensor chip for cancer cells detection with single cell resolution" IEEE SENSORS, Baltimore, MD, USA, 1-4 (2013).

[24] L. Ooi, L.Y. Heng, and I.C. Mori, "A high-throughput oxidative stress biosensor based on *Escherichia coli* roGFP2 cells immobilized in a k-carrageenan matrix", *Sensors* 15 (2), 2354–2368 (2015).

[25] J.-R. Fantino, F. Barras, and F. Denizot, "Sposensor: a whole-bacterial biosensor that uses immobilized *Bacillus subtilis* spores and a one-step incubation/detection process", *J. Mol. Microb. Biotech.* 17 (2), 90–95 (2009).

[26] T. Matsunaga, I. Karube, and S. Suzuki, "A specific microbial sensor for formic acid", *Eur. J. Appl. Microbiol.* 10 (3), 235–243 (1980).

[27] A. Adeniran, M. Sherer, and K.E.J. Tyo, "Yeast-based biosensors: design and applications", *FEMS Yeast Res.* 15 (1), 1–15 (2015).

[28] E. Savory, J. Sabarinathan, A. Sauer, and J.A. Scott, "An optoelectronic sensor for the monitoring of mould growth in concealed spaces", *Build. Environ.* 49, 9–16 (2012).

[29] A. Sangal, P. Pasini, and S. Daunert, "Stability of spore-based biosensing systems under extreme conditions", *Sensor Actuat. B-Chem.* 158 (1), 377–382 (2011).

[30] E. Ricca and S.M. Cutting, "Emerging applications of bacterial spores in nanobiotechnology", *J. Nanobiotechnol.* 1 (1), 6 (1-10) (2003).

[31] P. Setlow, "Resistance of bacterial spores", in *Bacterial Stress Responses*, ASM Press, Washington, DC, USA 2011.

[32] A. Driks, "*Bacillus subtilis* spore coat", *Microbiol. Mol. Biol. R.* 63 (1), 1–20 (1999).

[33] P. Setlow, "Germination of spores of *Bacillus* species: what we know and do not know", *J. Bacteriol.* 196 (7), 1297–1305 (2014).

[34] D. Paredes-Sabja, P. Setlow, and M.R. Sarker, "Germination of spores of *Bacillales* and *Clostridiales* species: mechanisms and proteins involved", *Trends Microbiol.* 19 (2), 85–94 (2011).

[35] W.L. Nicholson, N. Munakata, G. Horneck, H.J. Melosh, and P. Setlow, "Resistance of *Bacillus* endospores to extreme terrestrial and extraterrestrial environments", *Microbiol. Mol. Biol. R.* 64 (3), 548–572 (2000).

[36] P.T. McKenney, A. Driks, and P. Eichenberger, "The *Bacillus subtilis* endospore: assembly and functions of the multilayered coat", *Nat. Rev. Microbiol.* 11, 33-44 (2012).

[37] S.R. Sella, L.P. Vandenberghe, and C.R. Soccol, "Life cycle and spore resistance of spore-forming *Bacillus atrophaeus*", *Microbiol. Res.* 169 (12), 931–939 (2014).

[38] D. Wynn, S. Deo, and S. Daunert, "Engineering rugged field assays to detect hazardous chemicals using spore-based bacterial biosensors", *Meth. Enzymol.* 589, 51–85 (2017).

[39] X. Zhang, Z. Li, T. Zhou, Q. Zhou, Z. Zeng, X. Xu, and Y. Hu, "A quantum dot-spore nanocomposite pH sensor", *Talanta* 150, 184–189 (2016).

[40] Z. Zeng, L. Tian, Z. Li, L. Jia, X. Zhang, M. Xia, and Y. Hu, "Whole-cell method for phenol detection based on the color reaction of phenol with 4-Aminoantipyrine catalyzed by CotA laccase on endospore surfaces", *Biosens. Bioelectron.* 69, 162–166 (2015).

[41] O. Sahin, *Bacterial spore based energy system* 2011 (Patent, US20130285386A1).

[42] J. Oberländer, M. Mayer, A. Greeff, M. Keusgen, and M.J. Schöning, "Spore-based biosensor to monitor the microbicidal efficacy of gaseous hydrogen peroxide sterilization processes", *Biosens. Bioelectron.* 104, 87–94 (2018).

[43] D. L. Rosen, *Bacterial spore detection and quantification methods* 1997 (Patent, 5876960).

[44] M. B. Tabacco and L. C. Taylor, *Optical sensors for rapid, sensitive detection and quantitation of bacterial spores* 2000 (Patent, 6498041 B1).

[45] Y. Zhou, B. Yu, and K. Levon, "Potentiometric sensor for dipicolinic acid", *Biosens. Bioelectron.* 20 (9), 1851–1855 (2005).

[46] G.A. Campbell and R. Mutharasan, "Piezoelectric-excited millimeter-sized cantilever (PEMC) sensors detect *Bacillus anthracis* at 300 spores/mL", *Biosens. Bioelectron.* 21 (9), 1684–1692 (2006).

[47] M. Labib, A.S. Zamay, O.S. Kolovskaya, I.T. Reshetneva, G.S. Zamay, R.J. Kibbee, S.A. Sattar, T.N. Zamay, and M.V. Berezovski, "Aptamer-based viability impedimetric sensor for bacteria", *Anal. Chem.* 84 (21), 8966–8969 (2012).

[48] A.J. Baeumner, B. Leonard, J. McElwee, and R.A. Montagna, "A rapid biosensor for viable *B. anthracis* spores", *Anal. Bioanal. Chem.* 380 (1), 15–23 (2004).

[49] N. Tehri, N. Kumar, H.V. Raghu, and A. Vashishth, "Biomarkers of bacterial spore germination", *Ann. Microbiol.* 68 (9), 513–523 (2018).

[50] R.J. Doyle, F. Nedjat-Haiem, and J.S. Singh, "Hydrophobic characteristics of *Bacillus* spores", *Curr. Microbiol. (Current Microbiology)* 10 (6), 329–332 (1984).

[51] E. Galopin, G. Piret, S. Szunerits, Y. Lequette, C. Faille, and R. Boukherroub, "Selective adhesion of *Bacillus cereus* spores on heterogeneously wetted silicon nanowires", *Langmuir* 26 (5), 3479–3484 (2010).

[52] W.R. Bowen, A.S. Fenton, R.W. Lovitt, and C.J. Wright, "The measurement of *Bacillus mycoides* spore adhesion using atomic force microscopy, simple counting methods, and a spinning disk technique", *Biotechnol. Bioeng.* 79 (2), 170–179 (2002).

[53] U. Rönner, U. Husmark, and A. Henriksson, "Adhesion of *Bacillus* spores in relation to hydrophobicity", *J. Appl. Bacteriol.* 69 (4), 550–556 (1990).

[54] U. Husmark and U. Rönner, "Forces involved in adhesion of *Bacillus cereus* spores to solid surfaces under different environmental conditions", *J. Appl. Bacteriol.* 69 (4), 557–562 (1990).

[55] A. Turchanin, M. El-Desawy, and A. Gölzhäuser, "High thermal stability of cross-linked aromatic self-assembled monolayers: nanopatterning via selective thermal desorption", *Appl. Phys. Lett.* 90 (5), 053102 (1-3) (2007).

[56] C.M. Crudden, J.H. Horton, I.I. Ebralidze, O.V. Zenkina, A.B. McLean, B. Drevniok, Z. She, H.-B. Kraatz, N.J. Mosey, T. Seki, E.C. Keske, J.D. Leake, A. Rousina-Webb, and G. Wu, "Ultra stable self-assembled monolayers of N-heterocyclic carbenes on gold", *Nat. Chem.* 6 (5), 409–414 (2014).

[57] R.G. Acres, A.V. Ellis, J. Alvino, C.E. Lenahan, D.A. Khodakov, G.F. Metha, and G.G. Andersson, "Molecular structure of 3-aminopropyltriethoxysilane layers formed on silanol-terminated silicon surfaces", *J. Phys. Chem. C* 116 (10), 6289–6297 (2012).

[58] J.J. Richardson, M. Björnmalm, and F. Caruso, "Technology-driven layer-by-layer assembly of nanofilms", *Science* 348 (6233), aaa2491 (1-11) (2015).

[59] J.J. Harris and M.L. Bruening, "Electrochemical and in situ ellipsometric investigation of the permeability and stability of layered polyelectrolyte films", *Langmuir* 16 (4), 2006–2013 (2000).

[60] T.J. Park, K.-B. Lee, S.J. Lee, J.P. Park, Z.-W. Lee, S.-K. Choi, H.-C. Jung, J.-G. Pan, S.Y. Lee, and I.S. Choi, "Micropatterns of spores displaying heterologous proteins", *Journal of the American Chemical Society* 126 (34), 10512–10513 (2004).

[61] K.-B. Lee, Y.H. Jung, Z.-W. Lee, S. Kim, and I.S. Choi, "Biospecific anchoring and spatially confined germination of bacterial spores in non-biofouling microwells", *Biomaterials* 28 (36), 5594–5600 (2007).

[62] J. Wan, M.L. Johnson, R. Guntupalli, V.A. Petrenko, and B.A. Chin, "Detection of *Bacillus anthracis* spores in liquid using phage-based magnetoelastic micro-resonators", *Sens. Actuators, B* 127 (2), 559–566 (2007).

[63] B. Dhayal, W.A. Henne, D.D. Doorneweerd, R.G. Reifenberger, and P.S. Low, "Detection of *Bacillus subtilis* spores using peptide-functionalized cantilever arrays", *J. Am. Chem. Soc.* 128 (11), 3716–3721 (2006).

[64] Sang-Hun Lee, D. D. Stubbs, J. Cairney, and W. D. Hunt, Eds., "Real-time detection of bacteria spores using a QCM based immunosensor" SENSORS IEEE, Toronto, Canada, 1194-1198 (2003).

[65] S.K. Ghosh, V.P. Ostanin, C.L. Johnson, C.R. Lowe, and A.A. Seshia, "Probing biomolecular interaction forces using an anharmonic acoustic technique for selective detection of bacterial spores", *Biosens. Bioelectron.* 29 (1), 145–150 (2011).

[66] G. Acharya, D.D. Doorneweerd, C.-L. Chang, W.A. Henne, P.S. Low, and C.A. Savran, "Label-free optical detection of anthrax-causing spores", *J. Am. Chem. Soc.* 129 (4), 732–733 (2007).

[67] L. Fu, S. Li, K. Zhang, I.-H. Chen, J.M. Barbaree, A. Zhang, and Z. Cheng, "Detection of *Bacillus anthracis* spores using phage-immobilized magnetostrictive milli/micro cantilevers", *IEEE Sensors J.* 11 (8), 1684–1691 (2011).

[68] T.T. Nguyen, K.L. Sly, and J.C. Conboy, "Comparison of the energetics of avidin, streptavidin, neutravidin, and anti-biotin antibody binding to biotinylated lipid bilayer examined by second-harmonic generation", *Anal. Chem.* 84 (1), 201–208 (2012).

[69] A. Holmberg, A. Blomstergren, O. Nord, M. Lukacs, J. Lundeberg, and M. Uhlén, "The biotin-streptavidin interaction can be reversibly broken using water at elevated temperatures", *Electrophoresis* 26 (3), 501–510 (2005).

[70] J. Knurr, O. Benedek, J. Heslop, R.B. Vinson, J.A. Boydston, J. McAndrew, J.F. Kearney, and C.L. Turnbough, "Peptide ligands that bind selectively to spores of *Bacillus subtilis* and closely related species", *Applied and environmental microbiology* 69 (11), 6841–6847 (2003).

[71] V.A. Petrenko, "Landscape phage as a molecular recognition interface for detection devices", *Microelectronics Journal* 39 (2), 202–207 (2008).

[72] M. Tolba, O. Minikh, L.Y. Brovko, S. Evoy, and M.W. Griffiths, "Oriented immobilization of bacteriophages for biosensor applications", *Applied and environmental microbiology* 76 (2), 528–535 (2010).

[73] M.S. Zaman, A. Goyal, G.P. Dubey, P.K. Gupta, H. Chandra, T.K. Das, M. Ganguli, and Y. Singh, "Imaging and analysis of *Bacillus anthracis* spore germination", *Microscopy research and technique* 66 (6), 307–311 (2005).

[74] N. Andreeva, D. Bassi, F. Cappa, P.S. Cocconcelli, F. Parmigiani, and G. Ferrini, "Nanomechanical analysis of *Clostridium tyrobutyricum* spores", *Micron (Oxford, England : 1993)* 41 (8), 945–952 (2010).

[75] L. Häggström and N. Molin, "Calcium alginate immobilized cells of *Clostridium acetobutylicum* for solvent production", *Biotechnol Lett* 2 (5), 241–246 (1980).

[76] S. Matys, J. Raff, U. Soltmann, S. Selenska-Pobell, H. Böttcher, and W. Pompe, "Calcium dipicolinate induced germination of *Bacillus* spores embedded in thin silica layers: novel perspectives for the usage of biocers", *Chem. Mater.* 16 (26), 5549–5551 (2004).

[77] P.K. Stoimenov, R.L. Klinger, G.L. Marchin, and K.J. Klabunde, "Metal oxide nanoparticles as bactericidal agents", *Langmuir* 18 (17), 6679–6686 (2002).

[78] J. Han, R.B. Seale, P. Silcock, A.J. McQuillan, and P.J. Bremer, "The physico-chemical characterization of casein-modified surfaces and their influence on the adhesion of spores from a *Geobacillus* species", *Biofouling* 27 (5), 459–466 (2011).

[79] M.A. Kramer, R.L. Gieseck, B. Andrews, and A. Ivanisevic, "Spore-terminated cantilevers for chemical patterning on complex architectures", *J. Am. Chem. Soc.* 133 (25), 9627–9629 (2011).

[80] D. D. Williams and C.L. Turnbough, "Surface layer protein EA1 is not a component of *Bacillus anthracis* spores but is a persistent contaminant in spore preparations", *J. Bacteriol.* 186 (2), 566–569 (2004).

[81] H.-W. Shim, J.-H. Lee, B.-Y. Kim, Y.-A. Son, and C.-S. Lee, "Facile preparation of biopatternable surface for selective immobilization from bacteria to mammalian cells", *J. Nanosci. Nanotechnol.* 9 (2), 1204–1209 (2009).

[82] T.S. Sreeprasad, P. Nguyen, A. Alshogeathri, L. Hibbeler, F. Martinez, N. McNeil, and V. Berry, "Graphene quantum dots interfaced with single bacterial spore for bio-electromechanical devices: a graphene cytobot", *Scientific reports* 5, 9138 EP - (2015).

2 Theoretical aspects

In this chapter, theoretical details with regard to measurement methods of resistance temperature detectors (RTDs) and sensor principles of a H_2O_2 calorimetric sensor and a spore-based biosensor are presented. Additionally, fundamentals of surface functionalization on sensor substrates and methods to physically and electrochemically characterize them are introduced.

2.1 Sensing principles

2.1.1 Resistance temperature detectors (RTDs) and wire configurations

Most of calorimetric gas detecting principles are based on measuring the change of resistance of resistance temperature detectors (RTDs) because of their fairly linear resistance-temperature behavior. As the temperature of the metal increases, the amplitudes of the thermodynamic vibrations of its atomic nuclei increase as well. At the same time, the probability of free collisions increases between its free electrons and bound ions. Therefore, these interruptions of motion of the free electrons causes the resistance of the metal to increase [1].

The resistance of an RTD can be calculated from assuming that an RTD with a resistance R_T is measuring temperature nearby of some reference temperature T_o, which is normally considered to be 0 °C. Another assumption is that temperature is the only factor affecting the resistance of the RTD. As a result, applying Taylor series for T_o, gives a resistance R_T of the sensor temperature T °C as shown in Equation 2.1.

$$R_T = R_{T_0}\left[1 + \frac{1}{R_{T_0}}\left(\frac{\partial R_T}{\partial T}\right)_{T=T_0}\Delta T + \frac{1}{2!R_{T_0}}\left(\frac{\partial^2 R_T}{\partial T^2}\right)_{T=T_0}\Delta T^2 + \cdots + \frac{1}{n!R_{T_0}}\left(\frac{\partial^n R_T}{\partial T^n}\right)_{T=T_0}\Delta T^n + \cdots\right]$$

(Equation 2.1)

Here, R_{To} is its resistance at the reference temperature T_o and $\Delta T \approx T - T_o$.

In addition, further assuming a finite increase of temperature, neglecting fourth order terms and above and introducing the conventional definition for the coefficients A, B, and C of the resistance change, Equation 2.1 can be written as in Equation 2.2:

$$R_T = R_{T_0}[1 + A\Delta T + B\Delta T^2 + C\Delta T^3] \quad \text{(Equation 2.2)}$$

The coefficients *A*, *B* and *C* are supposed to be independent of temperature and are defined as follows:

$$A = \frac{1}{R_{T_0}}\left(\frac{\partial R_T}{\partial T}\right)_{T=T_0} \quad \text{(Equation 2.3)}$$

$$B = \frac{1}{2!R_{T_0}}\left(\frac{\partial^2 R_T}{\partial T^2}\right)_{T=T_0} \quad \text{(Equation 2.4)}$$

$$C = \frac{1}{3!R_{T_0}}\left(\frac{\partial^3 R_T}{\partial T^3}\right)_{T=T_0} \quad \text{(Equation 2.5)}$$

Using a linear temperature dependence for temperatures between 0 and 850 °C [2], assuming that T = 0 °C, this equation can be further simplified into Equation 2.6.

$$R_T = R_0(1 + \alpha T) \quad \text{(Equation 2.6)}$$

Here, it is worth to note that *α* is not the coefficient *A* from Equation 2.3, but the coefficient of resistance change with temperature, which is mostly expressed as an average value in a given temperature range. For instance, from a resistance range R_0 to R_{100} at their respective temperatures 0 °C and 100 °C, α is defined as in Equation 2.7.

$$\alpha = \frac{1}{R_0}\frac{R_{100} - R_0}{100} \quad \text{(Equation 2.7)}$$

Since the resistance is paramount to the proper performance of calorimetric sensors, a precise and accurate measurement of RTDs has to be carried out. This can be performed by so-called wire configurations [1, 3]. The simplest of them is by connecting the RTD to a bridging circuit (Wheatstone bridge) and using a 2-wire configuration (see Figure 2.1). In this case, the Wheatstone bridge is used to measure the unknown RTD resistance (R_T) by balancing the remaining three resistances (R_1, R_2 and R_3). The RTD is implemented to the bridging circuit by two wires (R_{L1} and R_{L2}). The balance condition is described by the Equation 2.8.

$$R_2(R_T + R_{L1} + R_{L2}) = R_1R_3 \quad \text{(Equation 2.8)}$$

This yields the resistance of the RTD (RT) as shown in Equation 2.9

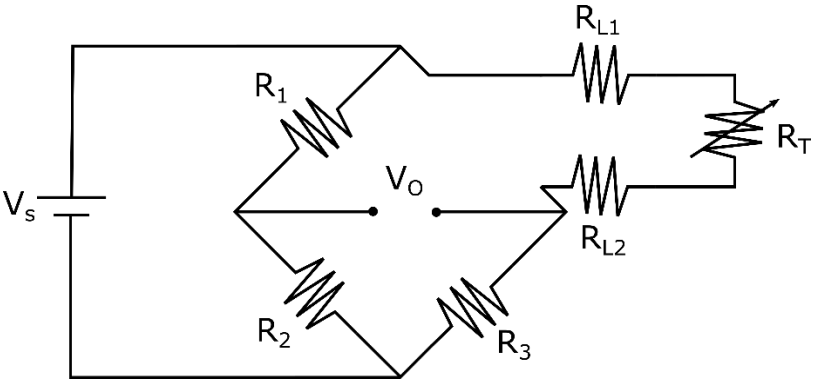

Figure 2.1. Wheatstone bridge connected to an RTD by a 2-wire configuration circuit.

$$R_T = \frac{R_1 R_3}{R_2} - (R_{L1} + R_{L2}) \qquad \text{(Equation 2.9)}$$

It can be seen from Equation 2.9 that the 2-wire configuration takes into account the resistance of the connecting wires and in some cases it can be inconvenient. For instance, during a calorimetric sensor measurement, if the change of resistance is smaller than the connecting wire resistance, the 2-wire configuration is not precise enough for the experiment. For this reason, the 3-wire configuration with R_{L1}, R_{L2} and R_{L3} can be used to get a more precise resistance measurement as shown in Figure 2.2.

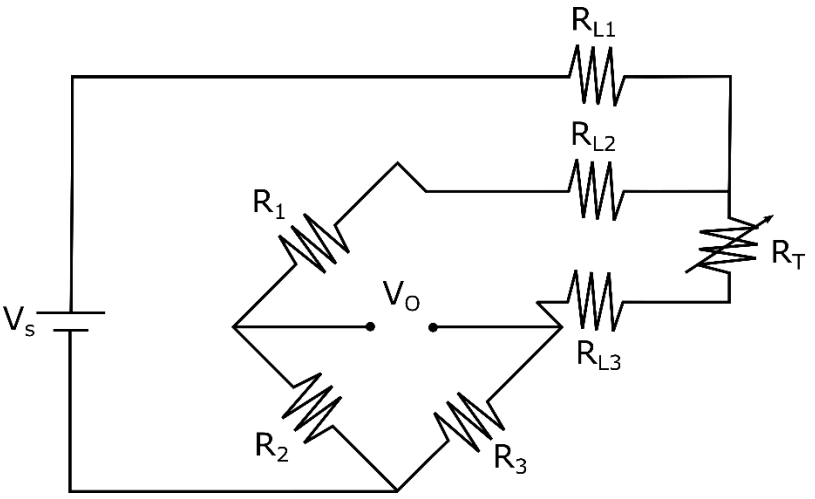

Figure 2.2. Wheatstone bridge connected to an RTD by a 3-wire configuration circuit.

The balancing condition for the 3-wire configuration is given as Equation 2.10.

$$R_2(R_T + R_{L2}) = R_3(R_1 + R_{L3}) \qquad \text{(Equation 2.10)}$$

Usually, with $R_{L2} = R_{L3} = R_L$, the RTD resistance is therefore:

$$R_T = \frac{R_1 R_3}{R_2} + R_L \qquad \text{(Equation 2.11)}$$

In symmetrical 3-wire bridges $R_2 = R_3$, thus Equation 2.11 becomes:

$$R_T = R_1 \qquad \text{(Equation 2.12)}$$

In this case, the measurement of the RTD is not influenced by the resistances of the connecting leads. However, connecting wires are manufactured with a certain tolerance, so not all have the same nominal resistance or temperature coefficient. The 3-wire method reduces the error coming from the wires in comparison to the 2-wire method, but it does not eliminate it completely. As a result, the 4-wire method is often preferred [4], since it offers the most precision from all the mentioned methods (see Figure 2.3).

Here, a constant current I_s passes through the RTD and its voltage V_o is separately measured; this eliminates the connecting wire resistances $R_{L1\text{-}4}$ and the RTD resistance R_T can be simply obtained from Equation 2.13.

$$R_T = \frac{V_0}{I_s} \qquad \text{(Equation 2.13)}$$

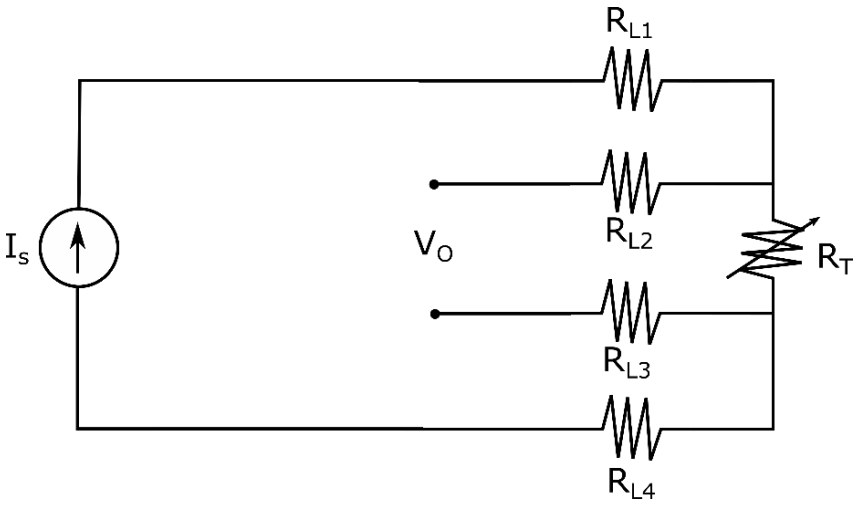

Figure 2.3. 4-wire configuration circuit for an RTD.

2.1.2 Calorimetric H_2O_2 sensing principle

Calorimetric sensors rely on determining the presence or concentration of a chemical by measurement of an enthalpy change produced by the chemical to be detected. Any chemical reaction or physisorption process releases or absorbs a certain quantity of heat from its

surroundings [5]. Depending on the transducing principle, they can be catalogued in: adsorptive-, catalytic- or thermal-conductive gas sensors [6]. Nevertheless, all of them produce a change of temperature in correlation to the gas to be detected.

In adsorptive gas sensors, the gas molecules get adsorbed onto a chemically sensitive layer (e.g., polymer) and therefore an increase of heat occurs. This, at the same time, causes a temperature change of a thermally insulated structure, which is sensed by a temperature sensor. As a result, a thermovoltage (Seebeck effect) change is obtained [7]. Moreover, in thermal-conductive gas sensors [8], two passivated resistance temperature detectors (RTDs) are heated. The gas under investigation is passed through one RTD, whereas the other is exposed to a reference gas (same gas components and flow, but lacking the investigated gas). This creates a difference of thermal conductivity between different gases and then, this is reflected in terms of a change of resistance on the active RTD (the one with the gas under investigation). In addition, in catalytic gas sensors, a differential setup is often used in a similar way than in thermal-conductive sensors. The main difference is that the active RTD is coated with a catalyst layer sensitive to the analyte. As both the catalyst-activated RTD and the passivated RTD are exposed to the analyte, an increase of temperature occurs only at the surface of the active RTD creating a temperature difference between them. This temperature difference can be then correlated to the increase of the analyte concentration.

This kind of catalytic calorimetric gas sensor has been extensively utilized to monitor gaseous hydrogen peroxide concentrations [9–16]; its principle is illustrated in Figure 2.1. The H_2O_2 sensor is composed of a differential setup measurement, where one RTD structure acts as a reference (passive) and the other one as a sensing element (active) for gaseous hydrogen peroxide. As the sensor is exposed to H_2O_2, a surface reaction results only at the catalytically activated (with MnO_2) part of the sensor, where hydrogen peroxide is decomposed into O_2 and H_2O. Several decomposition mechanisms of H_2O_2 by MnO_x have been suggested in literature [15, 17–19]. Among them, two different pathways may mainly occur: with or without electron exchange reaction between MnO_x and H_2O_2. For the former, the reaction takes place either by donating an electron from the surface to the H_2O_2 or the other way around [20–22] as shown in Equations 2.14 and 2.15.

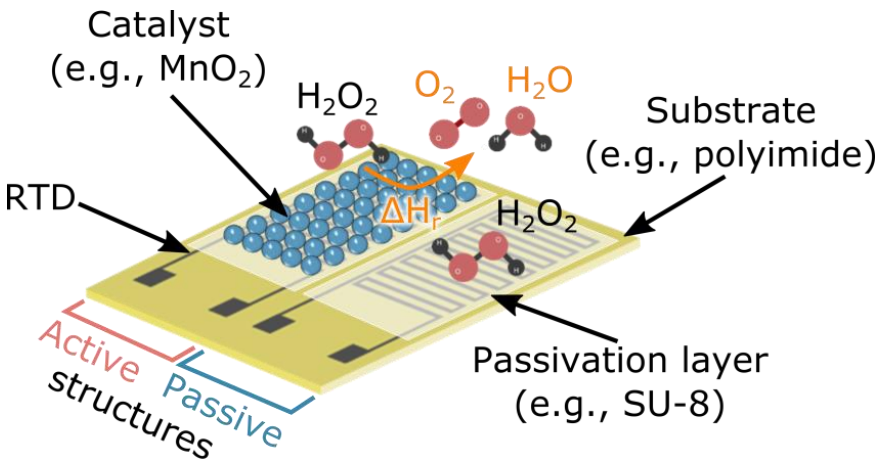

Figure 2.4. Schematic representation of a catalytic H_2O_2 gas sensor.

$$H_2O_2 + e^- \rightarrow OH^- + OH^{\cdot} \quad \text{(Equation 2.14)}$$

$$H_2O_2 \rightarrow H^+ + HO_2^{\cdot} + e^- \quad \text{(Equation 2.15)}$$

In the latter, the reaction takes place by fission of the O-O bond in H_2O_2, followed by the formation of hydroxyl radicals ($OH^{\cdot}$) as depicted in Equation 2.16; this is mainly presented on metal oxides at elevated temperatures [20, 23, 24].

$$H_2O_2 \rightarrow 2OH^{\cdot} \quad \text{(Equation 2.16)}$$

In addition, upon formation of $OH^{\cdot}$, further reactions arise as shown in Equations 2.17, 2.18 and 2.19.

$$OH^{\cdot} + H_2O_2 \rightarrow HO_2^{\cdot} + H_2O \quad \text{(Equation 2.17)}$$

$$HO_2^{\cdot} + H_2O_2 \rightarrow H_2O + O_2 + OH^{\cdot} \quad \text{(Equation 2.18)}$$

$$HO_2^{\cdot} + OH^{\cdot} \rightarrow H_2O + O_2 \quad \text{(Equation 2.19)}$$

The exothermic decomposition can be expressed as Equation 2.20.

$$2H_2O_2 \rightarrow 2H_2O + O_2 + \Delta H_r \quad \text{(Equation 2.20)}$$

Here, ΔH_r is the change of enthalpy of released heat reaction; in case of H_2O_2 evaporated at 240 °C, the enthalpy is ΔH_r = - 105.3 kJ mol^{-1}. The release of heat causes a temperature increase on the active part of the calorimetric sensor, which then can be correlated to the increase of hydrogen peroxide concentration [9, 12, 16].

2.1.3 Impedimetric sensing principle

Impedance spectroscopy is a technique to study the electrical properties of materials and their interfaces by means of electronically conducting electrodes. It can be applied to characterize dynamics of bound or mobile charges in the bulk or interfacial areas of all sorts of solid or liquid material, like ionic, semiconducting, mixed electronic-ionic or insulators [25]. The spore-based biosensor introduced in chapter 1 measures the electrical impedance of an interface (interdigitated electrodes) in alternate current (AC) steady state with constant direct current (DC) bias conditions. The impedance *Z* of such system is expressed as the voltage-time function *V(t)* divided by the resulting current-time function *I(t)*, as shown in Equation 2.21.

$$Z = \frac{V(t)}{I(t)} = \frac{V_0 \sin(2\pi f t)}{I_0 \sin(2\pi f t + \varphi)} \qquad \text{(Equation 2.21)}$$

Here, V_o and I_o are the maximum voltage and current, *f* is the frequency, *t* is the time, φ is the phase shift.

The impedance can be described in two different manners: as a Bode- or a Nyquist plot (see Figure 2.5). The former (Figure 2.5 a) shows the modulus |*Z*| and the phase shift φ as a function of the frequency *f*, whereas the latter (Figure 2.5 b) depicts the real Z_R and imaginary Z_I parts of the impedance *Z*.

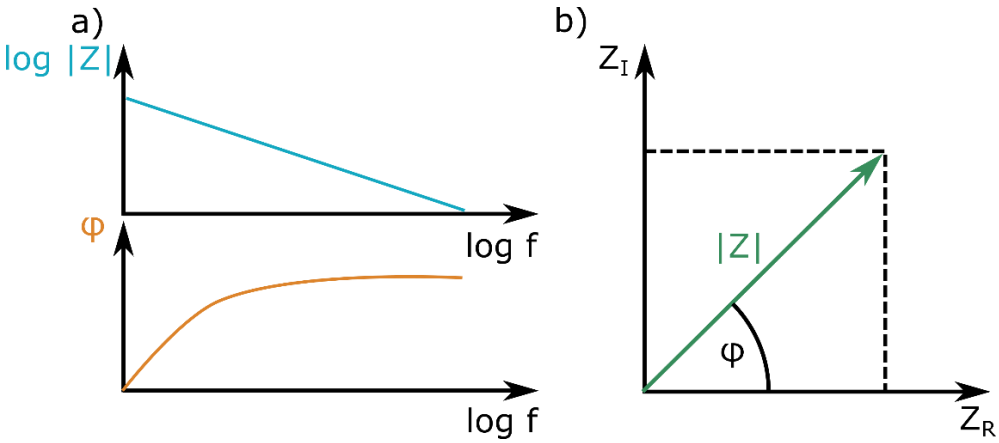

Figure 2.5. Bode (a)) and Nyquist (b)) plots of the impedance. In the Bode plot, the impedance is expressed as the modulus |*Z*| and the phase shift φ, whereas in the Nyquist plot by its real Z_R and imaginary Z_I parts (adapted from [25] with permission from John Wiley & Sons, Inc.).

The impedance can be expressed as a complex function using Euler's relationship. The potential *V(t)* and the current *I(t)* are described as follows, where $\omega = 2\pi f$:

$$V(t) = V_A e^{j\omega t} \quad \text{(Equation 2.22)}$$

$$I(t) = I_A e^{j\omega t - j\varphi} \quad \text{(Equation 2.23)}$$

$$Z = \frac{V_A e^{j\omega t}}{I_A e^{j\omega t - j\varphi}} = Z_A(\cos\varphi + j\sin\varphi) = Z_R + jZ_I \quad \text{(Equation 2.24)}$$

Equivalent circuits are commonly used to illustrate experimental impedance information, where ideal impedance elements are modeled in series and/or parallel. For instance, if a complex voltage *V(t)* (Equation 2.22) is applied to a pure resistor *R* or capacitor *C*, the impedance of a resistor Z_R or capacitor Z_C can be expressed as:

$$Z_R = \frac{V}{I_R} = \frac{V_A e^{j\omega t}}{\frac{V_A e^{j\omega t}}{R}} = R \quad \text{(Equation 2.25)}$$

$$Z_C = \frac{V}{I_C} = \frac{V_A e^{j\omega t}}{j\omega C V_A e^{j\omega t}} = \frac{1}{j\omega C} \quad \text{(Equation 2.26)}$$

An ideal resistor has no frequency dependence because its phase shift (φ) is 0°. On the contrary, an ideal capacitor has frequency dependence and its phase shift (φ) is -90°. However, most real systems possess a mixture of non-ideal impedance elements. Thus, different impedance- and phase values can be obtained at different frequencies. This can be exploited to record the impedance and phase to study interface phenomena at sensor surfaces.

Moreover, interdigitated electrodes (IDEs) can be used for impedimetric measurements to characterize surface phenomena. This electrode configuration has several benefits such as miniaturization, low cost, increase of the sensing area and sensitivity of the sensor [26]. IDEs have been used in combination with microorganisms to detect, for example, bacteriophage contamination in milk processing or bacteria [27, 28]. A schematic representation of such IDEs is shown in Figure 2.6. They consist of finger-like structures made out typically of Pt or Au, with a certain thickness *t*, width *w* and interspace between fingers *s* on an insulating substrate (e.g., glass, SiO_2). As it can be seen from the figure, the electric field (dotted blue lines) can be measured between the fingers, where the impedance between the substrate

material and the environment determines the initial impedance of the IDEs; this principle (see Figure 2.7 a) is applied to the spore-based biosensors introduced in chapter 1.

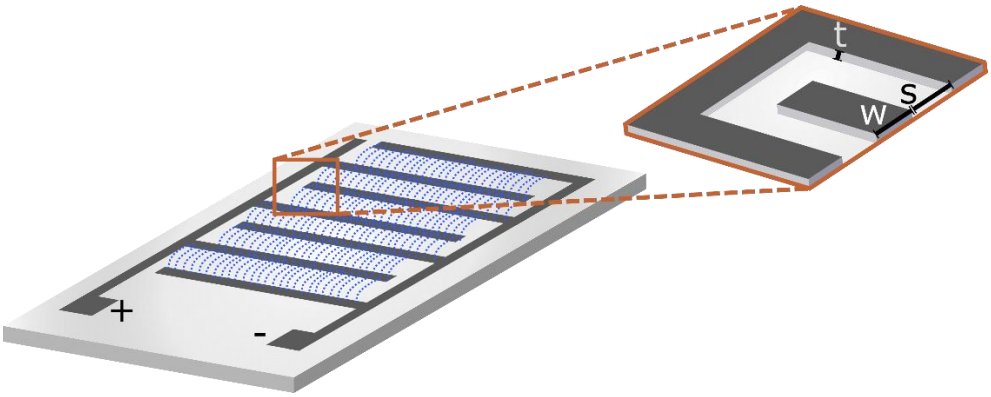

Figure 2.6. Schematic representation of interdigitated electrodes: the blue dotted lines represent the electric field between finger structures; *t* corresponds to the thickness of the electrodes, *w* to their width and *s* to the interspace between them.

In addition, non-conducting samples (e.g., spores) may change the overall capacitive behavior of the IDEs C_{IDE} (Figure 2.7 b) and this can be expressed [29] as:

$$C_{IDE} = L(N-1)\left(\frac{\varepsilon_0 \varepsilon_{r,t}}{2}\frac{\mathrm{K}\left((1-k^2)^{\frac{1}{2}}\right)}{\mathrm{K}(k)}\right) + 2\varepsilon_0 \varepsilon_{r,m}\frac{t}{s} \qquad \text{(Equation2.27)}$$

$$k = \cos\frac{\pi}{2}\frac{w}{s+w} \qquad \text{(Equation 2.28)}$$

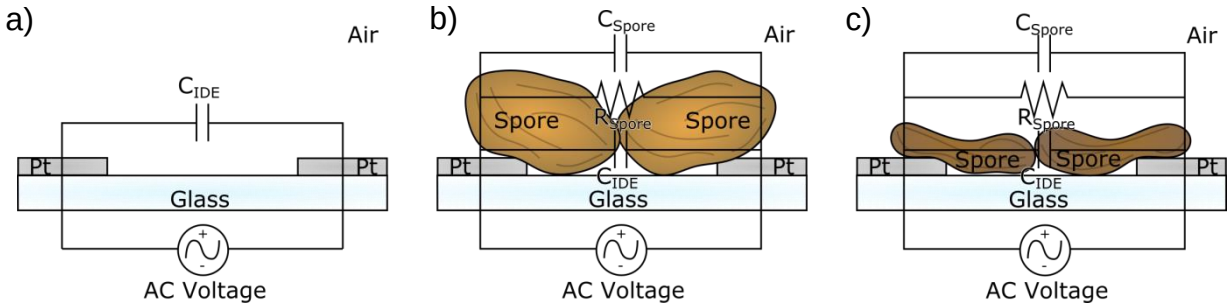

Figure 2.7 Equivalent circuit model for a spore-based biosensor; a) reference sensor (no spores are present), b) IDEs with spores and c) sterilized spores onto IDEs.

L represents the length of the electrode fingers and *N* the number of unit cells; ε_o is the vacuum permittivity and $\varepsilon_{r,t}$ is the total relative permittivity around the electrodes (reference sensor (Figure 2.7 a): air and glass, spore-based biosensor (Figure 2.7 b and c): glass and porous spore layer); *K(k)* describes the complete elliptic integral of the first kind to take into

consideration the fringing field surrounding the electrodes; the dimensions of the electrodes are expressed with the modulus *k* (Equation 2.28), where *w* and *s* are the width and interspace of the electrodes, respectively. The second term from Equation 2.27 represents the capacitance contribution due to the transverse field in the narrow region between the electrodes, where $\varepsilon_{r,m}$ describes the relative permittivity between the electrodes to describe the capacitance formed due to the transverse field (reference sensor (Figure 2.7 a): air, spore-based biosensor (Figure 2.7 b and c): porous spore layer) and *t* is the thickness of the electrodes.

In addition, capacitive (C_{spore}) and resistive (R_{spore}) behaviors may also be present from the porous spore layer as it has been shown in literature for bacterial cells [30]. After spore immobilization, the capacitance at the sensor surface increases (impedance decreases) probably due the porous spore layer that may facilitate electron transfer between IDEs. Furthermore, during sterilization, their morphology changes, provoking a further increase of capacitance (decrease of impedance) [31].

2.2 Surface functionalization

Functionalization (modification) of the sensor substrate to promote the coupling of spores onto them is frequently needed; to fulfill this task, SAMs are popularly implemented. SAMs consist of molecular assemblies that are formed by the adsorption of an active surfactant on a solid surface [32]. Several types of SAMs are available according to the substrate. These include organosilanes on hydroxylated surfaces (Si/SiO_2, Al/Al_2O_3, glass, etc.), alkanethiols on gold, alcohols and amines on platinum, and carboxylic acids on aluminum oxide and silver [33]. Organosilanes are taken as an example to demonstrate the principle of the SAMs formation.

2.2.1 Organosilanes

A silane is a silicon-based molecule containing four constituents (e.g., SiH_4); silanes that contain at least one carbon group are called organosilanes, which can have hydrogen-, oxygen- or halogen atoms directly attached to the silicon [34]. Figure 2.8 shows a general structure of an organosilane. It fundamentally consists of the silicon atom between two parts; the first part (hydrolyzable groups) covalently binds to inorganic substrates (e.g., glass)

and the second part (reactive group at the end of alkyl chain) facilitates the linkage to organic molecules.

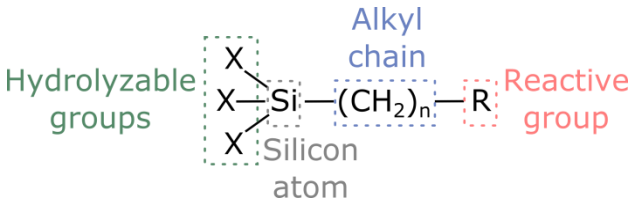

Figure 2.8 General structure of an organosilane. Adapted from [34] with permission from Elsevier.

The silanization process (formation course of organosilanes onto hydroxylated surfaces) is shown in Figure 2.9. In the first step of the silanization process, the alkoxy substituents (hydrolyzable groups) of the organosilane undergo hydrolysis to produce highly reactive silanols (Si-OH), which are required for the coupling to the hydroxylated substrate (Figure 2.9 a). These silanols may form hydrogen bonding laterally (between them (Figure 2.9 b) or vertically (between the hydroxyl groups of the substrate (Figure 2.9 d). A condensation step of the oligomers follows between them (Figure 2.9 c) proceeding as siloxanes (Si-O-Si) and another condensation takes place between the oligomers and the substrate; as a result, the organosilanes are covalently grafted onto the substrate. Although the silanization process is shown subsequently, these reactions can happen simultaneously after the first hydrolysis step [35].

The silanization process can be performed in two manners: in liquid or gas phase. During the gas-phase silanization, the substrates are placed in a closed chamber and the silane molecules are vaporized by heat or vacuum [34]; the substrates remain inside for a certain time and at the end, a uniform layer of silanes covalently attached to the substrate can be obtained. Furthermore, the liquid-phase silanization can be divided in two methods, namely dip-coating and drop-casting [34, 36]. In the dip-coating method, a substrate is immersed in a silane solution for a specific interval of time, whereas in the drop-casting method, the silane solution is drop-casted onto the substrates and incubated in the same fashion. Later on, the weakly bound silane molecules are removed and finally, a covalent bond can be attained by curing due to the loss of water (siloxane bonds replace the hydrogen ones between the silanes and the substrate).

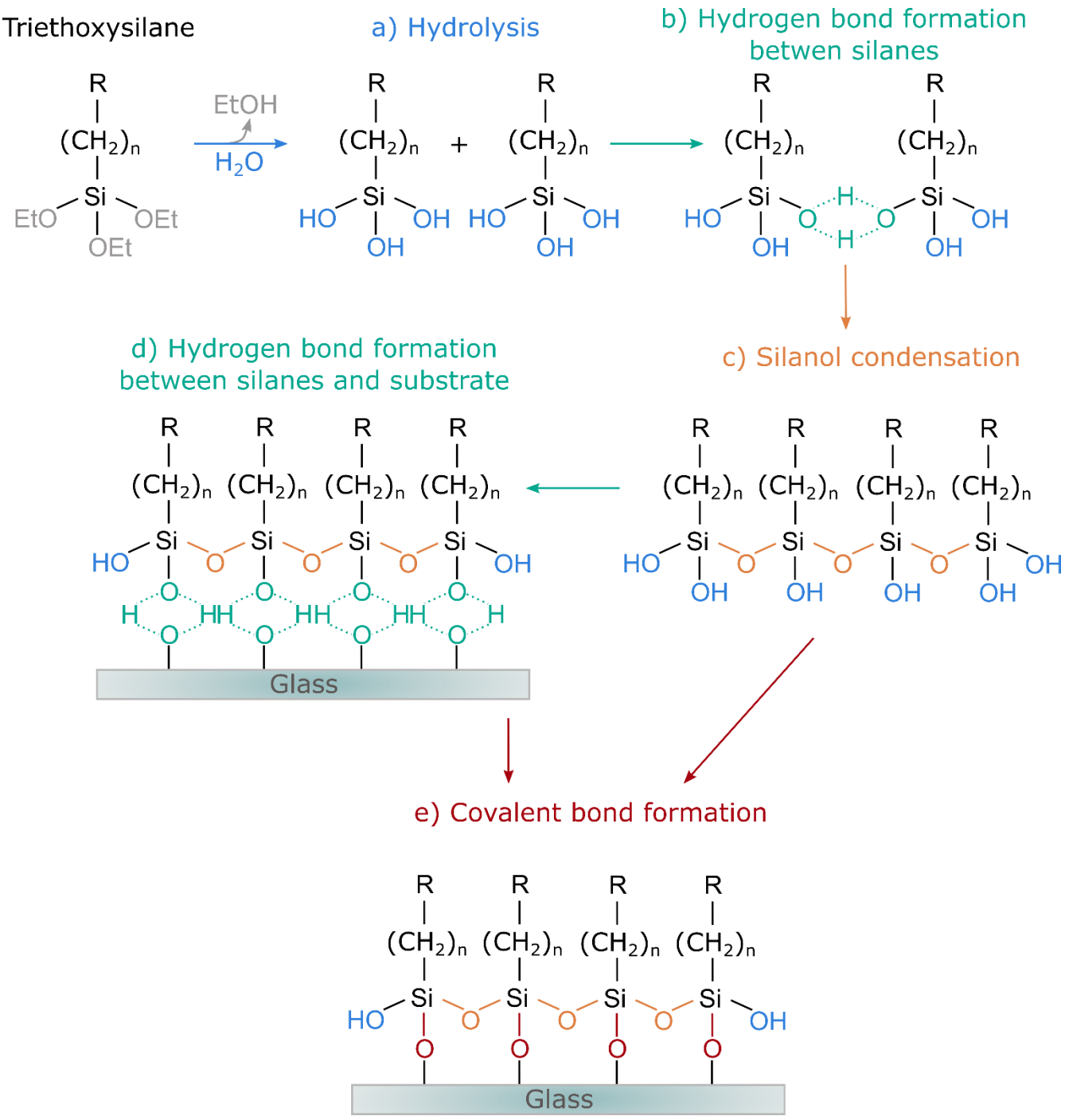

Figure 2.9 Silanization process: a) Highly reactive silanols are formed in the first step by hydrolysis of the alkoxysilane groups; for steps b) and d), the silanols undergo hydrogen bonding with other neighboring silanols and at the surface of the substrate; for steps c) and e), condensation of the organosilanes occurs between them and on the surface. Adapted from [34] with permission from Elsevier.

2.3 Characterization methods for surface functionalization and spore immobilization

2.3.1 Electrolyte-insulator-semiconductor (EIS) sensors

Capacitive electrolyte-insulator-semiconductor (EIS) sensors are field-effect (bio-)chemical devices that can be used for label-free monitoring of the adsorption and interaction of biomolecules [37]; for example, interface phenomena at the sensor surface can be investigated with this method. They are analogous to metal-insulator-semiconductor (MIS) structures. In the case, the metallic gate of the MIS structure is replaced by a sensor layer in contact with the analyte under a bias voltage resulting in an EIS sensor [38] as shown in Figure 2.10 (left).

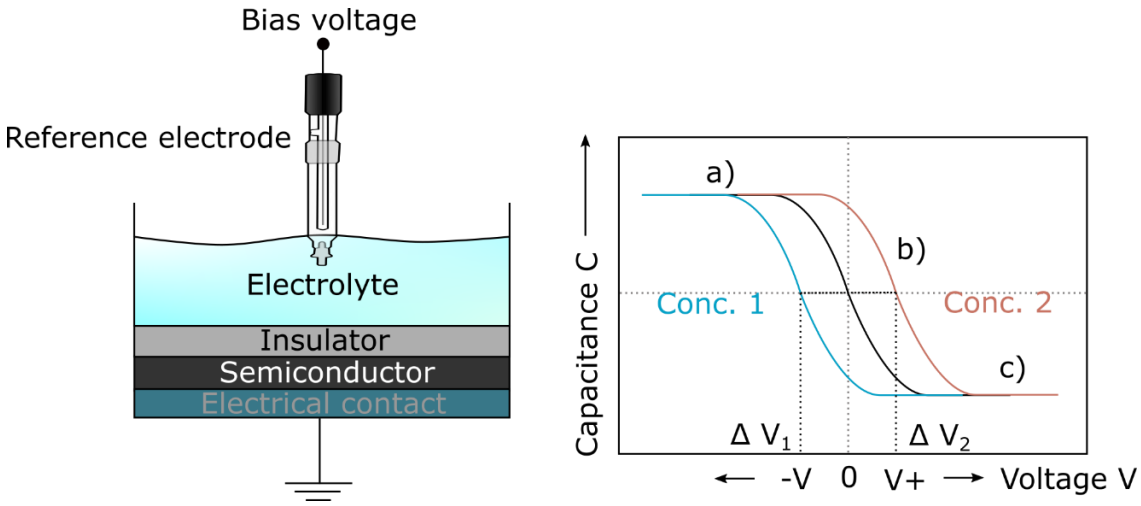

Figure 2.10 Schematic representation of an EIS structure (left) and its characteristic C-V (capacitance-voltage) curve (right); different concentrations provoke voltage shifts ΔV_1 and ΔV_2. In addition, three distinctive regions, for instance, in p-type semiconductors are depicted: a) accumulation, b) depletion and c) inversion of the C-V curve. Adapted from [38] with permission from CRC Press.

A bias voltage is usually applied to the semiconductor (e.g., silicon) between its electrical contact and a reference electrode. As a result, the charge carrier distribution at the insulator/semiconductor interface can be controlled by both an external dc voltage (V_B) and an electrochemical interaction between the electrolyte and the sensor surface (ΔV). The electrical behavior of the EIS structure is given by its small-signal capacitance. Depending on the applied V_B and a super-imposed ac voltage (e.g., 120 Hz, 20 mV), a characteristic C-V

(capacitance-voltage) curve can be obtained (Figure 2.10, right). For a p-type semiconductor, a negative bias voltage V_B ($V_B < 0$) on the reference electrode accumulates mobile charge carriers (i.e., positive holes) at the insulator/semiconductor interface (accumulation, Figure 2.10, right a). As V_B becomes positive ($V_B > 0$), the holes are displaced from the interface, generating a space-charge region (depletion, Figure 2.10, right b) at the semiconductor surface. In addition, when the potential becomes more positive ($V_B >> 0$), an inversion layer of accumulated electrons at the interface is created (inversion, Figure 2.10, right c). The integral capacitance *C*, corresponding to V_B is given in Equation 2.29.

$$\frac{1}{C} = \frac{1}{C_I} + \frac{1}{C_S} \qquad \text{(Equation 2.29)}$$

Here, C_I and C_S are the capacitance values of the sensor insulator and the space-charge region, respectively, with Equation 2.30.

$$C = \frac{\varepsilon_0 \varepsilon_r}{d} A \qquad \text{(Equation 2.30)}$$

Where, *A* is the area, *d* the thickness, ε_r the dielectric permittivity, and ε_0 the dielectric constant. Depending on the change of ion concentration in the analyte, a horizontal shift of the C-V curve is produced due to the electrochemical interaction (ΔV) [38].

Moreover, hydroxylation on sensor substrates is a typical procedure for further surface functionalization; this was exemplarily applied on EIS structures to study the effect of O_2 plasma on sensor substrates. While the hydroxylation was successful, the C-V curve of the EIS chip dramatically changed after being treated with oxygen plasma. Since this effect is unstable (dynamic), no further functionalization steps (e.g., APTES) can be accurately performed. Therefore, it is desirable to maintain a stable signal as well as a functionalized surface (hydroxylated); this effect is investigated in chapter 3.

2.3.2 Contact angle measurement

Contact angle measurements are broadly employed to analyze the surface chemistry of grafted surfaces such as self-assembly monolayers [39]. It is one of the common ways to measure the wettability of a material; the wetting is obtained by measuring the contact angle that the liquid forms in contact with solids or other liquids. The solid-liquid contact angle can

be described from the equilibrium of surface forces in the three-phase intersecting point as in Equation 2.31 [40] and shown in Figure 2.11.

$$\cos\theta = \frac{(\gamma_{SV}-\gamma_{SL})}{\gamma_{LV}} \qquad \text{(Equation 2.31)}$$

Here, Θ is the contact angle, γ_{LV} is the surface tension of the liquid in equilibrium with vapor, γ_{SV} is the surface tension of the solid surface in equilibrium with vapor and γ_{SL} represents the solid-liquid interfacial tension.

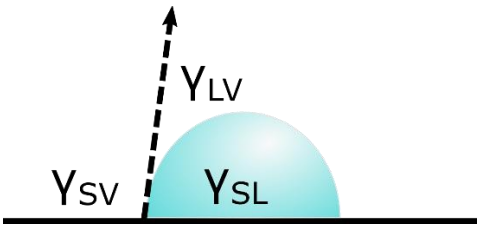

Figure 2.11. Schematic representation of the contact angle equilibrium. Adapted from [40] with permission from Elsevier.

Furthermore, if the contact angle between a liquid and a solid is less than 90°, the liquid is said to be hydrophilic: it will wet the surface spreading over it. However, if the contact angle is more than 90°, the liquid will stay on the surface as a sphere and it is considered as hydrophobic [41].

2.3.3 Atomic force microscopy (AFM)

In an atomic force microscope (AFM), a flexible cantilever, which is composed of a sharp tip at the end, is utilized to track sample topographies. This is performed by detecting the forces between the probe and samples with piconewton sensitivity [42]. AFM can not only be used to image surface topographies, but also for several applications. For instance, it can be used for nanoindentation, cell adhesion or biomolecular interactions [43]. Figure 2.12 shows a schematic representation of the AFM. Here, a laser beam coming from a laser diode (LD) is calibrated at the center of the position-sensitive photo diode (PSPD), which consists of four different photo diodes (A-D). As the tip approaches the sample, it experiences an attractive or repulsive force; as a result, the cantilever is bent toward or away from the sample surface. In case of bending, the beam path is shifted and this is captured in the PSPD. The bending angle is further controlled by means of a proportional-integral (PI) controller integrated to a Z-piezo actuator.

Different modes are available to scan surfaces with AFM such as contact-, non-contact- and intermittent (tapping) mode. In contact mode, the cantilever deflection is kept constant during the scan, i.e., the tip maintains direct contact with the sample. In addition, in non-contact mode and tapping mode, the cantilever vibrates at a certain frequency and this is measured instead of the deflection of the tip (considered in contact mode). In non-contact mode, the cantilever oscillates close to the sample surface without being in contact with it. This mode, however, is rarely used because of the possibility of the tip being attracted to the sample and therefore making contact with it. For this reason, tapping mode is a popular choice, since the cantilever oscillates and the tip makes repulsive contact with the sample surface at the lowest point of oscillation.

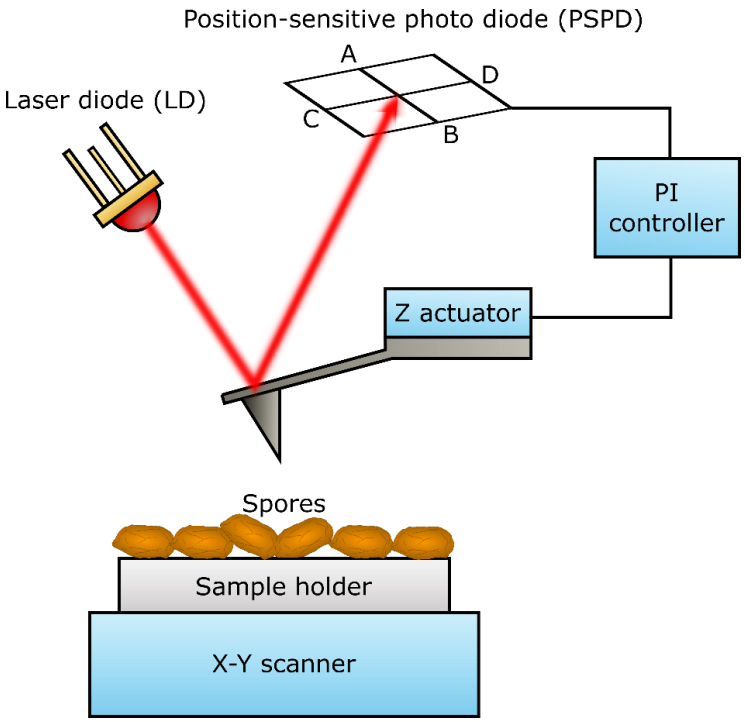

Figure 2.12. Schematic representation of the AFM. Adapted from [44] with permission from IOP Publishing.

2.3.4 Scanning electron microscopy (SEM)

A scanning electron microscope is commonly used for the observation of specimen surfaces with a much higher resolution (0.5 nm) than that of a light microscope (~200 nm) [45]. Many applications of SEM have been reported in literature, for instance, to measure thickness of films and thin coatings, surface morphology, height and lateral dimensions of nanometer-

sized materials or chemical composition and elemental analysis of nano- and micro-materials [46].

Moreover, the resolution *d* in a perfect optical system can be described by Abbe's equation:

$$d = \frac{0.612\lambda}{n \sin \alpha} \qquad \text{(Equation 2.32)}$$

Here, λ is the wavelength of imaging radiation, *n* the index of refraction of medium between point source and lens (relative to free space), and α is half the angle of the cone of light from specimen plane accepted by the objective (half aperture angle in radians); the expression $n \sin \alpha$ is often called numerical aperture (NA).

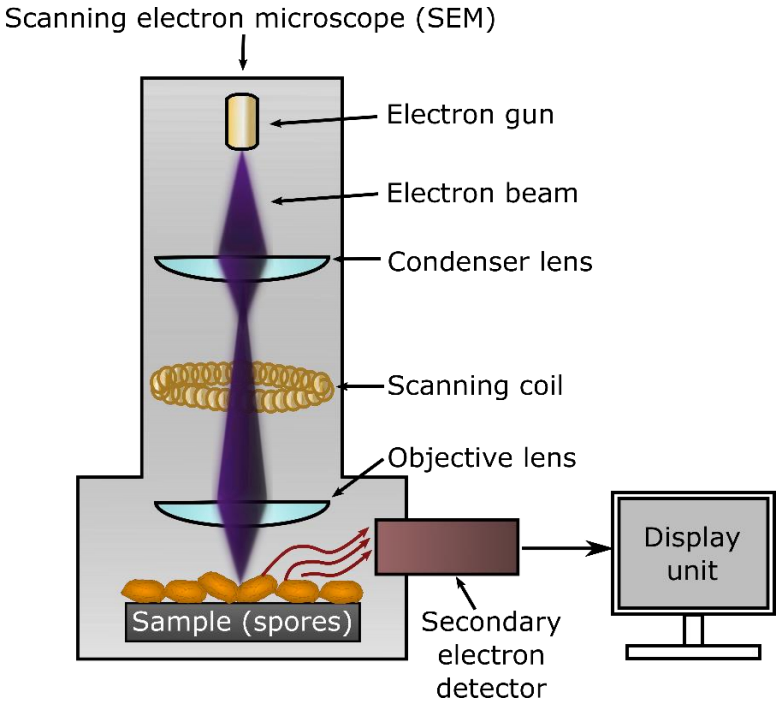

Figure 2.13. Schematic representation of a SEM. Adapted from [47].

A schematic representation of the SEM is shown in Figure 2.13. An electron beam is produced from an electron optical system consisting of an electron gun, a condenser lens and an objective lens (both of them are electromagnetic lenses). Additionally, a scanning coil is applied to scan the electron beam and other components; all these elements are kept at vacuum. When the sample is irradiated with the fine electron beam, emission of secondary electrons appears and this is recognized by a secondary electron detector. Finally, as the electron beam scans (two-dimensional scan) the sample, its topography can be observed and an image can be acquired from the detected secondary electrons.

2.3.5 Microbiological methods

Spores have been successfully recovered from different substrates utilizing a recovery solution consisting of a surfactant mixed in a buffer solution [48–50]. This can be exploited to measure the spore immobilization efficiency on substrates as shown in Figure 2.14.

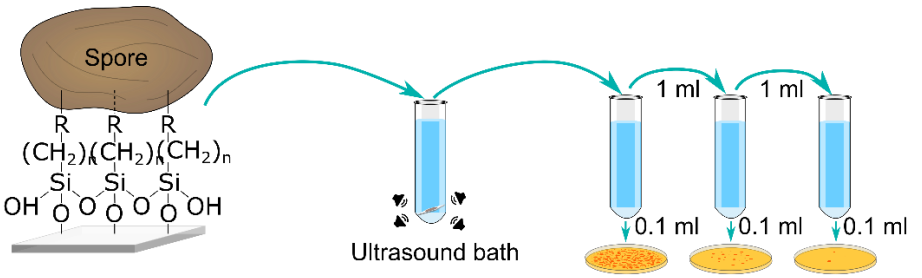

a) Spore immobilization b) Spore recovery c) Plate count method

Figure 2.14. Example of the spore immobilization a) with organosilanes and its recovery b), c). Adapted from [51].

The spore recovery is often performed by immersing the immobilized spores on substrates (Figure 2.14 a) in a solution consisting of a surfactant (e.g., Tween®80) and a buffer solution (e.g., Ringer solution). Then, it is submerged in an ultrasonic bath for a certain amount of time to loosen the spores from the surface. At the end, the non-immobilized spores remain in the solution and they can be serial-diluted and plate-counted (Figure 2.14 c).

The efficiency of the spore immobilization can be determined by visualizing the number of spores attached to the functionalized substrate (N_s) in comparison to the control substrate (N_c) as shown in Equation 2.33 or by the ratio r between the recovered spores (N_s) and the total number of spores from the main suspension (N_t) illustrated in Equation 2.34.

$$Efficiency = \left(1 - \frac{N_s}{N_c}\right) \times 100 \qquad \text{(Equation 2.33)}$$

$$r = \left(\frac{N_s}{N_t}\right) \times 100 \qquad \text{(Equation 2.34)}$$

References

[1] L. Michalski, Ed., "Temperature measurement", J. Wiley, Chichester, New York (2001).

[2] P.R.N. Childs, J.R. Greenwood, and C.A. Long, "Review of temperature measurement", *Rev. Sci. Instrum.* 71 (8), 2959–2978 (2000).

[3] D. Ibrahim, "Chapter 4 - RTD Temperature Sensors", in *Microcontroller-based Temperature Monitoring and Control*, Newnes, Oxford 2002.

[4] A. Tong, "Improving the accuracy of temperature measurements", *Sensor Rev.* 21 (3), 193–198 (2001).

[5] C. Hagleitner, A. Hierlemann, and H. Baltes, "CMOS single-chip gas detection systems: part II", *Sensors Update* 12 (1), 51–120 (2003).

[6] I. Bársony, C. Dücső, and P. Fürjes, "Thermometric gas sensing", in *Solid State Gas Sensing*, Springer Science and Business Media, Boston, MA 2009.

[7] N. Kerness, A. Koll, A. Schaufelbuhl, C. Hagleitner, A. Hierlemann, O. Brand, and H. Baltes, "N-well based CMOS calorimetric chemical sensors", *IEEE The Thirteenth Annual International Conference on Micro Electro Mechanical Systems*, 96–101 (2000).

[8] P.T. Walsh and T.A. Jones. *Chemical and Biochemical Sensors,* "Calorimetric chemical sensors", in *Sensors: A Comprehensive Survey*, VCH Verlagsgesellschaft mbH, Weinheim, Germany 1991.

[9] N. Näther, L.M. Juárez, R. Emmerich, J. Berger, P. Friedrich, and M.J. Schöning, "Detection of hydrogen peroxide (H_2O_2) at exposed temperatures for industrial processes", *Sensors (MDPI)* 6 (4), 308–317 (2006).

[10] N. Näther, H. Henkel, A. Schneider, and M.J. Schöning, "Investigation of different catalytically active and passive materials for realizing a hydrogen peroxide gas sensor", *Phys. Status Solidi A* 206 (3), 449–454 (2009).

[11] P. Kirchner, B. Li, H. Spelthahn, H. Henkel, A. Schneider, P. Friedrich, J. Kolstad, M. Keusgen, and M.J. Schöning, "Thin-film calorimetric H_2O_2 gas sensor for the validation of germicidal effectivity in aseptic filling processes", *Procedia Chem.* 1 (1), 983–986 (2009).

[12] P. Kirchner, B. Li, H. Spelthahn, H. Henkel, A. Schneider, P. Friedrich, J. Kolstad, M. Keusgen, and M.J. Schöning, "Thin-film calorimetric H_2O_2 gas sensor for the validation of germicidal effectivity in aseptic filling processes", *Sensor Actuat. B-Chem.* 154 (2), 257–263 (2011).

[13] P. Kirchner, J. Oberländer, H.-P. Suso, G. Rysstad, M. Keusgen, and M.J. Schöning, "Monitoring the microbicidal effectiveness of gaseous hydrogen peroxide in sterilization processes by means of a calorimetric gas sensor", *Food Control* 31 (2), 530–538 (2013).

[14] P. Kirchner, J. Oberländer, H.-P. Suso, G. Rysstad, M. Keusgen, and M.J. Schöning, "Towards a wireless sensor system for real-time H_2O_2 monitoring in aseptic food processes", *Phys. Status Solidi A* 210 (5), 877–883 (2013).

[15] J. Oberländer, P. Kirchner, H.-G. Boyen, and M.J. Schöning, "Detection of hydrogen peroxide vapor by use of manganese (IV) oxide as catalyst for calorimetric gas sensors", *Phys. Status Solidi A* 211 (6), 1372–1376 (2014).

[16] F. Vahidpour, J. Oberländer, and M.J. Schöning, "Flexible calorimetric gas sensors for detection of a broad concentration range of gaseous hydrogen peroxide: a step forward to online monitoring of food-package sterilization processes", *Phys. Status Solidi A* 215 (15), 1800044 (1–7) (2018).

[17] P. Kirchner, J. Oberländer, P. Friedrich, J. Berger, H.-P. Suso, A. Kupyna, M. Keusgen, and M.J. Schöning, "Optimization and fabrication of a calorimetric gas sensor built up on a polyimide substrate for H_2O_2 monitoring", *Phys. Status Solidi A* 208 (6), 1235–1240 (2011).

[18] D.B. Broughton, R.L. Wentworth, and M.E. Laing, "Mechanism of decomposition of hydrogen peroxide solutions with manganese dioxide. II", *J. Am. Chem. Soc.* 69 (4), 744–747 (1947).

[19] Y. Zhao, Z. Chen, X. Shen, and X. Zhang, "Kinetics and mechanisms of heterogeneous reaction of gaseous hydrogen peroxide on mineral oxide particles", *Environ. Sci. Technol.* 45 (8), 3317–3324 (2011).

[20] E. Giamello, P. Rumori, F. Geobaldo, B. Fubini, and M.C. Paganini, "The interaction between hydrogen peroxide and metal oxides. EPR investigations", *Appl. Magn. Reson.* 10 (1-3), 173–192 (1996).

[21] Y.N. Lee, R.M. Lago, J.L.G. Fierro, and J. González, "Hydrogen peroxide decomposition over $Ln_{1-x}A_xMnO_3$ (Ln = La or Nd and A = K or Sr) perovskites", *Appl. Catal. A-Gen.* 215 (1-2), 245–256 (2001).

[22] S.B. Kanungo, K.M. Parida, and B.R. Sant, "Studies on MnO_2—III. The kinetics and the mechanism for the catalytic decomposition of H_2O_2 over different crystalline modifications of MnO_2", *Electrochim. Acta* 26 (8), 1157–1167 (1981).

[23] L.P. Lindeman and J.C. Guffy, "Determination of the O –O bond energy in hydrogen peroxide by electron impact", *J. Chem. Phys.* 29 (1), 247–248 (1958).

[24] A. Hiroki and J.A. Laverne, "Decomposition of hydrogen peroxide at water-ceramic oxide interfaces", *J. Phys. Chem. B* 109 (8), 3364–3370 (2005).

[25] J.R. Macdonald and W.B. Johnson, "Fundamentals of Impedance Spectroscopy", in *Impedance Spectroscopy*, John Wiley & Sons, Hoboken, New Jersey 2005.

[26] M. Ibrahim, J. Claudel, D. Kourtiche, and M. Nadi, "Geometric parameters optimization of planar interdigitated electrodes for bioimpedance spectroscopy", *J. Electr. Bioimp.* 4 (1), 13–22 (2013).

[27] M. Mallén-Alberdi, N. Vigués, J. Mas, C. Fernández-Sánchez, and A. Baldi, "Impedance spectral fingerprint of *E. coli* cells on interdigitated electrodes: a new approach for label free and selective detection", *Sens. Biosensing Res.* 7, 100–106 (2016).

[28] G. Rosati, A. Cunego, F. Fracchetti, A. Del Casale, M. Scaramuzza, A. de Toni, S. Torriani, and A. Paccagnella, "Inkjet printed interdigitated biosensor for easy and rapid detection of bacteriophage contamination: a preliminary study for milk processing control applications", *Chemosens.* 7 (1), 8 (2019).

[29] J. Oberländer, Z.B. Jildeh, P. Kirchner, L. Wendeler, A. Bromm, H. Iken, P.H. Wagner, M. Keusgen, and M.J. Schöning, "Study of interdigitated electrode arrays using experiments and finite element models for the evaluation of sterilization processes", *Sensors (MDPI)* 15 (10), 26115–26127 (2015).

[30] N. Couniot, D. Flandre, L.A. Francis, and A. Afzalian, "Signal-to-noise ratio optimization for detecting bacteria with interdigitated microelectrodes", *Sens. Actuators, B* 189, 43–51 (2013).

[31] J. Oberländer, J. Arreola, C. Hansen, A. Greeff, M. Mayer, M. Keusgen, and M.J. Schöning, "Impedimetric biosensor to enable fast evaluation of gaseous sterilization processes", *Proceedings (MDPI)* 1 (4), 435 (2017).

[32] A. Ulman, "Formation and structure of self-assembled monolayers", *Chem. Rev.* 96 (4), 1533–1554 (1996).

[33] A. Ulman, "Part three - self-assembled monolayers", in *An Introduction to Ultrathin Organic Films*, Academic Press, San Diego 1991.

[34] G.T. Hermanson, "Silane coupling agents", in *Bioconjugate Techniques*, Academic Press, Amsterdam 2008.

[35] B. Arkles, "Hydrophobicity, hydrophilicity and silanes", *Paint and Coatings Industry* 22 (10), 114–125 (2006).

[36] Y. Yang, A.M. Bittner, S. Baldelli, and K. Kern, "Study of self-assembled triethoxysilane thin films made by casting neat reagents in ambient atmosphere", *Thin Solid Films* 516 (12), 3948–3956 (2008).

[37] Y.G. Vlasov, Y.A. Tarantov, and P.V. Bobrov, "Analytical characteristics and sensitivity mechanisms of electrolyte-insulator-semiconductor system-based chemical sensors-a critical review", *Anal. Bioanal. Chem.* 376 (6), 788–796 (2003).

[38] Schöning, M.J., Glück, O., Thust, M., "Electrochemical composition measurement", in *The Measurement, Instrumentation, and Sensors Handbook*, CRC Press, Boca Raton, Florida 1999.

[39] E.L. Decker, B. Frank, Y. Suo, and S. Garoff, "Physics of contact angle measurement", *Colloids and Surfaces A: Physicochemical and Engineering Aspects* 156 (1), 177–189 (1999).

[40] E. Marie and W. Torbjörn, "4 - Surface Analytical Techniques Applied to Cleaning Processes", in *Handbook for Cleaning/decontamination of Surfaces*, Elsevier, Amsterdam, Boston 2007.

[41] E. Drioli, A. Criscuoli, and E. Curcio, Eds., "Membrane Science and Technology : Membrane Contactors: Fundamentals, Applications and Potentialities", Elsevier (2006).

[42] M. Krieg, G. Fläschner, D. Alsteens, B.M. Gaub, W.H. Roos, G.J.L. Wuite, H.E. Gaub, C. Gerber, Y.F. Dufrêne, and D.J. Müller, "Atomic force microscopy-based mechanobiology", *Nat. Rev. Phys.* 1 (1), 41–57 (2019).

[43] H.-J. Butt, B. Cappella, and M. Kappl, "Force measurements with the atomic force microscope: Technique, interpretation and applications", *Surf. Sci. Rep.* 59 (1), 1–152 (2005).

[44] Y. Seo and W. Jhe, "Atomic force microscopy and spectroscopy", *Rep. Prog. Phys.* 71 (1), 16101 (2007).

[45] W. Zhou, R. Apkarian, Z.L. Wang, and D. Joy, "Fundamentals of scanning electron microscopy (SEM)", in *Scanning Microscopy for Nanotechnology: Techniques and Applications*, Springer New York, New York, NY 2007.

[46] K. Akhtar, S.A. Khan, S.B. Khan, and A.M. Asiri, "Scanning electron microscopy: principle and applications in nanomaterials characterization", in *Handbook of Materials Characterization*, Springer International Publishing, Cham 2018.

[47] JEOL, https://www.jeol.co.jp/en/applications/detail/891.html, downloaded at 12.11.2019.

[48] E. Dewhurst, D.M. Rawson, and G.C. Steele, "The use of a model system to compare the efficiency of ultrasound and agitation in the recovery of *Bacillus subtilis* spores from polymer surfaces", *J. Appl. Bacteriol.* 61 (4), 357–363 (1986).

[49] E.E. Sugimoto, A.J. Raasch, and R.M. Ehioba, "Recovery of bacterial spores dried on aluminium strips", *J. Appl. Bacteriol.* 80 (2), 147–152 (1996).

[50] K. Pruß, S. Stirtzel, and U. Kulozik, "Influence of the surface temperature of packaging specimens on the inactivation of *Bacillus* spores by means of gaseous H_2O_2", *J. Appl. Microbiol.* 112 (3), 493–501 (2012).

[51] J. Arreola, M. Mätzkow, M.P. Durán, A. Greeff, M. Keusgen, and M.J. Schöning, "Optimization of the immobilization of bacterial spores on glass substrates with organosilanes", *Phys. Status Solidi A* 213 (6), 1463–1470 (2016).

3 Effect of O_2 plasma on properties of electrolyte-insulator-semiconductor structures (*Physica Status Solidi (a) – applications and materials science*, 214, 9 (2017), 1700025 (1-6))

Julio Arreola[1,2], Michael Keusgen[2], and Michael J. Schöning[1,3]

[1] Institute of Nano- and Biotechnologies, Aachen University of Applied Sciences, Heinrich-Mußmann-Straße 1, 52428 Jülich, Germany

[2] Institute of Pharmaceutical Chemistry, Philipps-University Marburg, Marbacher Weg 6-10, 35032 Marburg, Germany

[3] Peter Grünberg Institute, Research Center Jülich GmbH, Wilhelm-Johnen-Straße, 52428 Jülich, Germany

Published in: *Physica Status Solidi (a) – applications and materials science*, 214, 9 (2017), 1700025 (1-6). Reprinted with permission from John Wiley & Sons, Inc.

Received 17 January 2017; **revised** 01 March 2017; **accepted** 07 March 2017

Keywords: annealing, electrolyte-insulator semiconductor sensor (EIS), hydroxylation, O_2 plasma, surface functionalization.

Abstract

Prior to immobilization of biomolecules or cells onto biosensor surfaces, the surface must be physically or chemically activated for further functionalization. Organosilanes are a versatile

option as they facilitate the immobilization through their terminal groups and also display self-assembly. Incorporating hydroxyl groups is one of the important methods for primary immobilization. This can be done, for example, with oxygen plasma treatment. However, this treatment can affect the performance of the biosensors and this effect is not quite well understood for surface functionalization. In this work, the effect of O_2 plasma treatment on EIS sensors was investigated by means of electrochemical characterizations: capacitance-voltage- (C-V) and constant capacitance (ConCap) measurements. After O_2 plasma treatment, the potential of the EIS sensor dramatically shifts to a more negative value. This was successfully reset by using an annealing process.

3.1 Introduction

The use of organosilanes has been widely applied in biosensors, for instance to immobilize enzymes, antibodies or microorganisms on top of the transducer structure [1–3]. It is a popular choice of coupling agents as they facilitate for further attachment of molecules through their terminal reactive groups (e.g., amines) and also display self-assembly behavior [4, 5]. The silanization process (formation of organosilanes on the surface) consists of four steps: hydrolysis, condensation, hydrogen bond formation and curing [6, 7]. In the first step, the organosilane groups are hydrolyzed to form highly reactive silanols (Si-OH). Then, in the second step, siloxanes are formed over the surface by means of silanols condensation. In the third step, the hydrolyzed organosilanes interact with the hydroxyl groups (OH) present on the transducer surface via hydrogen bonding. Finally, a covalent bond is formed between the silicon of the surface and the silicon of the organosilane with the associated loss of water molecules by curing [6, 8].

Prior to functionalizing the sensor surface with organosilanes, the surface must be activated by incorporating hydroxyl groups (hydroxylation); this can be done by chemical or physical treatments. Plasma methods have gained considerable popularity as they are easy to use, take only a few minutes and no special chemicals or waste removal is needed, since gaseous byproducts are removed under vacuum [9, 10]. However, in literature [3, 11–13] an influence of plasma treatments on the performance of biosensors has been reported. This phenomenon has been previously investigated by Szekeres et al. [14], where the effect of O_2 plasma on Si-SiO_2 systems was studied. They observed radiation damage as a result of the plasma treatment at different temperatures (from 20 °C to 300 °C). It was concluded that high temperature annealing is necessary to remove completely the radiation damage produced at substrate temperatures above 20 °C. Nevertheless, this effect is not completely well understood for surface functionalization. For instance, what is the hydrophilic behavior of the Si-SiO_2 structures after the annealing process?

Therefore, in this work, the effect of O_2 plasma is further investigated by means of electrolyte-insulator-semiconductor (EIS) sensors and contact angle measurements. An EIS sensor is very sensitive for the detection of (bio-)chemical reactions leading to chemical or

electrical changes at its interface; changes in the chemical composition of the analyte will induce changes in the capacitance of the EIS sensor [15, 16].

3.2 Experimental

3.2.1 Fabrication of the EIS sensor

A total of 30 nm of SiO_2 was thermally grown by dry oxidation at 1,000 °C for 30 min on a p-Si wafer (ρ = 1-10 Ωcm, <100>). After that, the oxide layer of the rear side was etched with HF and 300 nm Al were evaporated to function as ohmic contact to the p-Si wafer. Furthermore, the chips were diced into 10 x 10 mm^2 pieces and cleaned for 5 min sequentially in ultrasonic bath with acetone, isopropanol and deionized (DI) water.

3.2.2 Experimental setup

In Figure 3.1 the schematic cross-section of the measurement setup is shown. The EIS chips were mounted into an in-house measuring cell and sealed by an O-ring. The front side of the chip is in direct contact with the electrolyte, whereas the rear side is connected to the electrochemical workstation (Zennium, Zahner Elektrik, Germany). From the top side, an Ag/AgCl electrode (3 M KCl, Metrohm, Germany) was mounted as reference electrode. The contact area of the EIS chip was about 0.5 cm^2. All the measurements were performed in a dark Faraday cage at room temperature.

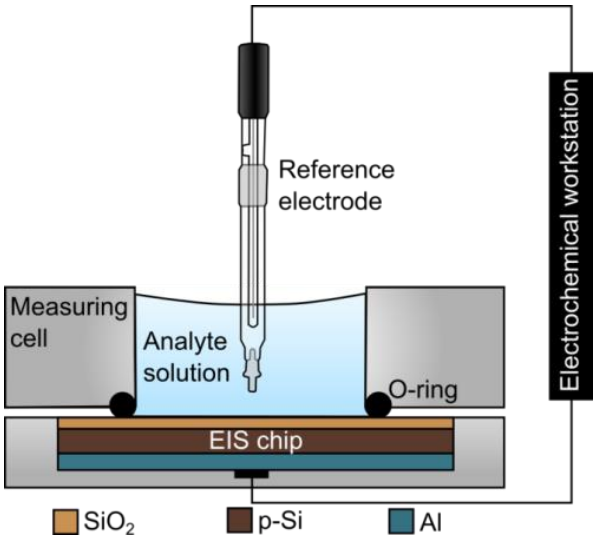

Figure 3.1 Schematic cross-section of the experimental setup.

The electrochemical characterization of the EIS chips was performed with capacitance-voltage- (C-V) and constant-capacitance (ConCap) measurements. For the C-V measurements a direct current polarization voltage from -3 V to 3 V (steps of 100 mV) was applied to set the working point of the EIS sensor. In order to measure the capacitance of the sensor, a small alternate current voltage (20 mV) and a frequency of 120 Hz were applied between the reference electrode and the rear side (Al) of the EIS sensor. All the measurements were carried out in phosphate buffered saline buffer (~0.33 mM ionic strength), pH 7.4. All potential values are referred to the reference electrode. For each treatment, the sensors chips were demounted and mounted again in the measuring cell. In addition, the buffer solution was disposed and replenished, accordingly. The pH of the buffer was controlled before and after measurements with a MPC227 pH/conductivity meter (Mettler-Toledo, Germany). A reference measurement was performed for every chip, which consisted in measuring the chip with the mentioned buffer and electrical conditions without any treatment. For the long-term measurements, the chips were stored in the measuring cell filled with PBS buffer and sealed with a wax film to avoid evaporation.

3.2.3 Hydroxylation

The EIS chips were hydroxylated by oxygen plasma treatment with 100 W (Femto PCCE, Diener electronic GmbH + Co. KG, Germany) for 2 min at 0.3 mbar. All EIS chips were directly utilized after being hydroxylated with the oxygen plasma treatment.

3.2.4 Annealing

A hot plate (RTC basic, Werke GmbH & Co. KG, Germany) was used to heat the EIS chips at 300 °C for 10 or 60 min.

3.2.5 Contact angle measurements

Water contact angles were measured on EIS chips before and after O_2 plasma treatments and annealing processes. The measurements were performed at room temperature using an optical contact angle system OCA (Dataphysics, Germany) and the data were analyzed with the software SCA 20.

3.3 Results and discussion

3.3.1 Effect of O_2 plasma on the EIS sensor

Figure 3.2 shows a C-V curve of an EIS sensor after it was treated with O_2 plasma. A shift of the C-V curve in the direction of negative voltages can be observed directly after the treatment, which decreases slowly and oscillates over time. The direction of the potential shifts depends on the charge of adsorbed molecules [17]. In this case, this may indicate that more positive charges are generated on the surface of the EIS chip after the plasma treatment.

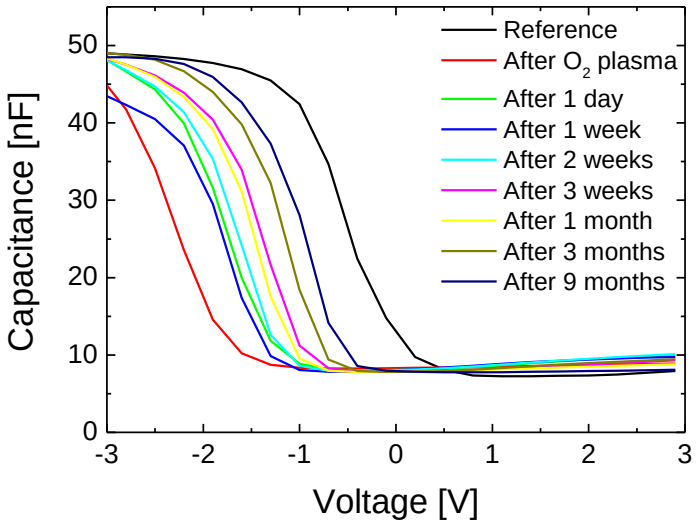

Figure 3.2 C-V curves of an EIS sensor after O_2 plasma treatment.

Oxygen plasma makes the surface of the chip more hydrophilic by removing contaminants and leaving silanols (Si-OH) groups at the sensor surface [18, 19]. Moreover, SiO_2 surfaces are known to possess a negative surface charge through its point of zero charge in aqueous solutions at pH = 2.5 [20] and the dissociation of terminal silanols groups [21]. In addition, the O_2 plasma activation (generation of hydroxyl groups) wear off in a scale of ~24 h [19] and it will probably not be still present after 9 months. Therefore, these positive charges are not likely to come from the sensor surface, but probably from penetration of excited species (ions and metastables) [11, 14, 22–24]. In order to verify this assumption, a series of plasma treatments investigations were performed as shown in Figure 3.3. In Figure 3.3, it can be observed that after a sequence of O_2 plasma treatments, the signal (potential) shifts towards a more negative voltage, the more plasma treatments are performed. In contrast to the C-V

operation mode, the ConCap measurement allows monitoring dynamic changes of the sensor signal. In this case, the drift behavior can be also determined for sensor chips treated with O_2 plasma (270 mV/10 min), which is larger than that of the reference sensor chip without oxygen plasma treatment (4 mV/10 min). Slow drifts in such electrolyte-SiO_2-Si system can also be related to both ions in-diffusion and buried OH sites [25].

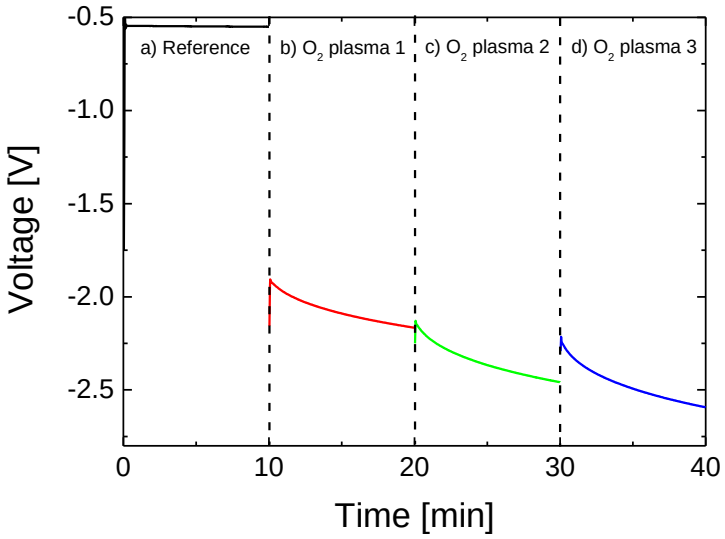

Figure 3.3 ConCap measurement of an EIS sensor after a series of O_2 plasma treatments. a) reference measurement, b) after the first O_2 plasma treatment, c) after the second O_2 plasma treatment, d) after the third O_2 plasma treatment.

3.3.2 Annealing effect on the EIS sensor

After the O_2 plasma treatment, the surface of the sensor was successfully activated by incorporating hydroxyl groups. At the same time, however, trapped charges within the substrate might be generated [14]. As a result, the sensor signal was dramatically changed as shown in the previous section.

Annealing has been reported to induce structural relaxation of the surface [26] and reduce the creation of plasma-induced radiation defects [14]. By doing this, the trapped charges could be released as shown in Figure 3.4. After the O_2 plasma treatment, the sensor signal was changed (-2.01 V). Furthermore, after the annealing process, the signal went nearly completely back (-0.32 V) to its initial reference value (-0.37 V). After 5 months, the EIS chip was measured again with a value of -0.35 V. This may indicate that the trapped charges inside of the substrate after the O_2 plasma treatment were released during the annealing process.

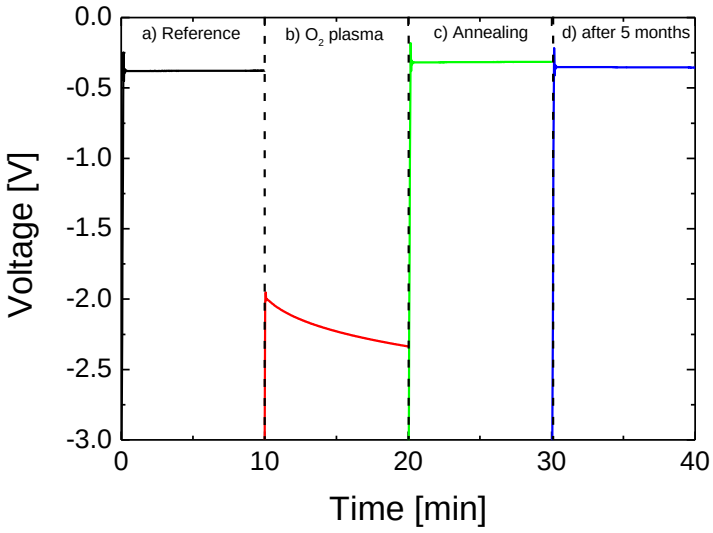

Figure 3.4 ConCap measurement of an EIS sensor. a) reference measurement, b) after O_2 plasma treatment, c) after annealing process, d) after 5 months after the annealing process was conducted.

Furthermore, a series of annealing processes was performed to investigate the isolated effect of the heat treatment on the EIS structure as shown in Figure 3.5.

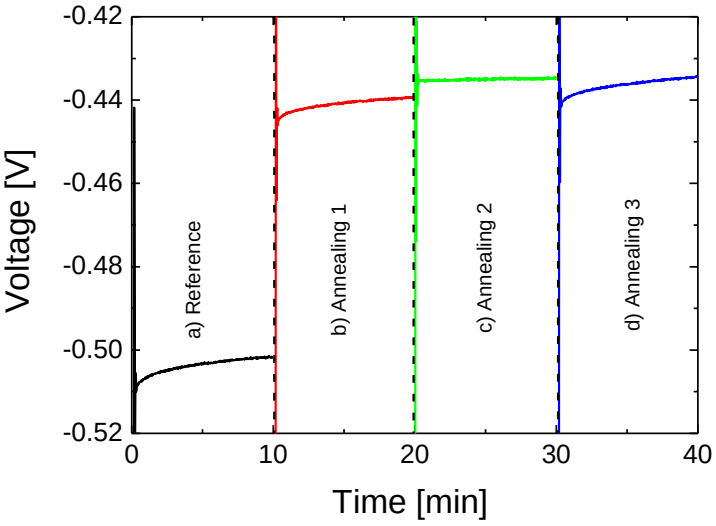

Figure 3.5 ConCap measurement of an EIS sensor after a series of 1 h annealing processes. a) reference measurement, b) after the first annealing process, c) after the second annealing process, d) after the third annealing process.

After annealing, a small potential shift of +0.06 V (absolute value: -0.44 V) can be observed in comparison with the starting reference value of -0.50 V. Later on, further annealing processes showed no significant changes of the sensor's signal, since these small changes could also be

attributed to the mounting and demounting of the EIS chip between treatments. In addition, during the measurements, a potential fluctuation up to ± 4 mV is expected [27]. A positive potential shift from the ConCap measurement may imply that more negative, less positive or trapped charges are present at the sensor's surface. After annealing it might be that these defects from the sensor chip are reduced by relaxing the surface into a more stable form. This positive shift of the signal might be due to this rearrangement and change of stoichiometry [28] by increasing the oxide quality at the interface region SiO_2/analyte significantly [29]. These results may support the suggested underlying mechanism from [14] to explain the creation of defects due to radiation or thermal treatments. During oxidation and/or postoxidation annealing, hydrogen can diffuse into the oxide creating Si-H or Si-OH bonds or can also remain as an interstitial form H_i. However, the Si-H bonds are not very stable and can be broken down with radiation, heat or charge transfer in a field as shown in the following reaction:

$$\equiv Si\text{-}H \leftrightarrow \equiv Si\cdot + H_i \qquad \text{(Equation 3.1)}$$

The trivalent radical ≡ Si· can be an interface state of acceptor or donor type depending on its oxidation state. In addition, the hydroxyl groups are metastable as well and may dissociate according to:

$$\equiv Si\text{-}OH \leftrightarrow \equiv Si\text{-}O\cdot + H_i \qquad \text{(Equation 3.2)}$$

The non-bridging oxygen from reaction (3.2) can act as an electron trap and the hydrogen atoms resulting from (3.1) and (3.2) are mobile and their migration may initiate a reaction creating additional defects near the interface according to:

$$\equiv Si\text{-}O\text{-}Si \equiv + H_i \leftrightarrow \equiv Si\text{-}OH + \equiv Si\cdot \qquad \text{(Equation 3.3)}$$

This again leads to the creation of a trivalent silicon radical and the replacement of bridging oxygen by an OH radical in the SiO_2 network. Therefore, defects may be generated by:

$$\equiv Si\text{-}H + \equiv Si\text{-}O\text{-}Si \equiv \leftrightarrow \equiv Si\cdot + \equiv Si^{+} + \equiv Si\text{-}OH \qquad \text{(Equation 3.4)}$$

One condition for the generation of stable defects of a trivalent silicon radical (≡Si·) and a trivalent-charged silicon (≡ Si^+) is the diffusion away of the hydroxyl group. The Si-OH groups from (3.3) and (3.4) together with Si-OH groups involved in the SiO_2 can participate in (3.2)

contributing with the creation of electron traps. It is important to note that these reactions are temperature-dependent: the temperature may assist or impede the creation of plasma-induced radiation defects.

Since in our experiments the annealing temperature was optimized at 300 °C, the rate of the reactions (3.3) and (3.4) increased and the generation of defects according to (3.4) as well, so that an intensive creation of electron traps may occur according to (3.2), resulting in a positive potential shift from Figure 3.5.

3.3.3 Contact angle measurements

Until now, all the annealing treatments were performed for 1 h. Figure 3.6 shows the typical effect of the O_2 plasma treatment and the annealing process on the EIS chips; after O_2 plasma treatment, the sensor's signal is dramatically changed and after annealing it was reset nearly to its reference value. Although the annealing process had a positive effect on the EIS sensor (resetting the sensor's signal), the hydrophilicity of the surface is as well a critical factor for surface functionalization. For this reason, water contact angle measurements were conducted to characterize the hydrophilicity of the EIS chips.

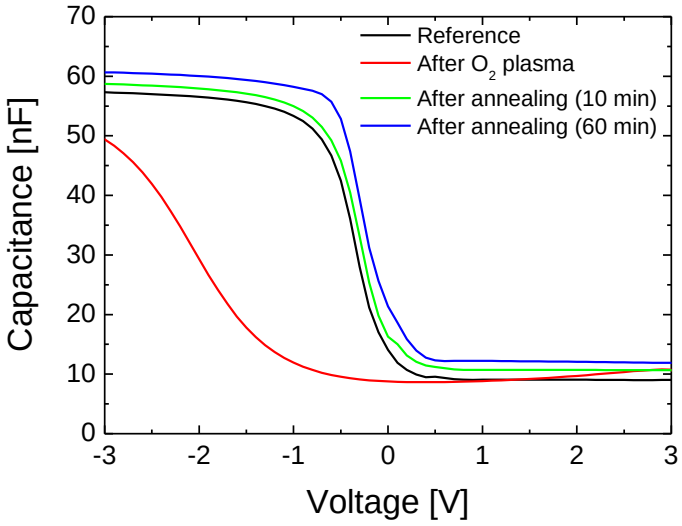

Figure 3. 6 C-V curves of an EIS sensor after O_2 plasma treatment and annealing processes (10 and 60 min).

As it can be seen in Table 3.1, the contact angle after O_2 plasma is nearly 0°, which is desired for silanization. However, after the annealing process of 60 min, the contact angle was increased to 60°, indicating the loss of the plasma activation. In order to maintain the

hydrophilicity of the surface after O_2 plasma treatment as well as the reset effect due to the annealing process, the annealing time and temperature were optimized for 10 min and 300 °C, respectively.

Table 3.1 Contact angle measurements of EIS chips after O_2 plasma treatments and annealing processes.

Treatment	Contact angle (°)
Reference	40
O_2 plasma	~1
Annealing (10 min)	6
Annealing (60 min)	60

Below this time and temperature, the signal does not go completely back to its initial value (results not shown). It can be seen the Table 3.1 (contact angle of 6° after the optimized annealing process) and from Figure 3.6, that the sensor's signal is as well reset and even closer to the reference value.

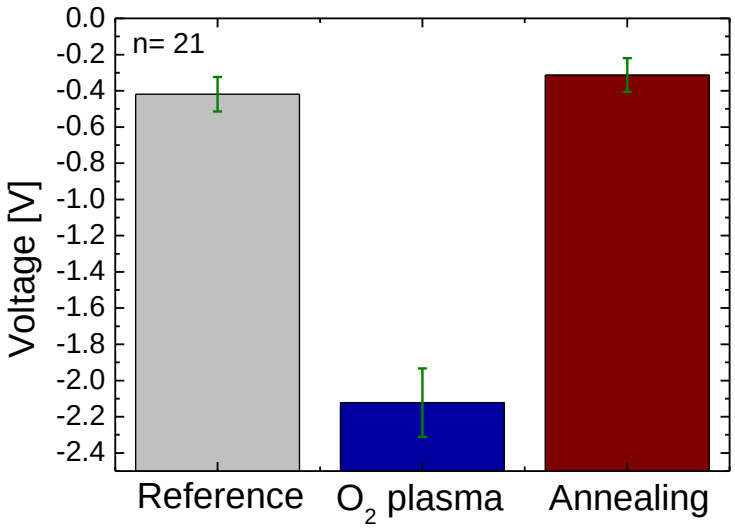

Figure 3.7 Potential shifts (ConCap measurement) after O_2 plasma treatment and annealing on the EIS sensor; n is the number of EIS sensors measured.

The potential shift changes after O_2 plasma treatment and annealing process are summarized in Figure 3.7. Note that the chips were first treated with O_2 plasma and after that with the annealing process. The reference potential was -0.41 ± 0.09 V, after O_2 plasma -2.12 ± 0.18 V and after annealing -0.31 ± 0.09 V. The effect of O_2 plasma treatment on EIS chips is highly reproducible as it can be seen from the 21 chips utilized. After the O_2 plasma treatment the sensor's signal shifts to a more negative value and after the annealing process goes back to its initial state. Changing the O_2 plasma exposure time from 2 min to 30 s made no difference at obtaining the same effect. Further parameters might have an additional influence such as O_2 plasma power, cooling rate after annealing and annealing atmosphere (all annealing processes were conducted at air).

3.4 Conclusions

In this work, the effect of O_2 plasma treatment on EIS chips was investigated by means of electrochemical characterizations (C-V- and ConCap measurements) and contact angle measurements. After the plasma treatment, a large potential shift of -2.12 ± 0.18 V was observed in comparison with the reference potential of -0.41 ± 0.09 V. This can be due to more negative, less positive or trapped charges within the Si/SiO_2 sensor structure. Furthermore, the potential shift due to the O_2 plasma treatment was successfully reset (-0.31 ± 0.09 V) by an additional annealing process. This probably releases the mentioned charges and improves the oxide quality. In addition, the annealing process was optimized (300 °C for 10 min) to obtain a hydrophilic surface as well as to maintain its reset effect of the sensor's signal.

In further investigations, the silanization process (e.g., with (3-(Aminopropyl)triethoxysilane) may be included as well as the effect of different hydroxylation methods.

Furthermore, endospores will be immobilized with silanization on different sensor chips (e.g., EIS, interdigitated electrodes). These sensors must be handled under harsh conditions (e.g., high temperatures >200 °C and an oxidizing atmosphere). Therefore, the use of this method may facilitate the reproducibility and sensibility of sensor chips by resetting their signal to the initial value after hydroxylation.

Acknowledgements

This work was financially supported by the Federal Ministry of Education and Research, Germany, Project: "ImpediPack" (Fund. No.: 03FH012I3). The authors are gratefully thankful to H. Iken for the fabrication of the EIS sensors, A. Poghossian for valuable discussions and revisions on the manuscript, and T. S. Bronder for support during the measurements.

References

[1] J. Arreola, M. Mätzkow, M.P. Durán, A. Greeff, M. Keusgen, and M.J. Schöning, "Optimization of the immobilization of bacterial spores on glass substrates with organosilanes", *Phys. Status Solidi A* 213 (6), 1463–1470 (2016).

[2] B. Barlen, S.D. Mazumdar, and M. Keusgen, "Immobilisation of biomolecules for biosensors", *Phys. Status Solidi A* 206 (3), 409–416 (2009).

[3] J. Gun, D. Rizkov, O. Lev, M.H. Abouzar, A. Poghossian, and M.J. Schöning, "Oxygen plasma-treated gold nanoparticle-based field-effect devices as transducer structures for bio-chemical sensing", *Microchimica Acta* 164 (3-4), 395–404 (2009).

[4] R.G. Acres, A.V. Ellis, J. Alvino, C.E. Lenahan, D.A. Khodakov, G.F. Metha, and G.G. Andersson, "Molecular structure of 3-aminopropyltriethoxysilane layers formed on silanol-terminated silicon surfaces", *J. Phys. Chem. C* 116 (10), 6289–6297 (2012).

[5] J. Landoulsi, M.J. Genet, K. El Kirat, C. Richard, S. Pulvin, and P.G. Rouxhet, "Silanization with APTES for controlling the interactions between stainless steel and biocomponents: reality vs. expectation", in *Biomaterials: Physics and Chemistry*, InTech, 2011.

[6] K. L. Mittal, *Silanes and Other Coupling Agents*, CRC Press, New York, 2009.

[7] C.M. Halliwell and A.E.G. Cass, "A factorial analysis of silanization conditions for the immobilization of oligonucleotides on glass surfaces", *Anal. Chem.* 73 (11), 2476–2483 (2001).

[8] B. Arkles, Y. Pan, and Y.M. Kim, "The role of polarity in the structure of silanes employed in surface modification", in *Silanes and Other Coupling Agents*, Volume 5, Brill, 2009.

[9] B.A. Langowski and K.E. Uhrich, "Oxygen plasma-treatment effects on Si transfer", *Langmuir* 21 (14), 6366–6372 (2005).

[10] K.S. Siow, L. Britcher, S. Kumar, and H.J. Griesser, "Plasma methods for the generation of chemically reactive surfaces for biomolecule immobilization and cell colonization - a review", *Plasma Process. Poly.* 3 (6-7), 392–418 (2006).

[11] E. Atanassova and A. Paskaleva, "Electrically active defects generated by MERIE and RIE-mode plasmas in thin SiO_2-Si structures", *Microelectron. Reliab.* 40 (3), 381–425 (2000).

[12] C. García Núñez, M. Sachsenhauser, B. Blashcke, A. García Marín, J.A. Garrido, and J.L. Pau, "Effects of hydroxylation and silanization on the surface properties of ZnO nanowires", *ACS Appl. Mater. Inter.* 7 (9), 5331–5337 (2015).

[13] O. Seitz, P.G. Fernandes, R. Tian, N. Karnik, H.-C. Wen, H. Stiegler, R.A. Chapman, E.M. Vogel, and Y.J. Chabal, "Control and stability of self-assembled monolayers under biosensing conditions", *J. Mater. Chem.* 21 (12), 4384-4392 (2011).

[14] A. Szekeres, S. Alexandrova, and K. Kirov, "The effect of O_2 plasma on properties of the Si-SiO_2 system", *Phys. Status Solidi A* 62 (2), 727–736 (1980).

[15] M.J. Schöning and A. Poghossian, "Bio FEDs (field-effect devices): state-of-the-art and new directions", *Electroanalysis* 18 (19-20), 1893–1900 (2006).

[16] M.J. Schöning and A. Poghossian, "Recent advances in biologically sensitive field-effect transistors (BioFETs)", *Analyst* 127 (9), 1137–1151 (2002).

[17] A. Poghossian, M. Weil, A.G. Cherstvy, and M.J. Schöning, "Electrical monitoring of polyelectrolyte multilayer formation by means of capacitive field-effect devices", *Anal. Bioanal. Chem.* 405 (20), 6425–6436 (2013).

[18] Q. Fu, T. Wagner, and M. Rühle, "Hydroxylated α-Al_2O_3 (0001) surfaces and metal/α-Al_2O_3 (0001) interfaces", *Surf. Sci.* 600 (21), 4870–4877 (2006).

[19] S. Kaya, P. Rajan, H. Dasari, D.C. Ingram, W. Jadwisienczak, and F. Rahman, "A systematic study of plasma activation of silicon surfaces for self sssembly", *ACS Appl. Mater. Inter.* 7 (45), 25024–25031 (2015).

[20] M. Kosmulski, "pH-dependent surface charging and points of zero charge. IV. Update and new approach", *J. Colloid Interface Sci.* 337 (2), 439–448 (2009).

[21] S.H. Behrens and D.G. Grier, "The charge of glass and silica surfaces", *J. Chem. Phys.* 115 (14), 6716–6721 (2001).

[22] S.P. Godfrey, J.P.S. Badyal, and I.R. Little, "Plasmachemical dehydroxylation of high surface area silica at room temperature", *J. Phys. Chem. B.* 105 (13), 2572–2577 (2001).

[23] E.H. Nicollian, C.N. Berglund, P.F. Schmidt, and J.M. Andrews, "Electrochemical charging of thermal SiO_2 films by injected electron currents", *J. Appl. Phys.* 42 (13), 5654–5664 (1971).

[24] J.N. Zemel, "Microfabricated nonoptical chemical sensors", *Rev. Sci. Instrum.* 61 (6), 1579–1606 (1990).

[25] Y.G. Vlasov, Y.A. Tarantov, and P.V. Bobrov, "Analytical characteristics and sensitivity mechanisms of electrolyte-insulator-semiconductor system-based chemical sensors: a critical review", *Anal. Bioanal. Chem.* 376 (6), 788–796 (2003).

[26] A.S. D'Souza and C.G. Pantano, "Hydroxylation and dehydroxylation behavior of silica glass fracture surfaces", *J. Am. Ceram. Soc.* 85 (6), 1499–1504 (2002).

[27] M. Turek, L. Ketterer, M. Claßen, H. Berndt, G. Elbers, P. Krüger, M. Keusgen, and M. J. Schöning, "Development and electrochemical investigations of an EIS- (electrolyte-insulator-semiconductor) based biosensor for cyanide detection", *Sensors* 7 (8), 1415–1426 (2007).

[28] N. Kumar, A. P. Tiwari, J. Kumar, and S. Panda, Eds., "Effect of post deposition annealing temperature of e-beam evaporated Ta_2O_5 films on sensitivities of electrolyte-insulator-semiconductor devices" 2nd International Symposium on Physics and Technology of Sensors (ISPTS), 214-218 (2015).

[29] D. Hiller, R. Zierold, J. Bachmann, M. Alexe, Y. Yang, J.W. Gerlach, A. Stesmans, M. Jivanescu, U. Müller, J. Vogt, H. Hilmer, P. Löper, M. Künle, F. Munnik, K. Nielsch, and M. Zacharias, "Low temperature silicon dioxide by thermal atomic layer deposition: investigation of material properties", *J. Appl. Phys.* 107 (6), 64314 (1-10) (2010).

4 Optimization of the immobilization of bacterial spores on glass substrates with organosilanes (Physica Status Solidi (a) – applications and materials science, 213, 6 (2016), 1463-1470)

Julio Arreola[1], Malte Mätzkow[1], Marlena Palomar Durán[2], Anton Greeff[2], Michael Keusgen[3], Michael J. Schöning[1]

[1] Institute of Nano- and Biotechnologies, Aachen University of Applied Sciences, Heinrich-Mußmann-Straße 1, 52428 Jülich, Germany

[2] Elopak EQS GmbH, Hanns-Martin-Schleyer-Straße 17, 41199, Mönchengladbach, Germany

[3] Institute of Pharmaceutical Chemistry, Philipps-University Marburg, Marbacher Weg 6-10, 35032 Marburg, Germany

Published in: *Physica Status Solidi (a) – applications and materials science*, 213, 6 (2016), 1463-1470. Reprinted with permission from John Wiley & Sons, Inc.

Received 09 November 2015; **revised** 18 February 2016; **accepted** 19 February 2016

Keywords: *Bacillus atrophaeus,* biosensors, endospores, immobilization, organosilanes, silanization.

Abstract

Spores can be immobilized on biosensors to function as sensitive recognition elements. However, the immobilization can affect the sensitivity and reproducibility of the sensor signal. In this work, three different immobilization strategies with organosilanes were optimized and characterized to immobilize *B. atrophaeus* spores on glass substrates. Five different silanization parameters were investigated: nature of the solvent, concentration of the silane, silanization time, curing process and silanization temperature. The resulting silane

layers were resistant to a buffer solution (e.g., Ringer solution) with a polysorbate (e.g., Tween®80) and sonication.

4.1 Introduction

Bacterial spores are dormant microorganisms that are highly resistant to a variety of treatments, including heat, radiation, pressurization and oxidizing agents [1–3]. In the dormant state the spores undergo no detectable metabolism, but are still capable of monitoring environmental changes. This robustness and flexibility make them really convenient to use, for instance, as a biocontrol of pests, probiotics or biological indicators [4–7].

In addition, spores can be immobilized on biosensor substrates (e.g., glass) to serve as sensitive or recognition elements [8]. The immobilization of the spores, however, is a critical factor; it may affect the sensitivity and reproducibility of the sensor signal. In order to overcome this problem, a robust surface functionalization method is needed. The functionalization method should maintain the identity and functionality of the sensor substrate as well as the integrity and viability of the spores. Several surface functionalization methods have been described in literature. Among them, covalent immobilization using self-assembled monolayers of organosilanes is a promising technique and has numerous advantages compared to others such as physioadsorption, gel entrapment or physical confinement [9–11].

Commonly, the silanization process (formation of organosilanes on a surface) consists of four steps: hydrolysis, condensation, hydrogen bond formation and curing [12, 13]. The first step involves the hydrolysis of the organosilane groups to form highly reactive silanols (Si-OH). In the second step, the silanols undergo condensation to form siloxanes (Si-O-Si) over the surface. In the third step, hydroxyl groups (OH) present on the surface interact with the hydrolyzed organosilanes via hydrogen bonding. In the last step, a covalent bond is formed between the silicon of the organosilane and the silicon of the surface with the associated loss of water molecules by curing. The water molecules present in the solvents used and on the surface are critical parameters that affect the monolayer formation [12, 14, 15]. Several other factors also influence the silanization process such as the nature of the solvent used, humidity, concentration of the silane, silanization time, temperature of the solution and the curing process [13, 16–18].

Silanization on glass substrates can be done in liquid or gas phase. In gas-phase silanization, the silane solution is vaporized on the samples under vacuum or heating [19]. In the case of liquid-phase silanization, it can be conducted with two different methods: i) by dipping the samples into the silane solution or ii) by drop-casting the silane solution onto the samples [19, 20]. Among them, silanization in liquid phase is accessible and easy to use. Although silanization is a very well-known process to functionalize solid surfaces, the field is known for inconsistent and low-reproducible data [21]. Therefore, a well-developed and optimized protocol to functionalize glass surfaces with organosilanes is lacking.

The aim of the present study is to immobilize spores on glass substrates, which can be used as a model system for a spore-based biosensor. One of the main advantages of using glass compared to semiconductor substrates (e.g., Si) is the lack of light sensitivity. This can be a major problem for semiconductor substrates when measuring where the light conditions may vary and it might compromise the reliability of the sensor signal.

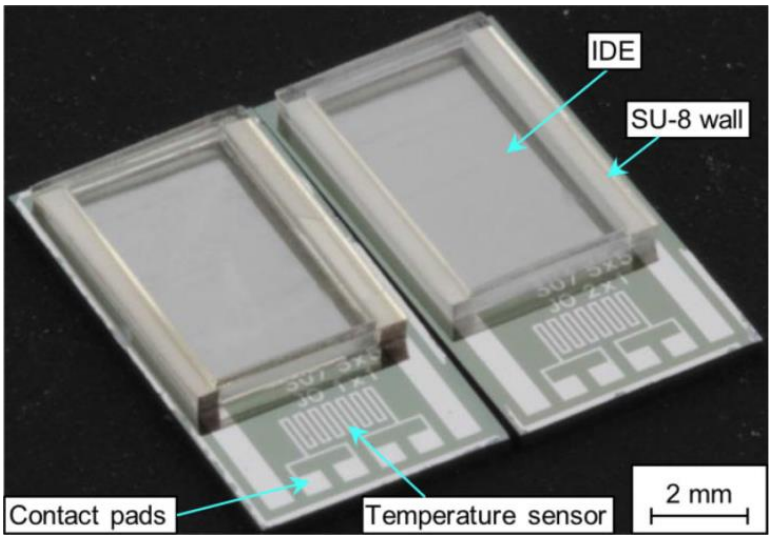

Figure 4.1 Spore-based biosensor from [8]. Differential set-up of two chips with temperature sensors and IDEs.

A spore-based biosensor was recently introduced [8] to evaluate the sterilization process in aseptic filling machines. Such biosensor can be seen in Figure 4.1. In short, it consists of temperature sensors and several interdigitated electrodes (IDEs), where the spores can be precisely confined and immobilized on one of the IDEs (due to walls of SU-8 photoresist) and the other IDE serves as reference sensor (differential measurement is desirable). The spore-based biosensor is then exposed to a H_2O_2 gas stream (e.g., 10 m^3/h) and heat (e.g., 240 °C);

as a result, a signal change (e.g., impedance) can be measured. Therefore, the immobilization of the spores is an important parameter because it might affect the signal change and reproducibility of the biosensor.

In this work, three different organosilanes are investigated for liquid-phase silanization and characterized by contact angle measurements, atomic force microscopy and a direct microbiological approach. Two organosilanes are used to immobilize spores of *Bacillus atrophaeus* (DSM 675) on glass substrates, namely (3-(Aminopropyl)triethoxysilane (APTES) and (3-(glycidyloxypropyl)trimethoxysilane (GPTMS). The third organosilane is applied to inhibit the attachment of the spores on the functionalized glass substrates, that is 1H,1H,2H,2H-Perfluorodecyltriethoxysilane (PFDTES). Chemical structures of the silanes studied in this report are summarized in Figure 4.2. In addition, the parameters: nature of the solvent used, concentration of the silane, silanization time, silanization temperature and curing process were investigated.

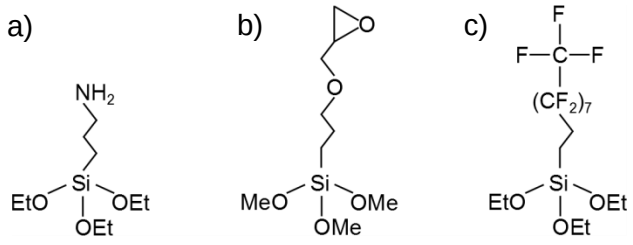

Figure 4.2 Chemical structures of the silanes investigated in this report. a) (3-(Aminopropyl)triethoxysilane (APTES), b) (3-(glycidyloxypropyl)trimethoxysilane (GPTMS), c) 1H,1H,2H,2H-Perfluorodecyltriethoxysilane (PFDTES).

4.2 Experimental

4.2.1 Materials

Borosilicate glass wafers, two-side polished, thickness of 1,000 ± 25 µm and cut into pieces of 10 x 10 mm² were purchased from MicroChemicals GmbH (Germany). (3-(Aminopropyl)triethoxysilane (APTES 98% v/v), (3-(glycidyloxypropyl)trimethoxysilane (GPTMS 98% v/v) and 1H,1H,2H,2H-Perfluorodecyltriethoxysilane (PFDTES 97% v/v) as well as toluene (99% v/v), ethanol (99% v/v), acetone (99% v/v), isopropanol (99% v/v), Tween®80, malachite green and safranin were obtained from Sigma-Aldrich (Germany). Plate count agar (PCA), Ringer solution tablets and manganese (II) sulphate monohydrate were obtained from

Merck Millipore (Germany). Meat extract dry and peptone from meat were purchased from VWR (Germany).

4.2.2 Surface functionalization

i) The glass substrates were cleaned to remove organic contamination in ultrasonic bath for 5 min for each step in acetone, isopropanol and deionized (DI) water, followed by drying under a stream of nitrogen gas. Subsequently, the glass substrates were hydrolyzed by oxygen plasma treatment with 100 W (Femto PCCE, Diener electronic GmbH + Co. KG) for 2 min. All glass substrates were directly used after being hydrolyzed with the oxygen plasma treatment.

ii) To optimize the liquid-phase silanization, the effect of both methods: a) dipping the samples in the silane solution or b) drop-casting the silane solution on the samples, was studied. Therefore, different solutions of 1% APTES, 1% GPTMS and 1% PFDTES in toluene for 1 h silanization were used. The glass substrates were then washed in ultrasonic bath for 5 min in toluene and ethanol, followed by curing for 1 h at 110 °C. All steps for silanization were conducted in a nitrogen glove box to reduce the effect of humidity on the silanization process.

iii) To study the effect of the solvent used on APTES, GPTMS and PFDTES, the glass substrates were cleaned as mentioned in the previous section and then five different solvents were investigated: DI water, ethanol, isopropanol, acetone, and toluene. A solution of 1% of each solvent was prepared with APTES, GPTMS and PFDTES, followed by silanization for 1 h. From this section on, the silanization was conducted with the optimal method by drop-casting. After the silanization, the glass substrates were washed and cured as mentioned earlier.

iv) The optimal solvent for each silane from the previous section was chosen to investigate the concentration of the silanes. The glass substrates were cleaned as before. For APTES, five different concentrations were studied, 0.01%, 0.10%, 0.25%, 0.50% and 1% in toluene for 1 h. In the case of GPTMS, 20%, 40%, 60%, 80% and 100% in isopropanol for 1 h and for PFTDES, 0.01%, 0.10%, 1%, 2.5% and 5% in toluene for 1 h were selected. The same washing and curing procedures used before were applied after the silanization.

v) The optimal parameters from the previous sections were chosen to study the silanization time. After cleaning the glass substrates as before, solutions of 1% APTES in toluene, 60% GPTMS in isopropanol and 1% PFDTES in toluene were prepared and five different silanization times were investigated: 30 min, 1 h, 2 h, 4h, and 24 h. After the silanization the glass substrates were washed and cured as mentioned earlier.

vi) To study the effect of the curing process during the silanization, the optimal parameters from the previous sections were used. The glass substrates were cleaned as before and silanized with 1% APTES in toluene for 1 h at room temperature, 60% GPTMS in isopropanol for 30 min at room temperature and 1% PFDTES in toluene for 1 h at 100 °C. After the silanization the glass substrates were washed as before and different curing times at 110 °C were investigated: 15 min, 30 min, 1 h, 2 h, and 4 h.

vii) Until now, all the optimization of the silanization parameters was conducted at room temperature. To investigate the effect of the silanization temperature, the optimized parameters were used. The glass substrates were cleaned as in the previous section, followed by silanization of 1% APTES in toluene for 1 h, 60% GPTMS in isopropanol for 30 min and 1% PFDTES in toluene for 1 h. The silanization was conducted at different temperature of 40 °C, 60 °C, 80 °C, 100 °C and 110 °C, followed by the same washing steps and cured at 110 °C for 1 h for APTES and PFDTES and 30 min for GPTMS.

4.2.3 Contact angle measurement (CA)

Water contact angles were measured on the glass substrates after the optimization of the silanization process. The measurements were conducted at room temperature using an optical contact angle system OCA (Dataphysics, Germany) and the data were analyzed with the software SCA 20. Reported values are an average of measurements conducted at three different regions on the samples.

4.2.4 Atomic force microscopy (AFM)

A BioMat Workstation (JPK Instruments, Germany) was used to record AFM images at 512 pixels per line, scanning at 0.2-0.4 Hz. The samples were imaged after the optimization of the silanization process at ambient conditions in tapping mode, using silicon cantilevers (Arrow

NCR, NanoWorld AG, Switzerland) with a spring constant of 42 N/m and resonant frequency of 285 kHz. The scanned areas were 2x2 μm^2.

4.2.5 Bacterial culture, sporulation and spore purification

The *Bacillus atrophaeus* strain (DSM 675) was obtained from IVV Fraunhofer, Germany. All procedures were conducted aseptically under a laminar flow hood. For culturing, *B. atrophaeus* cells were grown at 30 °C in 10 ml of complex medium [22] (3 g/l meat extract dry, 5 g/l peptone) for 24 h. The sporulation was then initiated by inoculation of all the cells in 200 ml of freshly complex medium with 10 mg/l $MnSO_4$ [22] and were incubated at 30 °C for 7 days. After the incubation time, the spores were harvested by centrifugation at 4,000 rpm (A-4-81; Centrifuge 5810R, Eppendorf, Germany) at 20 °C and resuspended in Ringer solution with 0.01% Tween®80. The spores were then washed at least five times in Ringer solution with 0.01 % Tween®80 and three times in DI water. Subsequently, the spores were pasteurized in water bath at 80 °C for 20 min, centrifuged and resuspended in 70% (v/v) ethanol solution. The spore suspension was free of vegetative cells (>95%) as determined by staining the spores with malachite green and safranin using Schaefer and Fulton's method [23]. The spore concentration was determined by serial dilutions and plating, resulting in a final concentration of 10^8 CFU/ml.

4.2.6 Microbiological evaluation of the immobilization of the spores

The optimization of the silanization process was evaluated using the spore recovery method, serial dilutions and spread-plate method (Figure 4.3). To evaluate the efficiency of the immobilization of the spores, after the glass substrates were silanized, 10 µl of the spore suspension of *B. atrophaeus* were inoculated onto each of the glass substrates and dried under a laminar flow hood for 30-120 min. The immobilized spores were recovered by resuspending the glass substrates in test tubes with 10 ml Ringer solution with 0.01% Tween®80 and placing them in ultrasonic bath for 10 min. Subsequently, each spore suspension was diluted by serial dilutions, spread-plated on PCA and cultivated at 30 °C for 24 h. The spores were then counted and the efficiency was defined as the number of spores remained onto the silanized glass substrates after the spore recovery compared to the control glass substrates (cleaned as mentioned in the previous section, without silanization); the less spores in the suspension (more spores on the silanized glass substrates), the better the

efficiency. The *Efficiency* (%) was calculated as shown in Equation 4.1, where N_s is the number of the recovered spores from the silanized glass substrate and N_c is the number of the recovered spores from the control glass substrate.

$$\text{Efficiency} = \left(1 - \frac{N_s}{N_c}\right) \times 100 \qquad \text{(Equation 4.1)}$$

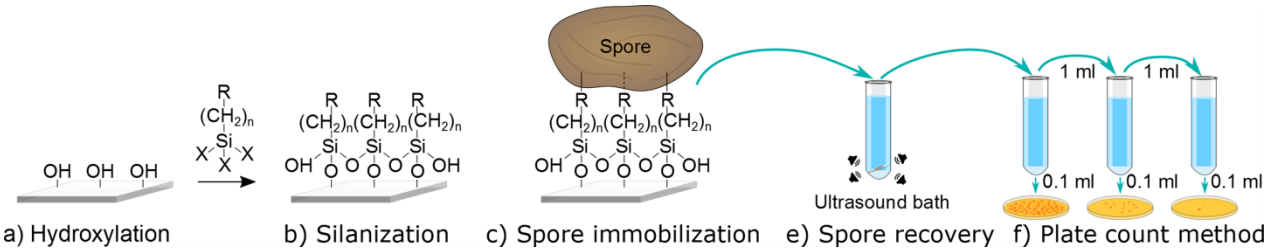

Figure 4.3 Schematic process of surface functionalization with organosilanes (a, b), spore immobilization (c) and microbiological evaluation for the immobilization of the spores (e, f).

4.3 Results and discussion

4.3.1 Optimization of the liquid-phase silanization

Dip-coating is one of the most used methods of silanization in liquid phase. However, very little has been studied about other silanization methods, such as drop-casting [20]. Both of these methods were investigated for APTES, GPTMS and PFDTES as shown in Figure 4.4. Silanization by drop-casting (Figure 4.4 b) shows slightly better efficiencies for GPTMS and PFDTES compared to silanization by dip-coating (Figure 4.4 a). Furthermore, the efficiency for APTES was notably relevant compared in a similar way to the mentioned methods. It can be noted that for the evaluation of the immobilization of spores, several factors are intrinsically involved to create a more robust self-assembled monolayer (SAM) in the evaluation method per se. For example, in this case the resulting SAM shall be stable in a buffer solution (Ringer solution) with a polysorbate (0.01% Tween®80) in ultrasonic bath. This may indicate the SAM formed of APTES for dip-coating and drop-casting methods, might not be influenced by the evaluation conditions and purely by the effect of both methods. The higher efficiency for APTES using the drop-casting method might result from

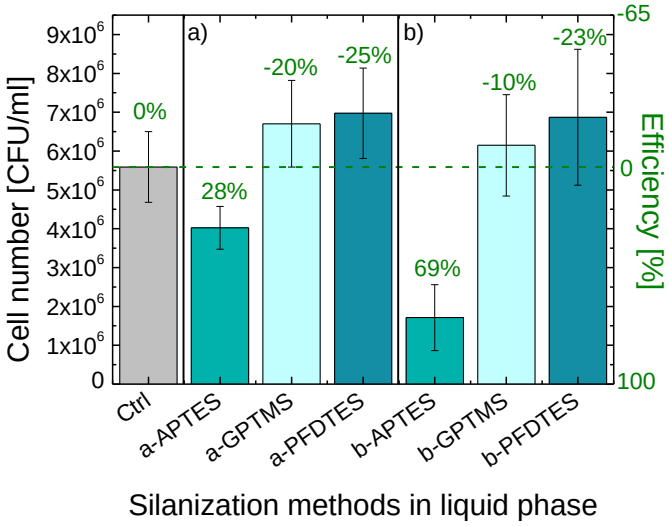

Figure 4.4 Comparison of two different silanization methods in liquid phase for APTES, GPTMS and PFDTES. a) dip-coating, b) drop-casting.

the surface tension associated with the APTES droplet and the hydrolyzed surface of the glass substrate, probably increasing the density of the silane molecules adsorbed onto the surface. On the other hand, the efficiencies for GPTMS and PFDTES may be influenced by the evaluation conditions. The unexpected efficiency for GPTMS for both methods might be due to further reactivity of the SAM during the evaluation conditions, forcing immobilized spores to detach from the surface. In addition, the efficiency for PFDTES was as expected; it was negative meaning spore detachment from the glass substrate was observed.

4.3.2 Nature of the solvent

The quality of the SAM depends on the amount of water in solution [12, 14, 15]. Incomplete monolayers are formed in the absence of water [17, 24], whereas excess of water results in rapid polymerization in solution and polysiloxane deposition of the surface [25–27]. Different commonly used solvents for silanization were investigated as shown in Table 4.1. For APTES toluene showed the best results with an efficiency of 69%, followed by ethanol with 66%. For GPTMS the best results were obtained using isopropanol with -6%. Although the results are not as they would have been expected, since a negative efficiency means detachment from the spores due to the immobilization, at this point the other silanization parameters were not optimized yet. For PFDTES acetone, DI water and toluene showed similar efficiencies of -85%, -85%, and -81%, respectively. The lower standard deviation of toluene compared to

acetone and DI water favoured it to be considered as the best solvent for PFDTES in order to guarantee the detachment of spores (that is required in that case).

Table 4.1 Experimental results of the silanization parameters investigated in this report (n = 4 samples have been investigated for each parameter). Cell number is the total number of colonies counted from the microbiological experiments with their standard deviation.

Parameter	Subparameter	APTES *		GPTMS *		PFDTES *	
		Cell number (10^6 CFU/ml)	Efficiency (%)	Cell number (10^6 CFU/ml)	Efficiency (%)	Cell number (10^6 CFU/ml)	Efficiency (%)
Nature of the solvent	Acetone	5.07 ± 1.64	-22	5.53 ± 0.39	-33	7.68 ± 0.64	-85
	Ethanol	1.40 ± 0.46	66	5.75 ± 0.65	-38	6.97 ± 0.68	-68
	DI water	3.54 ± 1.60	15	7.69 ± 0.99	-85	7.70 ± 0.98	-85
	Isopropanol	6.97 ± 2.17	-68	4.41 ± 0.56	-6	7.05 ± 0.74	-69
	Toluene	1.28 ± 0.51	69	7.90 ± 0.94	-90	7.53 ± 0.50	-81
Concentration of the silane	0.01%	2.57 ± 0.37	38	-	-	6.36 ± 0.74	-53
	0.1%	2.53 ± 0.19	39	-	-	5.44 ± 0.55	-31
	0.25%	2.44 ± 0.21	41	-	-	-	-
	0.5%	1.20 ± 0.33	71	-	-	-	-
	1%	0.93 ± 0.07	78	-	-	12.2 ± 0.63	-192
	2.5%	-	-	-	-	12 ± 1.27	-189
	5%	-	-	-	-	10.01 ± 0.55	-143
	20%	-	-	2.02 ± 0.35	51	-	-
	40%	-	-	2.67 ± 0.21	36	-	-
	60%	-	-	1.34 ± 0.57	68	-	-
	80%	-	-	3.23 ± 0.48	22	-	-
	100%	-	-	1.62 ± 0.28	61	-	-
Silanization time	30 min	3.05 ± 0.21	27	1.17 ± 0.56	72	5.14 ± 0.71	-24
	1 h	2.02 ± 0.11	51	2.46 ± 1.64	41	6.01 ± 0.84	-44
	2 h	2.88 ± 0.6	31	2.07 ± 1.21	50	4.78 ± 0.67	-15
	4 h	3.90 ± 0.31	6	1.96 ± 1.55	53	4.29 ± 0.61	-3
	24 h	1.62 ± 0.15	61	2.73 ± 1.10	34	4.86 ± 0.68	-17
Curing process	15 min	4.50 ± 0.48	-8	2.65 ± 0.74	36	4.46 ± 0.51	-7
	30 min	4.86 ± 0.34	-17	1.31 ± 0.20	69	4.53 ± 0.35	-9
	1 h	1.96 ± 0.37	53	3.91 ± 0.84	6	5.28 ± 0.96	-27
	2 h	1.57 ± 0.84	62	2.92 ± 1.24	30	4.88 ± 0.56	-17
	4 h	1.09 ± 0.60	74	3.71 ± 0.38	11	5.02 ± 0.38	-21
Temperature	40 °C	4.20 ± 1.1	-1	2.15 ± 0.28	48	5.42 ± 1.33	-30
	60 °C	1.10 ± 0.07	97	2.33 ± 0.36	44	3.45 ± 0.15	17
	80 °C	3.02 ± 0.15	93	1.57 ± 0.16	62	4.78 ± 0.52	-15
	100 °C	4.52 ± 0.25	-9	1.37 ± 0.19	67	7.45 ± 0.93	-79
	110 °C	4.10 ± 0.68	2	2.12 ± 0.20	49	3.30 ± 0.26	21

* Control: 4.16 ± 0.55 10^6 CFU/ml and 0% efficiency.

4.3.3 Concentration of the silane

Different concentrations of APTES, GPTMS, and PFDTES were investigated as shown in Table 4.1. For APTES, the efficiency of the immobilization of the spores was increased along with the concentration of the silane. In this case, 0.5% and 1% showed similar efficiencies of 71% and 78%, respectively. The concentration of 1% for APTES, however, had the lowest standard deviation and was selected for further optimization. In addition, for GPTMS, much higher concentrations were taken due to the previous unexpected results. As it can be seen in Table 4.1, with higher concentrations of GPTMS the efficiency increases (i.e., spores are immobilized on the glass substrate). The best efficiencies were with a concentration of 60%, followed by a concentration of 100%. It can be noted that even though the concentration of 100% had better standard deviation compared to that of 60%, a white film could be seen (data not shown) on the glass substrate, probably meaning excess of polymerization during the silanization process. This might not be desirable later because it might affect the performance of the biosensor. For this reason, the concentration of 60% GPTMS was used for further experiments. Furthermore, the best concentrations for PFDTES were 1% and 2.5%, with the efficiencies of -192% and -189%, respectively. The concentration of 1% was chosen, since it had the lowest standard deviation compared to that of 2.5%.

4.3.4 Silanization time

Several silanization times were investigated for APTES, GPTMS, and PFDTES as shown in Table 4.1. For APTES, the best efficiency was 61% for 24 h. This silanization time, however, was not taken into consideration due to a white film formed (data not shown) on the glass substrate. Thus, the second best silanization efficiency of 51% for 1 h was selected as the optimal silanization time for APTES. For GPTMS the best silanization time was 72% for 30 min and for PFTDES -44% for 1 h. Generally, the formation of the SAM depends on the reaction time during the silanization process, increasing the thickness of the silane layer with time [20, 28]. In our case, however, no correlation could be seen regarding the silanization time and efficiencies, probably meaning different stabilities of the SAM depending on the silanization time due to the evaluation process.

4.3.5 Curing process

The results of the different curing times investigated for APTES, GPTMS and PFDTES are shown in Table 4.1. The best efficiency of 74% for 4 h was observed for APTES. It can be seen that the efficiency increases along with the different curing times investigated. Although the efficiency of 4 h was the best, the efficiency of 1 h was selected due to its lower standard deviation compared to the others and shorter time. For GPTMS and PFDTES the best efficiencies were 69% for 30 min and -27% for 1 h. In both cases, no correlation could be found between efficiency and curing times. The curing process has been shown to result in cross-linking of organosilane molecules, covalent bond formation to the silica surface, increasing of the resistant against hydrolysis and increasing of the mechanical stability of the organosilane layer [17, 29]. The increasing of the efficiency for APTES along the curing process might be due to the good stability of the silane layer for the evaluation conditions, whereas for GPTMS and PFDTES, the stability of their silane layers seems to be highly affected by the evaluation process.

4.3.6 Temperature

Different silanization temperatures were investigated for APTES, GPTMS and PFDTES as shown in Table 4.1. (please note that all former experiments in sections 4.3.1-4.3.5 have been performed at room temperature). For APTES, the best two efficiencies were 97% and 93% at 60 °C and 80 °C, respectively. For GPTMS and PFDTES the best efficiencies were obtained at 100 °C with 67% and -79%, accordingly. It was again noticeable a white film formation for APTES for all the different silanization temperatures investigated and as mentioned earlier (section 4.3.3) this is not desirable in our case. For this reason, the optimal silanization temperature for APTES was at room temperature. For GPTMS no significant effect was observed compared to room temperature and it was selected as well as the optimal temperature for GPTMS. For PFDTES 100 °C with an efficiency of -79% showed the best result. The temperature effect on the silanization process may be due the acceleration of the kinetics of the organosilanes by increasing their mobility in the solvent and increasing the reaction rate for silanization [30]. For APTES the efficiencies are distinctly increased at 60 °C and 80 °C, but are quite low for the other investigated temperatures; this probably might be due to the capillary forces associated in the drying process at different temperatures. The effect of temperature for GPTMS might be negligible due to the higher evaporation rate of

isopropanol, probably evaporating too fast already at 40 °C. For PFDTES no correlation could be found between efficiencies and temperature.

4.3.7 Contact angle measurements

Water contact angle measurements were conducted to characterize the hydrophilicity or hydrophobicity of the surfaces after silanization. As it can be seen in Figure 4.5 a) and Table 4.2, for APTES the resulting contact angle was 63°, which is consistent with amino-terminated SAMs from the literature [30, 31]. The hydrophilic behavior resulting from the amino-terminated SAMs can be explained by covalent bonding with the amino groups of the spore coat, since the spore coat is mainly composed of proteins with minor amounts of carbohydrates and lipids [32]; another covalent interaction might be between the carboxyl groups from the spore coat and the amino-terminated SAMs. Furthermore non-covalent interactions (hydrophobic forces) between the alkyl moieties and the spore coat could be involved as well due to the SAM orientation. For GPTMS the contact angle was unexpectedly 91° (Table 4.2 and Figure 4.5 b). Generally, reported values from literature for GPTMS are in the range from 34° to 70° [33–35]. However, the silanization parameters for GPTMS were optimized taking into account the resistance of GPTMS against the evaluation conditions (buffer solution with polysorbate). Commonly used parameters for GPTMS were considered at the beginning of the optimization procedure while studying different methods of silanization in liquid phase (see section 4.3.1).

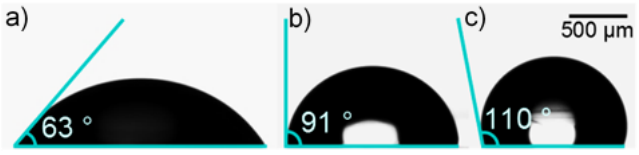

Figure 4.5 Contact angle measurements on glass substrates after silanization with a) APTES, b) GPTMS and c) PFDTES.

A negative effect (negative efficiency) for GPTMS was noticeable probably suggesting that even though some SAMs for GPTMS reported in literature [33–35] will be successfully formed, they might not be stable under the evaluation conditions used in this report. Furthermore, the high contact angle for GPTMS is probably due to the exposure of the alkyl fragments at the surface [35]. This may indicate not only the binding between some epoxy groups and spore coat, but also hydrophobic interactions contributing to the stability of the SAM formed.

Moreover, for PFDTES (Table 4.2 and Figure 4.5 c) the resulting contact angle was 110°, suggesting high hydrophobicity, likely due to the high packing density of the perfluoroalkylsilanes in the SAMs. In addition, the inertness and lipophobic behavior of the SAM formed can inhibit the interaction between perfluoroalkyl moieties and the spore coat, hindering the attachment of spores to the glass substrate silanized with PFDTES.

Table 4.2 Contact angle measurements and roughness of different organosilanes.

Silane	CA (°)	R_q (nm)
Control	≈ 0	0.32
APTES	63	0.98
GPTMS	91	1.34
PFDTES	110	0.99

4.3.8 Atomic force microscopy

AFM was used for further characterization of the morphology and roughness (Rq) of the silanized glass substrates. Figure 4.6 shows representative images of the surface topography for APTES, GPTMS and PFDTES. Figure 4.6 a) was taken as reference; the glass substrate was cleaned as described in section 4.2.2 without hydroxylation. For APTES (Figure 4.6 b) the SAM formed was smooth with a roughness of 0.98 nm (Table 4.2), probably indicating high orderly densities of silane layers on the glass substrate. For GPTMS (Figure 4.6 c) the SAM was partially smooth with a roughness of 1.34 nm (Table 4.2). However, some domains could be seen with a height from 5 nm to 10 nm, likely due to the partial lateral aggregation of terminal groups within the monolayers [35]. Moreover, a similar case can be seen for PFDTES (Figure 4.6 d), where the height of the domains is less than 8 nm with a roughness of 0.99 nm (Table 3.2).

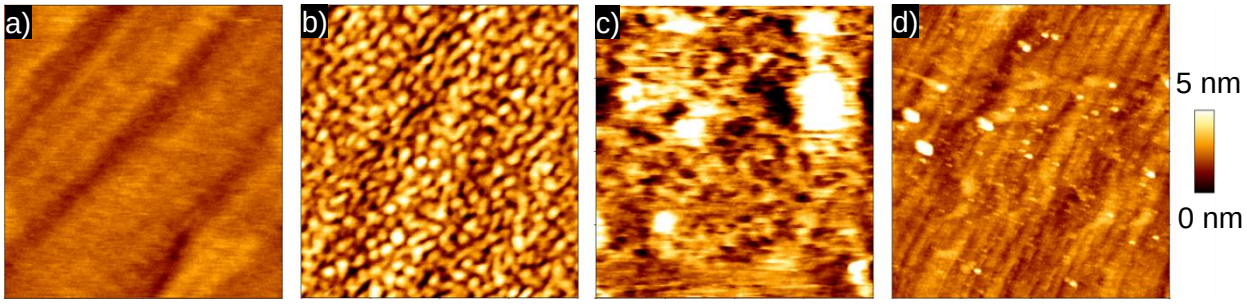

Figure 4.6 Atomic force microscopy images (height) of the silanization on glass substrates (2x2 µm²) with different organosilanes. a) Control, b) APTES, c) GPTES, d) PFDTES.

4.4 Conclusions

In the present work, three different organosilanes (APTES, GPTMS, PFDTES) were investigated for the immobilization of bacterial spores (*B. atrophaeus* DSM 675) on glass substrates, which were used as a model system for spore-based biosensors. In addition, the immobilization of the spores was evaluated by microbiological experiments and the silanized glass substrates were characterized by contact angle measurements and AFM. Different silanization parameters were optimized such as nature of the solvent, concentration of the silane, silanization time, curing time and temperature. The optimized organosilanes were intrinsically resistant to a buffer solution (e.g., Ringer solution) with a polysorbate (e.g., Tween®80) and sonication due to the evaluation process employed in this study. For APTES and GPTMS the spores were successfully immobilized on the glass substrates, whereas for PFDTES the attachment of the spores to the glass substrates was inhibited as expected. Moreover, the contact angle measurements showed higher hydrophobic behavior for GPTMS in contrast to previous reports, suggesting the exposure of alkyl residues at the surface; this might help to increase the resistance of the silane layer to the evaluation process. For APTES and PFDTES the contact angles were in agreement with those expected and reported in literature. Furthermore, from the AFM data it can be seen a smooth and orderly silane layer for APTES, whereas the silane layers for GPTMS and PFDTES were only partially smooth likely due to small domains.

Further investigations may include studying SAM-spore-coat interactions with further silanes (including carboxyl groups, e.g., EDC/NHS coupling), the silanization process on different sensor surface materials (e.g., platinum) and to investigate the influence of the silane layer

on spore-based biosensors, specifically the sensor signal (e.g., by means of impedance measurements).

Acknowledgements

This research was financially supported by the Federal Ministry of Education and Research (Germany), project "Impedipack". The authors are gratefully thankful to Prof. Dr. P. Siegert and Prof. Dr. J. Bongaerts for access to the microbiology laboratory to conduct microbiological evaluations, Prof. Dr. T. Mang for access to the instrument for contact angle measurements, T. Bronder, S. Dantism and J. Oberländer for valuable discussions.

References

[1] W.L. Nicholson, N. Munakata, G. Horneck, H.J. Melosh, and P. Setlow, "Resistance of *Bacillus* endospores to extreme terrestrial and extraterrestrial environments", *Microbiol. Mol. Biol. R.* 64 (3), 548–572 (2000).

[2] B. Setlow, C.A. Loshon, P.C. Genest, A.E. Cowan, C.A. Setlow, and P. Setlow, "Mechanisms of killing spores of *Bacillus subtilis* by acid, alkali and ethanol", *J. Appl. Microbiol.* 92 (2), 362–375 (2002).

[3] P. Setlow, "Spores of *Bacillus subtilis*: their resistance to and killing by radiation, heat and chemicals", *J. Appl. Microbiol.* 101 (3), 514–525 (2006).

[4] D.G. Allison, "A review: taking the sterile out of sterility", *J. Appl. Microbiol.* 87 (6), 789–793 (1999).

[5] R.M. La Ragione, G. Casula, S.M. Cutting, and M.J. Woodward, "*Bacillus subtilis* spores competitively exclude *Escherichia coli* O78:K80 in poultry", *Vet. Microbiol.* 79 (2), 133–142 (2001).

[6] B. Rotman and M.A. Cote, "Application of a real-time biosensor to detect bacteria in platelet concentrates", *Biochem. Biophys. Res. Commun.* 300 (1), 197–200 (2003).

[7] W.A.M. Wolken, J. Tramper, and M.J. van der Werf, "What can spores do for us?", *Trends Biotechnol.* 21 (8), 338–345 (2003).

[8] J. Oberländer, A. Bromm, L. Wendeler, H. Iken, M.P. Durán, A. Greeff, P. Kirchner, M. Keusgen, and M.J. Schöning, "Towards a biosensor to monitor the sterilization efficiency of aseptic filling machines", *Phys. Status Solidi A* 212 (6), 1299–1305 (2015).

[9] A. del Campo and I.J. Bruce, "Substrate patterning and activation strategies for DNA chip fabrication", in *Immobilisation of DNA on Chips,* Springer, Berlin, 2005.

[10] F.W. Hyde, G.R. Hunt, and La Errede, "Immobilization of bacteria and *Saccharomyces cerevisiae* in poly(tetrafluoroethylene) membranes", *Appl. Environ. Microb.* 57 (1), 219–222 (1991).

[11] E. Timofeev, "Regioselective immobilization of short oligonucleotides to acrylic copolymer gels", *Nucleic Acids Res.* 24 (16), 3142–3148 (1996).

[12] B. Arkles, "Hydrophobicity, hydrophilicity and silanes", *Paint Coat. Ind.* 22 (10), 114–125 (2006).

[13] C.M. Halliwell and A.E.G. Cass, "A factorial analysis of silanization conditions for the immobilization of oligonucleotides on glass surfaces", *Anal. Chem.* 73 (11), 2476–2483 (2001).

[14] A.N. Parikh, B. Liedberg, S.V. Atre, M. Ho, and D.L. Allara, "Correlation of molecular organization and substrate wettability in the self-assembly of n-alkylsiloxane monolayers", *J. Phys. Chem.* 99 (24), 9996–10008 (1995).

[15] P. Silberzan, L. Leger, D. Ausserre, and J.J. Benattar, "Silanation of silica surfaces. A new method of constructing pure or mixed monolayers", *Langmuir* 7 (8), 1647–1651 (1991).

[16] N. Aissaoui, L. Bergaoui, J. Landoulsi, J.F. Lambert, and S. Boujday, "Silane layers on silicon surfaces: mechanism of interaction, stability, and influence on protein adsorption", *Langmuir* 28 (1), 656–665 (2012).

[17] D.L. Angst and G.W. Simmons, "Moisture absorption characteristics of organosiloxane self-assembled monolayers", *Langmuir* 7 (10), 2236–2242 (1991).

[18] A.V. Krasnoslobodtsev and S.N. Smirnov, "Effect of water on silanization of silica by trimethoxysilanes", *Langmuir* 18 (8), 3181–3184 (2002).

[19] G.T. Hermanson, "Silane coupling agents", in *Bioconjugate Techniques*, Academic Press, Amsterdam 2008.

[20] Y. Yang, A.M. Bittner, S. Baldelli, and K. Kern, "Study of self-assembled triethoxysilane thin films made by casting neat reagents in ambient atmosphere", *Thin Solid Films* 516 (12), 3948–3956 (2008).

[21] C.R. Vistas, A.C.P. Águas, and G.N.M. Ferreira, "Silanization of glass chips—a factorial approach for optimization", *Appl. Surf. Sci.* 286, 314–318 (2013).

[22] Deutsche Sammlung von Mikroorganismen und Zellkulturen, DSMZ, Braunschweig, http://www.dsmz.de, downloaded at 12.11.2019.

[23] A.B. Schaeffer and M.D. Fulton, "A simplified method of staining endospores", *Science* 77 (1990), 194 (1933).

[24] C.P. Tripp and M.L. Hair, "An infrared study of the reaction of octadecyltrichlorosilane with silica", *Langmuir* 8 (4), 1120–1126 (1992).

[25] J.D. Le Grange, J.L. Markham, and C.R. Kurkjian, "Effects of surface hydration on the deposition of silane monolayers on silica", *Langmuir* 9 (7), 1749–1753 (1993).

[26] A. Ulman, "Formation and structure of self-assembled monolayers", *Chem. Rev.* 96 (4), 1533–1554 (1996).

[27] S.R. Wasserman, Y.T. Tao, and G.M. Whitesides, "Structure and reactivity of alkylsiloxane monolayers formed by reaction of alkyltrichlorosilanes on silicon substrates", *Langmuir* 5 (4), 1074–1087 (1989).

[28] S.G. Thakurta and A. Subramanian, "Fabrication of dense, uniform aminosilane monolayers. A platform for protein or ligand immobilization", *Colloids and Surfaces A: Physicochemical and Engineering Aspects* 414, 384–392 (2012).

[29] J. Kim, P. Seidler, C. Fill, and L.S. Wan, "Investigations of the effect of curing conditions on the structure and stability of amino-functionalized organic films on silicon substrates by Fourier transform infrared spectroscopy, ellipsometry, and fluorescence microscopy", *Surf. Sci.* 602 (21), 3323–3330 (2008).

[30] J.A. Howarter and J.P. Youngblood, "Optimization of silica silanization by 3-aminopropyltriethoxysilane", *Langmuir* 22 (26), 11142–11147 (2006).

[31] W. Wang and M.W. Vaughn, "Morphology and amine accessibility of (3-aminopropyl) triethoxysilane films on glass surfaces", *Scanning* 30 (2), 65–77 (2008).

[32] A. Driks, "*Bacillus subtilis* spore coat", *Microbiol. Mol. Biol. R.* 63 (1), 1–20 (1999).

[33] J.M. Goddard and D. Erickson, "Bioconjugation techniques for microfluidic biosensors", *Anal. Bioanal. Chem.* 394 (2), 469–479 (2009).

[34] M.H. Lee, D. Boettiger, P. Ducheyne, and R.J. Composto, "Self-assembled monolayers of omega-functional silanes: A platform for understanding cellular adhesion at the molecular level", in *Silanes and Other Coupling Agents*, Volume 4, CRC Press, 2007.

[35] I. Luzinov, D. Julthongpiput, A. Liebmann-Vinson, T.A. Cregger, M.D. Foster, and V.V. Tsukruk, "Epoxy-terminated self-assembled monolayers: molecular glues for polymer layers", *Langmuir* 16 (2), 504–516 (2000).

5 Surface functionalization for spore-based biosensors with organosilanes (*Electrochimica Acta*, 241 (2017), 237-243)

Julio Arreola[1,2,†], Jan Oberländer[1,2,†], M. Mätzkow[1], Michael Keusgen[2], Michael J. Schöning[1,3,*]

[1] Institute of Nano- and Biotechnologies, Aachen University of Applied Sciences, Campus Jülich, 52428 Jülich, Germany

[2] Institute of Pharmaceutical Chemistry, Philipps-University Marburg, Marbacher Weg 6-10, 35032 Marburg, Germany

[3] Peter Grünberg Institute, Research Center Jülich GmbH, 52425 Jülich, Germany

[†]These authors contributed equally to this work.

Published in: *Electrochimica Acta*, 241 (2017), 237-243. Reprinted with permission from Elsevier.

Received 30 January 2017; **revised** 03 April 2017; **accepted** 28 April 2017

Keywords: biosensor, silanization, *Bacillus atrophaeus*, endospores, immobilization.

Abstract

In the present work, surface functionalization of different sensor materials was studied. Organosilanes are well known to serve as coupling agent for biomolecules or cells on inorganic materials. 3-(Aminopropyl)triethoxysilane (APTES) was used to attach microbiological spores for the first time to an interdigitated sensor surface. The functionality and physical properties of APTES were studied on isolated sensor materials, namely silicon dioxide (SiO_2) and platinum (Pt) as well as the combined material on sensor level. A

predominant immobilization of spores could be demonstrated on SiO_2 surfaces. Additionally, the impedance signal of APTES-functionalized sensor chips has been investigated.

5.1 Introduction

Under stressful environments (e.g., nutrient-limiting conditions), a variety of bacteria of *Bacilli* and *Clostridia* genus produce spores: a dormant (i.e., no detectable metabolism) cell type, that can withstand a wide range of different stresses such as heat, radiation and oxidizing agents [1–3]. During the dormant state, the spores nonetheless are still able to monitor changes in their surroundings, making them suitable for use as sensitive or recognition elements in biosensor systems [4–8].

Recently, a first type of spore-based biosensor was suggested to evaluate sterilization processes in aseptic filling machines [9]. Such biosensor is illustrated in Figure 5.1. It consists of a glass substrate with temperature sensors and several interdigitated electrodes (IDEs) as transducer elements, where the spores can be immobilized on one of the IDEs due to walls of SU-8 photoresist, whereas the other IDE is utilized as reference sensor (differential setup measurement).

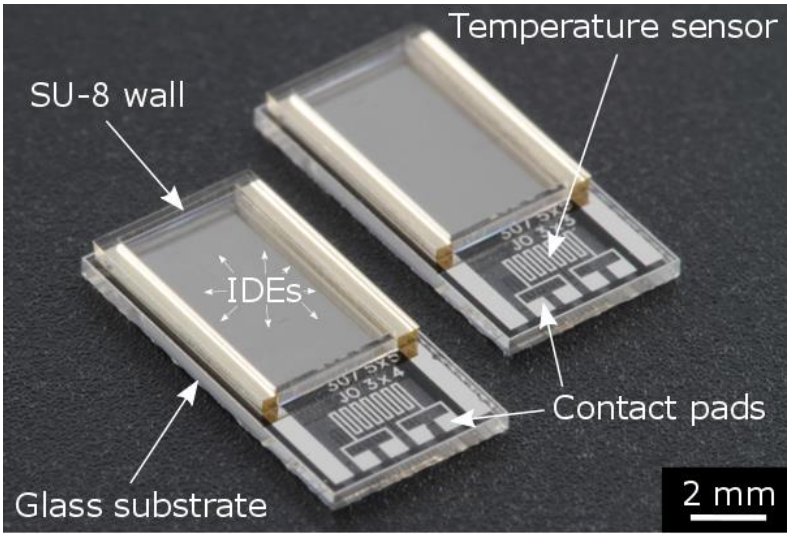

Figure 5.1 Spore-based biosensor. Differential set-up of two glass chips with temperature sensors and interdigitated electrodes (IDEs).

The principle of the spore-based biosensor is depicted in Figure 5.2. First, the spores are chemically immobilized (e.g., via silanization) onto the sensor surface to prevent any detachment during the sterilization process. Then, the biosensor is exposed to a vaporized hydrogen peroxide (H_2O_2) hot gas stream (e.g., 240 °C, 10 m^3h^{-1}) and the sensor signal change (e.g., impedance) before and after sterilization is evaluated. The signal change can be

correlated to the morphology deformation of the spores due to the H_2O_2 concentration. In general, the H_2O_2 concentration applied defines the grade of sterilization in aseptic food processes and the dosed H_2O_2 concentration can serve as a sensor signal to monitor the sterilization efficiency [10, 11]. Nonetheless, for industrial standards, additional microbiological challenge test routines such as end-point test and count-reduction test are necessary for validation [12]. A reliably functioning spore-based biosensor might enable the combination of both, the standard microbiological tests and H_2O_2 monitoring by chemical gas sensors.

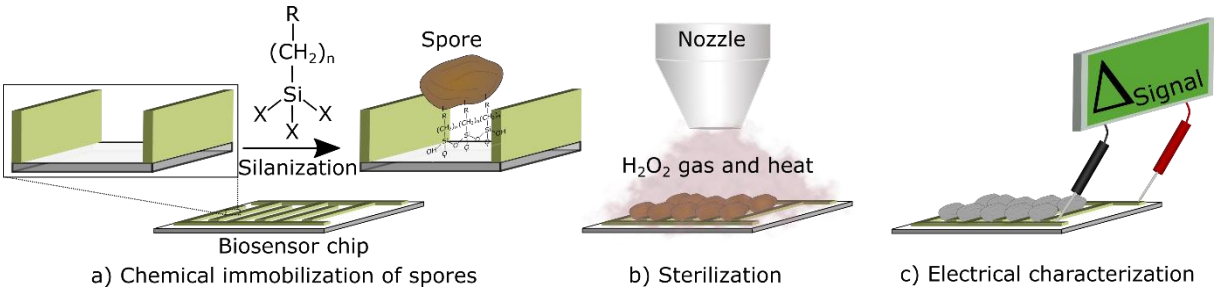

Figure 5.2 Principle of the spore-based biosensor. The spores are chemically immobilized onto the sensor substrate (a). Then, the spore-based biosensor is sterilized with H_2O_2 and heat (b) and finally due to the sterilization process, the morphology of the spores is compromised and this causes a change on the sensor signal (c).

On the other hand, for developing a spore-based biosensor for sterilization processes the immobilization of spores is the most challenging aspect in order to ensure its reliability and reproducibility. Organosilanes have been used previously to functionalize glass substrates to provide moieties suitable for covalent attachment of spores [13, 14]. They are a versatile option as they promote the attachment of molecules through their terminal reactive groups (e.g., amines) and show likewise self-assembly behavior [15, 16]. Generally, the silanization process (organosilane formation on a surface) involves four phases: hydrolysis, condensation, hydrogen bond formation and curing [17, 18]. In the first phase, the organosilane groups are hydrolyzed to form highly reactive silanols (Si-OH). During the second phase, the silanols undergo condensation to form siloxanes (Si-O-Si) over the surface. In the third phase, the hydroxyl groups (OH) from the surface interact with the hydrolyzed organosilanes via hydrogen bonding. In the last phase, the silicon of the organosilane and the silicon of the surface are covalently bonded with the associated loss of water molecules by curing.

In the present work, two biosensor substrates (SiO_2, Pt) are functionalized with the organosilane 3-(Aminopropyl)triethoxysilane (APTES) and characterized by means of atomic force microscopy, contact angle measurement and microbiological evaluation tests for the immobilization of *Bacillus atrophaeus* spores (DSM 675). Furthermore, the influence of the silane layer on the biosensors' signal is investigated by means of impedance spectroscopy measurements.

5.2. Experimental

5.2.1 Materials

The following chemicals have been used for the surface functionalization and the microbiological methods: APTES (98% v/v), toluene (99% v/v), ethanol (99% v/v), acetone (99% v/v), isopropanol (99% v/v), Tween®80 were obtained from Sigma-Aldrich. Plate count agar (PCA), Ringer solution tablets and manganese (II) sulphate monohydrate were obtained from Merck Millipore. Dry meat extract and peptone from meat were purchased from VWR.

5.2.2 Fabrication of the silicon oxide (SiO_2), platinum (Pt) substrates and sensors

5.2.2.1 SiO_2 substrates

As initial material a boron-doped silicon wafer (ρ = 1-10 Ωcm, <100>) was chosen with 30 nm of SiO_2 thermally grown by dry oxidation at 1,000 °C for 30 min. For the further functionalization and characterizations, the wafer was diced into 10 x 10 mm^2 pieces and cleaned for 5 min sequentially in ultrasonic bath with acetone, isopropanol and deionized (DI) water, respectively.

5.2.2.2 Pt substrates

The platinum substrates were fabricated (to characterize the sensor electrode material) as follows: 10 nm of Ti and 100 nm of Pt were deposited on a glass wafer (Borofloat33®, Schott, Germany) with an e-beam evaporation process (Univex 350, Leybold). In addition, the wafer was diced into 10 x 10 mm^2 pieces and cleaned for 5 min sequentially in ultrasonic bath with acetone, isopropanol and deionized (DI) water.

5.2.2.3 Sensor fabrication

For the sensor fabrication conventional photolithography methods were applied. The fabrication steps are summarized in Figure 5.3. In a first step, titanium and platinum were deposited on a glass wafer by an e-beam evaporation process. The thicknesses of these metal layers were chosen as 10 nm and 100 nm, respectively. A negative photoresist AZ 2020 nLOF was applied as masking layer for the subsequent reactive ion-etching (RIE) process. The lithography mask applied to pattern the photoresist layer defines the IDE structures with a finger width and gap of 5 µm. A total number of 614 electrode fingers and a length of 3.25 mm is resulting in a sensing area of about 20 mm². The metal layers were patterned by a reactive ion-etching process (RIE, Plasmalab 100, Oxford Instruments plc, United Kingdom) (Figure 5.3 e). Oxygen plasma was applied to remove the photoresist masking layer (Figure 5.3 f)). An SU-8 wall was fabricated to enable a precise immobilization of microbiological samples on the IDE (Figure 5.3 g). After these fabrication steps the wafer was diced into single chips size of 5 x 10 mm². The single sensors were cleaned in acetone, isopropanol and DI water prior to further characterization and functionalization procedures.

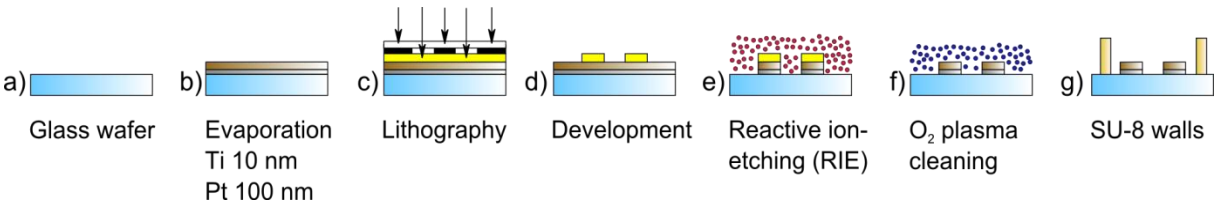

Figure 5.3 Schematic view of the sensor fabrication steps: a) cleaned glass wafer, b) deposition of the electrode materials, c-d) structuring of a photoresist etching mask, e) transfer of the electrode pattern by reactive ion-etching, f) removal of photoresist mask, g) SU-8 walls to define the sensor-active regions with immobilized spores onto the interdigitated electrodes.

5.2.3 Surface functionalization

Pt-, SiO_2 substrates and the sensors were silanized with a modified protocol for the immobilization of bacterial spores developed in [13].

5.2.3.1 Hydroxylation

The mentioned substrates and sensors were firstly cleaned to remove organic contaminants in a series of ultrasonic baths for 5 min for each step in acetone, isopropanol and deionized (DI) water, respectively. Subsequently, their surface was activated with hydroxyl groups (hydroxylation) by oxygen plasma treatment (Femto PCCE, Diener electronic GmbH + Co. KG) at 100 W for 2 min.

5.2.3.2 APTES

For the silanization with APTES the drop-casting method was applied for all substrates and sensors. A solution of 1% APTES in toluene was pipetted onto the surfaces and incubated for 1 h. In order to avoid unwanted reactions (e.g., polymerization) from the organosilane under atmosphere conditions, the silanization has been performed in a glove box under nitrogen atmosphere.

The excess of APTES was washed out from the substrates and sensors with a series of ultrasonic baths in toluene and ethanol for 5 min each step. At the end, a curing process was performed to increase stability of the organosilanes by cross-linking of the silane molecules. The substrates and the sensors were cured at 110 °C for 1 h.

5.2.4 Physical characterizations of the SiO_2- and Pt substrates

5.2.4.1 Contact angle measurements

Contact angle measurements on all substrates were conducted to demonstrate the successful surface functionalization. Therefore, the water contact angles were measured before and after the silanization process. The optical contact angle system OCA (Dataphysics, Germany) was used for the measurements performed at room temperature and the data were analyzed with the software SCA 20.

5.2.4.2 Atomic force microscopy

The morphology and topology of the samples were analyzed with a BioMat Workstation (JPK Instruments, Germany). The surface roughness was chosen to quantify these analyses. The scans (2 x 2 μm^2) were performed in tapping mode at 512 pixels per line, scanning at 0.2-0.4

Hz under ambient conditions. Silicon cantilevers (Arrow NCR, NanoWorld AG, Switzerland) with a spring constant of 42 N/m and resonant frequency of 285 kHz were used.

5.2.4.3 Scanning electron microscopy

Surface characterizations of the functionalized sensor surface have been conducted on a Jeol JSM-7800F (Japan) scanning electron microscope.

5.2.4.4 Ellipsometry

The thickness of the APTES layer was characterized by spectroscopic nulling ellipsometry (EP3, Accurion GmbH, Germany). The angle of incidence used was 65° over a wavelength range of 360-1002 nm.

5.2.5 Microbiological methods

5.2.5.1 Bacterial culture, sporulation and spore purification

The strain of *Bacillus atrophaeus* (DSM 675) was purchased from IVV Fraunhofer, Germany. All procedures were performed aseptically under a laminar flow hood. Bacterial culture, sporulation and spore purification were carried out as stated in [13]. *B. atrophaeus* cells were grown at 30 °C in 10 ml of complex medium (3 g/l meat extract dry, 5 g/l peptone) for 24 h. The sporulation was initiated by inoculation of all cells in 200 ml of freshly complex medium with 10 mg/l $MnSO_4$ and an incubation at 30 °C for 7 days. After the incubation, the spores were harvested by centrifugation at 4,000 rpm (A-4-81; Centrifuge 5810R, Eppendorf, Germany) at 20 °C and then resuspended in Ringer solution with 0.01% Tween®80. After this, the spores were washed at least five times in Ringer solution with 0.01% Tween®80 and three times in DI water. Subsequently, the spores were pasteurized in a water bath at 80 °C for 20 min, centrifuged and resuspended in DI water. The spore suspension was free of vegetative cells (>95%). The spore concentration was determined by serial dilutions and plating, resulting in a final concentration of 10^8 CFU/ml.

5.2.5.2 Microbiological evaluation

In order to evaluate the efficiency of the silanization process, the spore recovery method, serial dilutions and spread-plate methods were utilized [13]. For the spore recovery, 10 µl of the main spore suspension of *B. atrophaeus* were inoculated onto different silanized and non-

silanized surfaces and dried under a laminar flow hood for 60 min. The immobilized spores were recovered from the surfaces by resuspending them in 10 ml of Ringer solution with 0.01% Tween®80 and placing them in ultrasonic bath for 10 min. After that, each spore suspension was diluted by serial dilutions, spread-plated on PCA and cultivated at 30 °C for 24 h. The colony forming units (CFU) were counted and a final cell concentration (CFU/ml) of the recovered spores was obtained (N_s). The number of spores of the different solutions was compared to the total cell concentration (CFU/ml) found in the main spore suspension (N_t). As a result, the ratio (r) between recovered spores (N_s) and the total number of spores from the main suspension (N_t) can be determined by:

$$\mathrm{r} = \left(\frac{\mathrm{N_s}}{\mathrm{N_t}}\right) \times 100 \qquad (5.1)$$

In Eq. (5.1), the lower the N_s concentration, the better the silanization process (i.e., more spores remained on the substrates or sensors).

5.2.6 Electrical characterization of the sensors

In order to characterize the electrical parameters of the silane layer on the sensors, impedance measurements were performed. All measurements were conducted on a point-probe station with a precision LCR meter (E4980A, Agilent Technologies, United States). An excitation voltage of 0.02 V without a DC bias was applied. The impedance characteristics were monitored over a frequency range between 200 Hz and 200 kHz. In order to avoid effects of air humidity- and temperature variations the measurements were conducted in a vacuum chamber.

5.3. Results and discussion

5.3.1 Physical characterizations of APTES on SiO_2- and Pt substrates

5.3.1.1 Contact angle measurements

Water contact angle measurements were performed to characterize the hydrophilicity or hydrophobicity of the SiO_2 and Pt substrates after silanization with APTES as shown in Tab. 5.1. Control chips were used as a reference and cleaned in a series of ultrasonic baths for 5 min for each step in acetone, isopropanol and deionized DI water, respectively. For SiO_2, a contact angle of 73° was obtained with APTES. This value is in good agreement with amino-

terminated films from literature [19, 20]. Furthermore, the contact angle of Pt after APTES was 98°. Water contact angles after silanization on Pt surfaces are similar than that from SiO_2 [21]. In our experiment, the contact angle on Pt was more hydrophobic in comparison with that of SiO_2. This difference may come from the lack of oxide species produced after O2 plasma (i.e., the less oxide species, the less OH groups available), since no significant differences were found between contact angles before and after O_2 plasma treatments for Pt (data not shown). Therefore, the silanization process might be unfavorably affected for Pt, probably indicating alkyl fragments exposed at the surface [15]. Moreover, the outermost layer of the spore coat (spore surface) is mainly formed from proteins, including CotB, CotC, CotG and CotZ [22, 23]. APTES may bind to these proteins by their N- or C-termini producing a covalent bond by cross-linking due to the nature of the spore deposition (i.e., a droplet of DI water with spores is let dried at the sensor surface). In addition, non-covalent interactions (hydrophobic forces) between the alkyl fragments and the spores coat may be involved due to the orientation of the silane layer.

Table 5.1 Contact angle measurements and roughness of Pt- and SiO_2 substrates silanized with APTES.

Material	Silane	Contact angle (°)	Roughness (Rq) (nm)
SiO_2	Control	47	0.11
	APTES	73	0.86
Pt	Control	72	2.72
	APTES	98	6.57

5.3.1.2 Atomic force microscopy and ellipsometry

The morphology and roughness (R_q) of the silanized SiO_2 and Pt was further characterized with AFM and ellipsometry. Representative images of their surface topography for APTES are shown in Figure 5.4. Figure 5.4 a) and 5.4 c) were taken as a reference and were cleaned as described in section 5.2.3.1. The increase of roughness (R_q) for SiO_2 (0.11 nm compared to 0.86 nm) and Pt (2.72 nm compared to 6.57 nm) silanized with APTES suggest the presence

of an organic layer as it can be also seen from Tab. 5.1. In addition, the increases of roughness can be attributed to domains or agglomeration of APTES molecules on the surface of SiO_2 (Figure 5.4 b) and Pt (Figure 5.4 d). These domain diameters for SiO_2 are in the range from 5 nm to 10 nm and for Pt from 5 nm to 30 nm. Furthermore, the APTES thickness obtained with ellipsometry was 6.1 ± 1.15 nm.

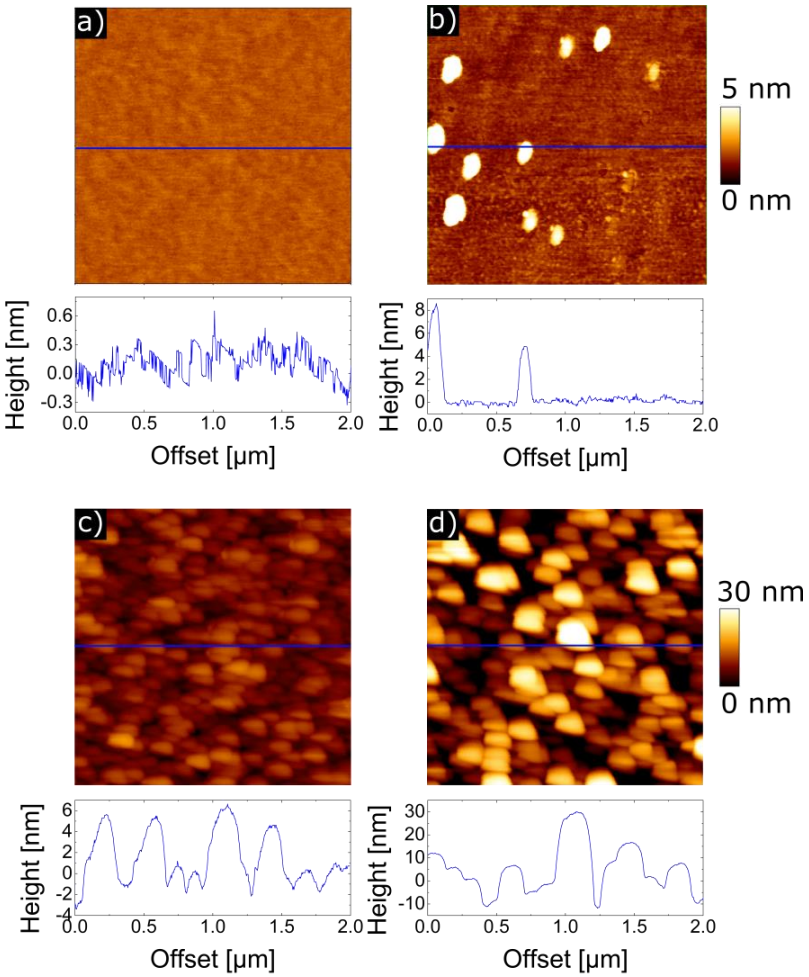

Figure 5.4 Atomic force microscopy images 2 x 2 µm² (height) of the silanization on SiO_2- and Pt substrates with APTES. a) control SiO_2, b) SiO_2 with APTES, c) control Pt, d) Pt with APTES.

5.3.2 Microbiological evaluation of the SiO_2-, Pt substrates and sensors

The results of the immobilization study of spores with APTES on SiO_2-, Pt substrates and interdigitated sensor chips are depicted in Figure 5.5. The control substrates were cleaned as mentioned in section 5.2.3.1 without further silanization. For SiO_2 and Pt no significant

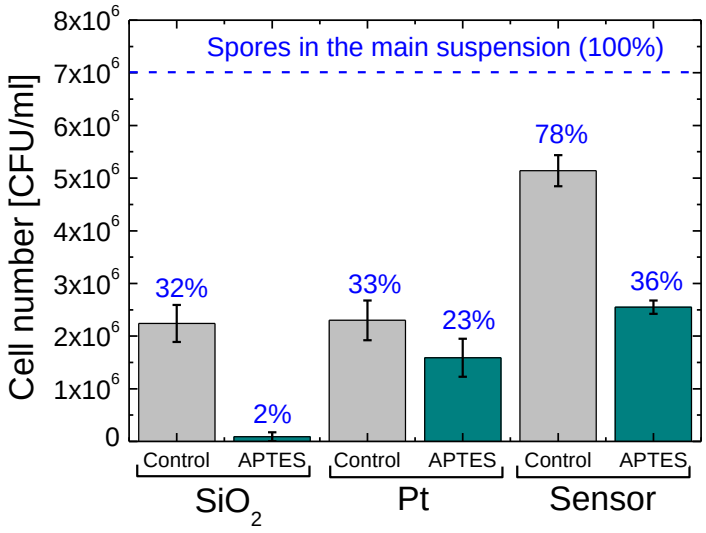

Figure 5.5 Microbiological evaluation of the immobilization of the spores with APTES on SiO_2, Pt and interdigitated sensor chips. The error bars indicate the standard deviations of four samples for each group.

difference could be observed between substrates with a spore recovery of 32% and 33%, respectively. The opposite case was found for the sensor with a spore recovery of 78%. There are several factors that can affect the adhesion strength between the spores and the substrates such as hydrophobic interactions, surface topography or spore's surface [24]. In this case, no difference could be observed between a relatively smooth (SiO_2) and a rough (Pt) surface. However, a combination of both surfaces and a change from a 2D surface to a 3D surface (sensor) showed a substantial decrease of the spore adhesion. Since both materials alone remained almost the same, this may suggest that the decrease of the spore adhesion may be affected by the 3D geometry of the IDEs. Future studies should address this influence in more detail. Moreover, the results exhibit that the best immobilization of spores could be achieved on APTES-functionalized SiO_2 surfaces, as only 2% of the spores could be recovered. In comparison to that of the Pt substrate, 23% of the spores were found in the solution. A reason for the reduced or lower adhesion could be the higher hydrophobicity and roughness of the surface (sections 5.3.1, 5.3.2) compared to that of the SiO_2 substrates. In combination with the applied method to evaluate the immobilization, the bonding between APTES layer and the Pt surface might be less stable in the buffer solution as for the SiO_2 substrate [25]. As a result, the silane molecules probably detach from the Pt surface at the mentioned conditions. Furthermore, for the sensors, 36% of the spores were decoupled. Since the sensor consists mainly of a combination of both materials (glass (SiO_2) and Pt), it is

probably expected that the percentage of detached spores would be between those values. However, the geometry of the IDE structures may play as well an important role in the immobilization of spores due to the spore recovery method. This may be illustrated in Figure 5.6; Figure 5.6 a-c) shows SiO_2, Pt and the biosensor substrates, respectively.

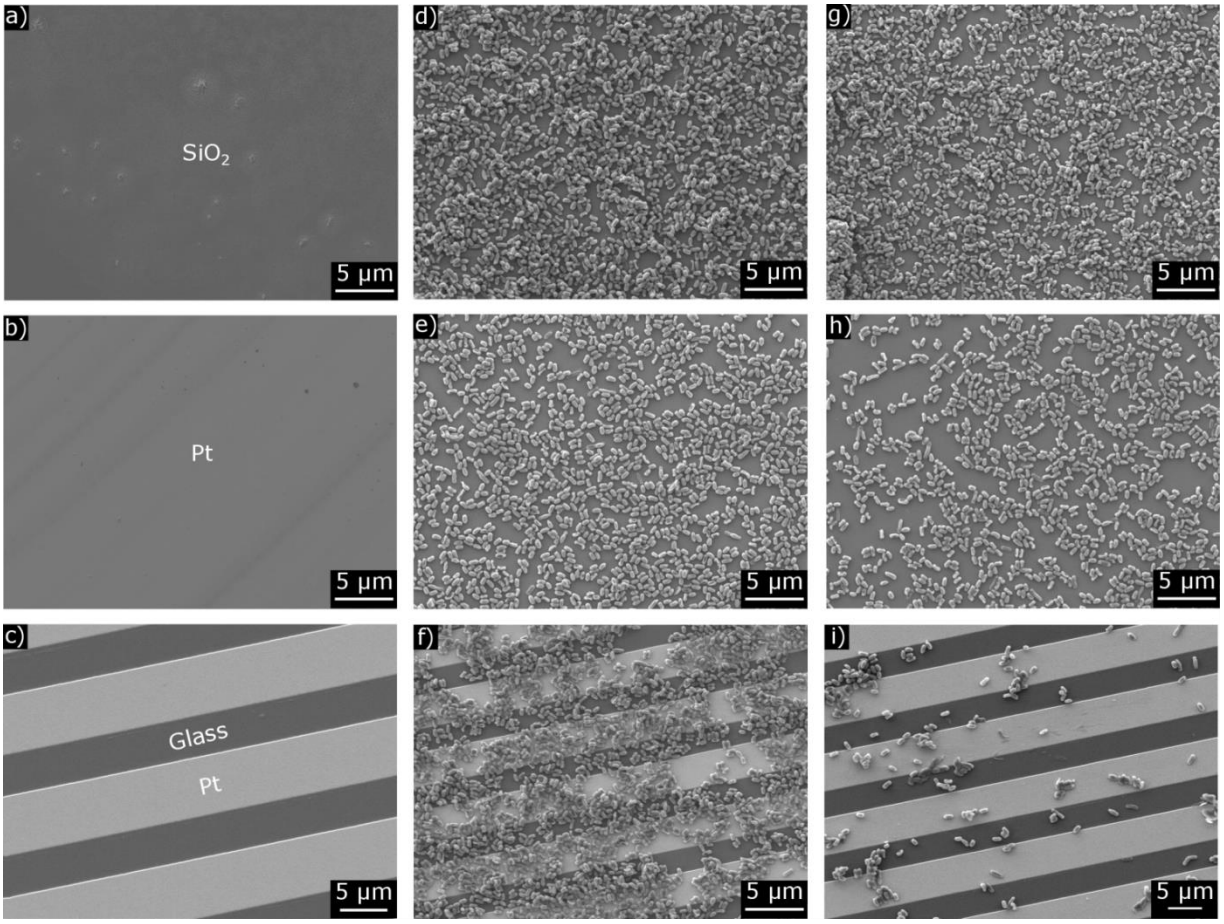

Figure 5.6 Scanning electron microscope images of the spore recovery method. APTES-functionalized surfaces for: a) SiO_2, b) Pt and c) biosensor chips with interdigitated electrodes. Immobilized spores on their respective surfaces (d-f). Remaining spores on the sensor surface after the spore recovery method (g-i).

In addition, in Figure 5.6 d-f) spores immobilized on their respective surfaces can be observed. Finally, after the spore recovery method, the spores are detached (Figure 5.6 g-i) so they can be found in their respective spore suspension. One of the main differences between the substrates and the sensors is the 3D structure obtained from the IDEs. The spores seem to attach better to the planar surfaces (substrates) compared to their 3D counterparts on the sensor structure. This result can be observed for all the surfaces from the control groups (Figure 5.5). Therefore, future investigations will explicitly study the influence of the 3D

geometry of the IDEs (e.g., thickness of Pt electrodes) with respect to the *B. atrophaeus* attachment on the sensor surface. Nevertheless, APTES has been shown to enhance the attachment of spores for all the investigated substrates distinctly.

5.3.3 Impedance measurements of the sensors with APTES

To study the influence of APTES on the sensor signal, impedance characterizations were performed before and after the sensor functionalization. As a base line the newly produced and cleaned sensor structures were investigated under vacuum conditions to exclude external disturbing factors such as variations of air humidity and temperature.

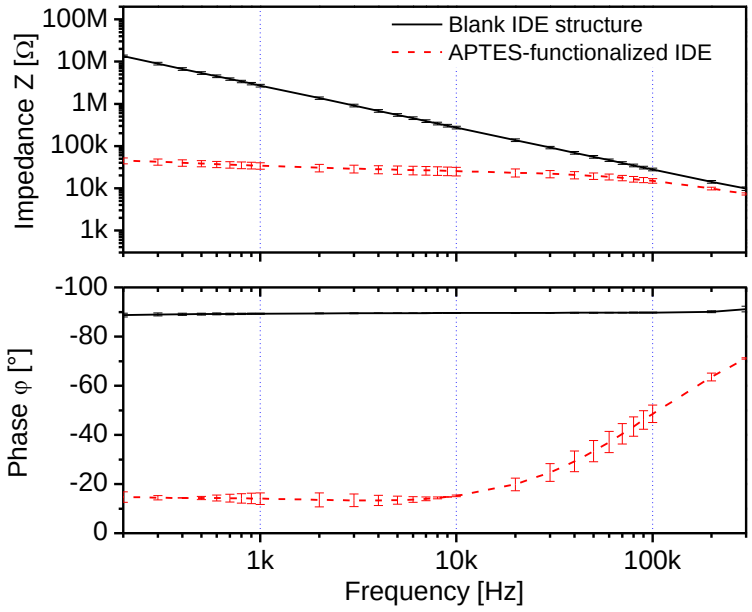

Figure 5.7 Bode plots of interdigitated electrodes before (black line) and after functionalization with APTES (red-dashed line). Lines represent the mean values of three independent sensors and the error bars indicate the standard deviations.

The resulting impedance signal depicts a capacitive sensor behavior, negative slope of the impedance plot and a phase of about -90° (Figure 5.7 (black plots) in impedance (top) and phase diagram (bottom)). The Bode diagram shows the mean and standard deviation of three independent IDE structures. After functionalization of the sensor surface with APTES the impedance signal was recorded again (Figure 5.7). In comparison to the impedance plot of a non-functionalized sensor, it can be observed that the sensor impedance decreased, and a resistive characteristic is present (phase of about -20°). This increase in electrical conductivity can be interpreted by different hypotheses. For instance, the APTES molecules can serve as

electron donor on the surface to be functionalized and enhance thereby the electrical conductivity [26–29]. Another possible assumption is that the permittivity between the electrode structure changes due to the adsorbed APTES monolayer as investigated in [30], whereby the capacitive characteristics are changing at frequencies above 10 kHz. Furthermore, the improved conductivity could also be related to electron tunneling effects occurring in the self-assembled monolayer, as discussed by [31, 32]. The change of electrical properties of the APTES functionalization combined with the microbiological spores at the sensor surface is subject of the ongoing research. Succeeding experiments will focus on signal changes of the immobilized spores as well as in combination with the sterilization process at various process conditions such as different H_2O_2 concentrations.

5.4. Conclusions

In this work, the surface functionalization of transducer chips for biosensors with the organosilane APTES has been investigated. The immobilization of bacterial spores was studied on different materials to be applied in sensor fabrication, namely silicon dioxide (SiO_2), platinum (Pt) and the combination on sensor level consisting of glass (SiO_2) and platinum. In a first attempt, the silanization has been proven by analyzing the wettability by means of contact angle measurements. These measurements have demonstrated successful surface modifications. Furthermore, AFM- and ellipsometric analyses have been conducted to study the surface morphology as well as the resulting change in surface roughness (R_q) supporting the successful coupling of APTES.

Moreover, a microbiological evaluation of the immobilization of spores on the substrates (SiO_2, Pt) and sensors with APTES was performed. SiO_2 showed the best immobilization of the spores. In addition, the immobilization of spores on Pt was negatively affected by the high hydrophobicity and roughness of the silane layer. Furthermore, the detachment of the spores was influenced by the geometry of the IDEs as well as by the silanization on the mixture of both investigated materials.

Additionally, electrochemical studies of the sensors have been realized under vacuum conditions. The electrochemical measurements have revealed a change in the impedance spectrum after silanization with APTES. The functionalized sensors demonstrated resistive behavior at low frequencies (200 Hz-10 kHz). In future, electrochemical characterizations

combining the APTES functionalization together with the microbiological spores on the sensor surface need to be performed.

Acknowledgements

The project was financially supported by the Federal Ministry of Education and Research, Germany, Project: "ImpediPack" (Fund. No.: 03FH012I3). The authors are gratefully thankful to Prof. Dr. P. Siegert and Prof. Dr. J. Bongaerts for access to the microbiology laboratory to conduct microbiological evaluations, Prof. Dr. T. Mang for access to the instrument for contact angle measurements, H. Iken for assisting the fabrication of the spore-based biosensors, D. Rolka for the scanning electron microscopy measurements and L. Breuer for the ellipsometry measurements.

References

[1] W.L. Nicholson, N. Munakata, G. Horneck, H.J. Melosh, and P. Setlow, "Resistance of *Bacillus* endospores to extreme terrestrial and extraterrestrial environments", *Microbiol. Mol. Biol. R.* 64 (3), 548–572 (2000).

[2] B. Setlow, C.A. Loshon, P.C. Genest, A.E. Cowan, C.A. Setlow, and P. Setlow, "Mechanisms of killing spores of *Bacillus subtilis* by acid, alkali and ethanol", *J. Appl. Microbiol.* 92 (2), 362–375 (2002).

[3] P. Setlow, "Spores of *Bacillus subtilis*: their resistance to and killing by radiation, heat and chemicals", *J. Appl. Microbiol.* 101 (3), 514–525 (2006).

[4] D.G. Allison, "A review: taking the sterile out of sterility", *J. Appl. Microbiol.* 87 (6), 789–793 (1999).

[5] N. Kumar, G. Thakur, H.V. Raghu, N. Singh, P.K. Sharma, V.K. Singh, A. Khan, M. Balhara, L.R. Avinash, S. Kouser, N. Tehri, R. Gopaul, and S. Arora, "Bacterial spore based biosensor for detection of contaminants in milk", *J. Food. Process. Technol.* 04 (11), 1–6 (2013).

[6] R.M. La Ragione, G. Casula, S.M. Cutting, and M.J. Woodward, "*Bacillus subtilis* spores competitively exclude *Escherichia coli* O78:K80 in poultry", *Vet. Microbiol.* 79 (2), 133–142 (2001).

[7] M.L. López Rodriguez, C. Benimeli, R.E. Madrid, and C.E. Giacomelli, "A simple *Streptomyces* spore-based impedimetric biosensor to detect lindane pesticide", *Sensor Actuat. B-Chem.* 207, 447–454 (2015).

[8] B. Rotman and M.A. Cote, "Application of a real-time biosensor to detect bacteria in platelet concentrates", *Biochem. Bioph. Res. Co.* 300 (1), 197–200 (2003).

[9] J. Oberländer, A. Bromm, L. Wendeler, H. Iken, M.P. Durán, A. Greeff, P. Kirchner, M. Keusgen, and M.J. Schöning, "Towards a biosensor to monitor the sterilization efficiency of aseptic filling machines", *Phys. Status Solidi A* 212 (6), 1299–1305 (2015).

[10] P. Kirchner, Y.A. Ng, H. Spelthahn, A. Schneider, H. Henkel, P. Friedrich, J. Kolstad, J. Berger, M. Keusgen, and M.J. Schöning, "Gas sensor investigation based on a catalytically activated thin-film thermopile for H_2O_2 detection", *Phys. Status Solidi A* 207 (4), 787–792 (2010).

[11] P. Kirchner, J. Oberländer, H.-P. Suso, G. Rysstad, M. Keusgen, and M.J. Schöning, "Monitoring the microbicidal effectiveness of gaseous hydrogen peroxide in sterilization processes by means of a calorimetric gas sensor", *Food Control* 31 (2), 530–538 (2013).

[12] Verband Deutscher Maschinen- und Anlagenbau e.V. (VDMA), "Code of practice: filling machines of VDMA hygiene class V: testing the effectiveness of packaging sterilization devices", *VDMA-Fachverbandsschriften* 6, 1–16 (2008).

[13] J. Arreola, M. Mätzkow, M.P. Durán, A. Greeff, M. Keusgen, and M.J. Schöning, "Optimization of the immobilization of bacterial spores on glass substrates with organosilanes", *Phys. Status Solidi A* 213 (6), 1463–1470 (2016).

[14] T.J. Park, K.-B. Lee, S.J. Lee, J.P. Park, Z.-W. Lee, S.-K. Choi, H.-C. Jung, J.-G. Pan, S.Y. Lee, and I.S. Choi, "Micropatterns of spores displaying heterologous proteins", *J. Am. Chem. Soc.* 126 (34), 10512–10513 (2004).

[15] R.G. Acres, A.V. Ellis, J. Alvino, C.E. Lenahan, D.A. Khodakov, G.F. Metha, and G.G. Andersson, "Molecular structure of 3-aminopropyltriethoxysilane layers formed on silanol-terminated silicon surfaces", *J. Phys. Chem. C* 116 (10), 6289–6297 (2012).

[16] J. Landoulsi, M.J. Genet, K. El Kirat, C. Richard, S. Pulvin, and P.G. Rouxhet, "Silanization with APTES for controlling the interactions between stainless steel and biocomponents: reality vs. expectation", in *Biomaterials: physics and chemistry,* InTech, 2011.

[17] B. Arkles, "Hydrophobicity, hydrophilicity and silanes", *Paint Coat. Ind.* 22 (10), 114–125 (2006).

[18] C.M. Halliwell and A.E.G. Cass, "A factorial analysis of silanization conditions for the immobilization of oligonucleotides on glass surfaces", *Anal. Chem.* 73 (11), 2476–2483 (2001).

[19] S.E. Asenath and W. Chen, "How to prevent the loss of surface functionality derived from aminosilanes", *Langmuir* 24 (21), 12405–12409 (2008).

[20] J.A. Howarter and J.P. Youngblood, "Optimization of silica silanization by 3-aminopropyltriethoxysilane", *Langmuir* 22 (26), 11142–11147 (2006).

[21] J.C. Chang and B.C. Wheeler. *Using Multi-Electrode Arrays,* "Pattern technologies for structuring neuronal networks on MEAs", in *Advances in Network Electrophysiology*, Springer Science and Business Media, Boston 2006, 153-189.

[22] A. Iwanicki, I. Piątek, M. Stasiłojć, A. Grela, T. Lęga, M. Obuchowski, and K. Hinc, "A system of vectors for *Bacillus subtilis* spore surface display", *Microb. Cell Fact.* 13 (1), 30–38 (2014).

[23] J.-G. Pan, S.-K. Choi, H.-C. Jung, and E.-J. Kim, "Display of native proteins on *Bacillus subtilis* spores", *FEMS Microbiol. Lett.* 358 (2), 209–217 (2014).

[24] C. Faille, C. Jullien, F. Fontaine, M.-N. Bellon-Fontaine, C. Slomianny, and T. Benezech, "Adhesion of *Bacillus* spores and *Escherichia coli* cells to inert surfaces. Role of surface hydrophobicity", *Can. J. Microbiol.* 48 (8), 728–738 (2002).

[25] M. Zhu, M.Z. Lerum, and W. Chen, "How to prepare reproducible, homogeneous, and hydrolytically stable aminosilane-derived layers on silica", *Langmuir* 28 (1), 416–423 (2012).

[26] J. Kong and H. Dai, "Full and modulated chemical gating of individual carbon nanotubes by organic amine compounds", *J. Phys. Chem. B.* 105 (15), 2890–2893 (2001).

[27] J. Li and N. Wu, *Biosensors Based on Nanomaterials and Nanodevices*, CRC Press, Boca Raton, Florida, USA 2013, 375-389.

[28] M. Song, J.-W. Kang, D.-H. Kim, J.-D. Kwon, S.-G. Park, S. Nam, S. Jo, S. Yoon Ryu, and C. Su Kim, "Self-assembled monolayer as an interfacial modification material for highly efficient and air-stable inverted organic solar cells", *Appl. Phys. Lett.* 102 (14), 143303-143305 (2013).

[29] T.H. Tran, J.-W. Lee, K. Lee, Y.D. Lee, and B.-K. Ju, "The gas sensing properties of single-walled carbon nanotubes deposited on an aminosilane monolayer", *Sensor Actuat. B-Chem.* 129 (1), 67–71 (2008).

[30] A. Markov, K. Greben, D. Mayer, A. Offenhäusser, and R. Wördenweber, "In situ analysis of the growth and dielectric properties of organic self-assembled monolayers: a way to tailor organic layers for electronic applications", *ACS Appl. Mater. Inter.* 8 (25), 16451–16456 (2016).

[31] S. Casalini, C.A. Bortolotti, F. Leonardi, and F. Biscarini, "Self-assembled monolayers in organic electronics", *Chem. Soc. Rev.* 46 (1), 40–71 (2017).

[32] C.S.S. Sangeeth, A. Wan, and C.A. Nijhuis, "Equivalent circuits of a self-assembled monolayer-based tunnel junction determined by impedance spectroscopy", *J. Am. Chem. Soc.* 136 (31), 11134–11144 (2014).

6 Toward an immobilization method for spore-based biosensors in oxidative environment (*Electrochimica Acta*, 302 (2019), 394-401)

Julio Arreola[1,2], Michael Keusgen[2], Michael J. Schöning[1,3]

[1] Institute of Nano- and Biotechnologies, Aachen University of Applied Sciences, Campus Jülich, 52428 Jülich, Germany

[2] Institute of Pharmaceutical Chemistry, Philipps-University Marburg, Marbacher Weg 6-10, 35032 Marburg, Germany

[3] Institute of Complex Systems 8, Research Centre Jülich GmbH, 52425 Jülich, Germany

Published in: *Electrochimica Acta*, 302 (2019), 394-401. Reprinted with permission from Elsevier.

Received 19 September 2018; **revised** 08 January 2019; **accepted** 26 January 2019

Keywords: biosensor, spores, *Bacillus atrophaeus*, APTES, immobilization.

Abstract

Microbiological investigations are the state-of-the-art method to evaluate aseptic sterilization machines. Recently, different sensors have been introduced to overcome these time-consuming and lab-intensive procedures, for example, calorimetric sensors or spore-based biosensors. The former are developed from microbiological spores, which have to be properly immobilized on the sensor's surface to provide a reliable and consistent sensor signal in order to evaluate sterilization processes with gaseous hydrogen peroxide. Still, no stable, oxidation-resistant and harmless immobilization technique exists for the immobilization of

bacterial spores. The aim of this work is, therefore, to elaborate an oxidation-resistant functionalization method to immobilize *B. atrophaeus* spores for spore-based biosensors.

6.1 Introduction

Gaseous hydrogen peroxide (H_2O_2) is one of the most used sterilants for packaging in the aseptic food industry [1]. It is also a strong oxidant and effective against a wide range of microorganisms such as bacteria, spores, fungi, and viruses [2–5] as it provides hydroxyl-free radicals, which disrupt essential cell components, including lipids, proteins, and DNA [6]. The state-of-the-art method utilized to validate such a sterilization process is via microbiological analyses. Despite the fact that these methods are well-standardized and reliable, they are still slow and labor-intensive. As a result, novel electrochemical sensor methods have been recently developed to overcome these issues. For instance, H_2O_2 concentrations in aseptic filling machines have been measured by means of calorimetric sensors [7, 8] and the microbicidal efficacy of sterilization processes has been evaluated using spore-based biosensors [9]. This type of spore-based biosensor (Figure 6.1) consists of a glass substrate with a meander-type structure as temperature sensor and several interdigitated electrodes (IDEs) as transducer elements, where the spores can be immobilized on one of the IDEs and the other one acts as a reference sensor (differential measurement setup).

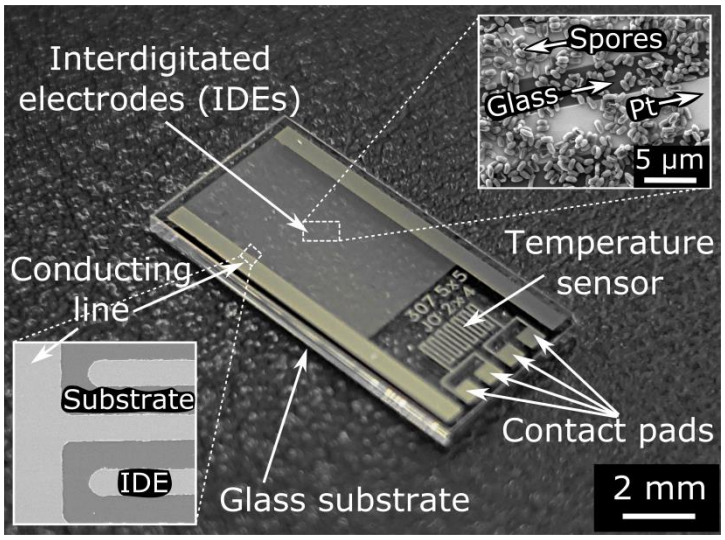

Figure 6.1 Spore-based biosensor. Glass sensor chip consisting of temperature sensors and interdigitated electrodes (IDEs). Inlets show the IDE area with spores (upper right) and connection between IDE and conducting line (exemplary, bottom left).

The spore-based biosensor is consequently exposed to an oxidative environment (H_2O_2 concentration up to 7.6% v/v and temperature up to 300 °C) for a short time (< 2 s) and finally, the sensor's signal change (e.g., impedance) can be evaluated. This change is then correlated

to the grade of morphological deformation of the spores depending on the H_2O_2 concentration. The additional temperature sensor allows controlling of the overall temperature of the spore-based biosensor and then, can deliver an additional parameter describing the process conditions during industrial sterilization cycles.

The functionalization strategy to immobilize the spores is a crucial aspect because it will substantially influence the reproducibility, sensitivity and overall performance of the biosensor. Organosilanes have been earlier employed for spore immobilization [10–12] as they support the attachment of organic molecules to an inorganic surface. Specifically, 3-(Aminopropyl)triethoxysilane (APTES) is a popular choice because it can form an amine-reactive film that exhibits self-assembly behavior. The reaction (silanization) involves four stages: hydrolysis, condensation, hydrogen bond formation and curing [13, 14]. First, the alkoxysilane groups are hydrolyzed to form extremely reactive silanols. In the second stage, these silanols condensate to form siloxanes. Hydrogen bond formation is followed in the third stage between the hydrolyzed alkosysilanes and the OH groups of the sensor substrate. At the end, a covalent bond is developed from the silane's silicon and the surface's silicon resulting in a loss of water by curing. The whole silanization process can, however, take place simultaneously after hydrolysis. Several parameters affect the silanization process, for instance: solvent, humidity, silane concentration, silanization time, temperature of the solution and the curing process [14–17]. Since the working environment of the sensor is oxidative, the immobilization layer is desired to be stable against hydrogen peroxide at high temperatures and should not affect the sensor's signal during the sterilization process. A schematic of the functionalization and sterilization process is shown in Figure 6.2. First, the sensor chips are hydroxylated to provide OH groups for further silanization (Figure 6.2 a). Then, the chips are silanized with APTES (Figure 6.2 b) as mentioned in section 6.2.3.2. After that, the spores are immobilized from a water- or ethanol-based suspension onto the sensor's surface (Figure 6.2 c). Finally, the APTES-modified spore-based biosensors are sterilized (Figure 6.2 d).

Until now, to the best of our knowledge, no stable, oxidation-resistant and harmless immobilization layer has been developed for the immobilization of bacterial spores. Therefore, the aim of this study is to investigate the influence of gaseous hydrogen peroxide on APTES-functionalized spore-based biosensors for the immobilization of *Bacillus*

atrophaeus spores (DSM 675). Here, different parameters such as the solvent of APTES (toluene, ethanol) and of the spore suspension (water, ethanol) were investigated and characterized by means of impedimetric- and contact angle measurements, microbiological evaluation tests for the immobilization of spores, ellipsometric- and atomic force microscopic measurements.

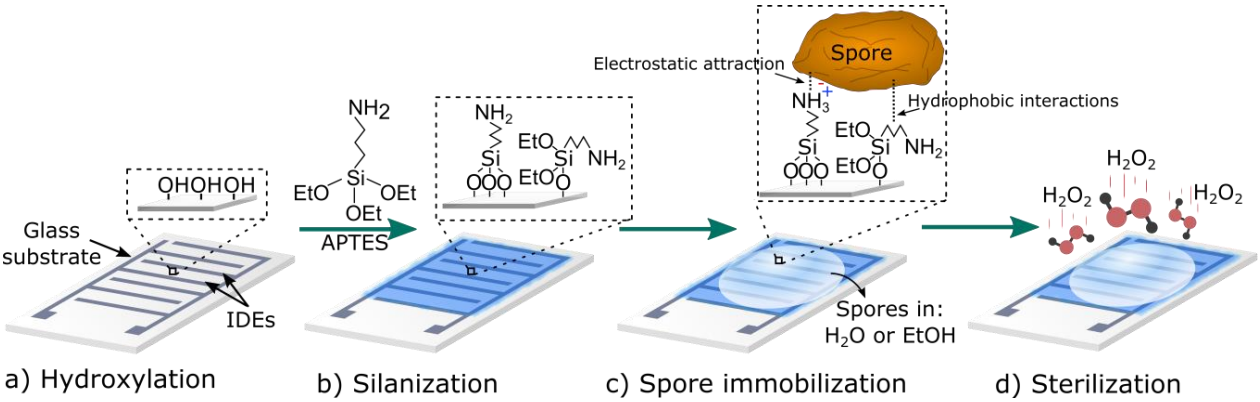

Figure 6.2 Schematic of the functionalization and sterilization on the spore-based biosensor. The sensor chip is hydroxylated (a), followed by silanization with APTES (b). The spores contained in a water- or ethanol-based solution are then immobilized on the sensor surface (c), and at the end, the APTES-funtionalized spore-based biosensor is sterilized with gaseous hydrogen peroxide (d).

6.2 Materials and methods

The objectives and experimental methods performed in the present work are depicted in Figure 6.3. The main objective (as mentioned before) is to develop a stable APTES layer against gaseous hydrogen peroxide. Because of the nature of the spore immobilization (liquid phase), a sub-objective is also investigated regarding the stability of the APTES layer with water- or ethanol-based solutions.

Si/SiO_2 substrates were used as a model system for spore-based biosensors due to technical limitations from glass substrates with transducer structures for contact angle-, ellipsometric- and atomic force microscopic measurements. Therefore, the presence of the APTES layer, the wettability of the substrate and the APTES thickness and roughness after water- or ethanol aliquots deposited on Si/SiO_2 substrates and sterilization, were investigated by these methods.

Furthermore, the efficiency of APTES for the immobilization of spores and the evaluation of the APTES stability were conducted by means of microbiological approaches and impedimetric measurements on spore-based biosensors, respectively.

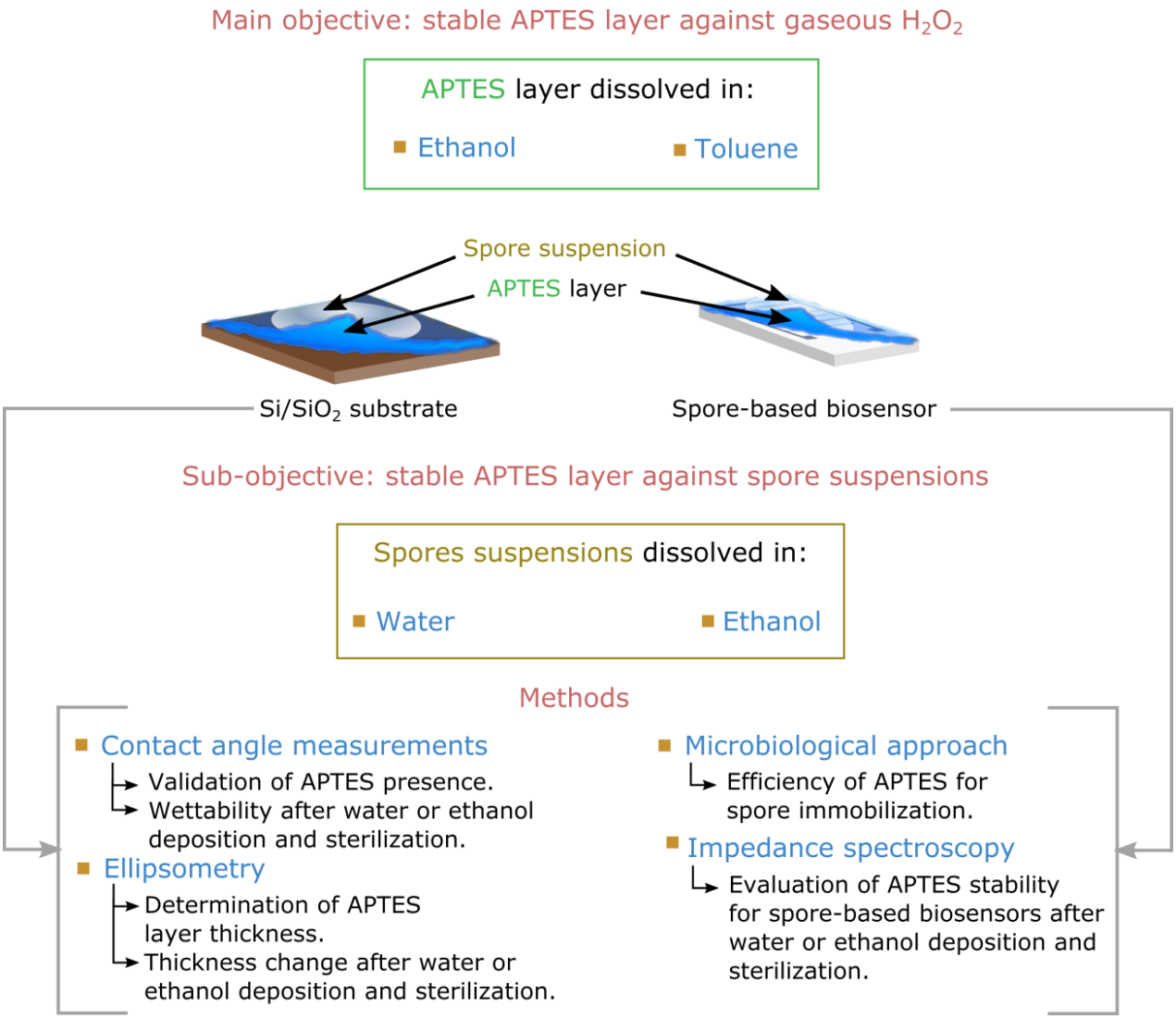

Figure 6.3 Objectives and methodology of the experimental investigations.

6.2.1 Materials

3-(Aminopropyl)triethoxysilane (APTES, 98% v/v), acetone (99% v/v), ethanol (99% v/v), isopropanol (99% v/v), toluene (99% v/v) and Tween®80 were obtained from Sigma-Aldrich (Germany). Manganese (II) sulphate monohydrate and Ringer solution pellets were purchased from Merck Millipore (Germany). Plate count agar (PCA), dry meat extract and peptone from meat were purchased from VWR International (Germany). The adhesion promoter Ti prime, the photoresist AZ®5214E, the developer AZ®326 MIF and TechniStrip®Micro D350 (DMSO) were obtained from Microchemicals GmbH (Germany).

6.2.2 Sensor fabrication

6.2.2.1 Si/SiO_2 substrates

80 nm of SiO_2 was thermally grown by dry oxidation at 1,000 °C for 30 min on a boron-doped silicon wafer (ρ = 1-10 Ωcm, <100>). The wafer was then diced into 10 x 10 mm^2 pieces and cleaned sequentially for 5 min in ultrasonic bath with acetone, isopropanol and deionized (DI) water.

6.2.2.2 Spore-based biosensor

Conventional photolithography methods were used for the sensor fabrication. Here, borosilicate glass wafers were dehydrated by heating up to 180 °C for at least 10 min. Then, the adhesion promoter Ti prime was spin-coated at 4,000 rpm for 30 s and prebaked at 120 °C for 2 min. Afterwards, in a similar way, the positive photoresist AZ®5214E was also spin-coated and prebaked at 95 °C for 5 min. The desired structures were transferred to the photoresist by a mask aligner (Süss MicroTec AG, Germany) with a UV light source of 365 nm. The wafer was then developed with AZ®326 MIF for 50 s. In addition, 10 nm titanium and 100 nm platinum were deposited by e-beam evaporation process and the final structures were obtained by a lift-off process with TechniStrip®Micro D350 (DMSO). Finally, the wafer was diced into chips with dimensions of 5 x 10 mm^2. The finger width and gap of the interdigitated structures was 5 µm with a total number of 614 electrodes, a length of 3.25 mm and a sensing area of 20 mm^2. The chips were cleaned in acetone, isopropanol and DI water for further experiments.

For the inoculation of spores onto the sensors, 10 µl of the spore suspension (water- or ethanol-based) with a final spore concentration of least 10^6 CFU/ml (colony forming unit per milliliter) were pipetted, distributed along the sensor and air-dried under sterile conditions.

6.2.3 Silanization

Si/SiO_2 substrates and spore-based sensors were silanized with an optimized protocol for the immobilization of bacterial spores introduced in [10].

6.2.3.1 Hydroxylation

The surface of the Si/SiO_2 substrates and the sensors was activated with hydroxyl groups (hydroxylation) by oxygen plasma treatment (Femto PCCE, Diener electronic GmbH + Co. KG, Germany) at 100 W for 2 min.

6.2.3.2 APTES

The silanization process was carried out under nitrogen atmosphere in a glove box to avoid unwanted reactions due to atmospheric conditions (e.g., humidity). The drop-casting method was used for all substrates and sensors. An aliquot of 1% APTES contained in toluene or ethanol was pipetted onto the surfaces and incubated for 1 h. Later on, the surfaces were washed with a series of baths in toluene or ethanol and ethanol for 5 min each step to remove the excess of APTES. Lastly, the substrates and the sensors were cured at 110 °C for 1 h in an air circulation oven (Heraeus UT 6P, Kendro Laboratory Products GmbH, Germany) to increase the stability of the APTES by cross-linking.

6.2.4 Physical and impedimetric characterizations

6.2.4.1 Contact angle measurements (CA)

Water contact angle measurements were performed to validate the surface functionalization, to study the wettability on APTES-modified Si/SiO_2 substrates after air-drying aliquots of water and ethanol for approximately 30 minutes and to analyze the effect of gaseous hydrogen peroxide on them. For this reason, the measurements were taken before and after the sterilization process with an optical contact angle system OCA (Dataphysics, Germany) at room temperature and the data were processed with the software SCA 20.

6.2.4.2 Ellipsometry

Spectroscopic nulling ellipsometry (EP3, Accurion GmbH, Germany) was used to determine the thickness of the APTES layers on Si/SiO_2 substrates. The angle of incidence (AOI) utilized was 70° over a wavelength range of λ = 360-1002 nm. The thickness and refractive index n of the APTES layer was obtained using the Cauchy dispersion function (APTES: A_n = 1.413, B_n = 6265 nm^2 [18]):

$$n = A_n + \frac{B_n}{\lambda^2} \quad \text{(Equation 6.1)}$$

APTES-modified Si/SiO_2 substrates without any further treatment were used as reference for the ellipsometric measurements; they were exposed to the same laminar air flow as the rest of the chips during the drying process of the water or ethanol droplets.

6.2.4.3 Atomic force microscopy (AFM)

The BioMat Workstation (JPK Instruments, Germany) was used to scan and study the topography by quantification of the surface roughness from the APTES-modified surfaces (Si/SiO_2) after sterilization. Silicon cantilevers (Arrow NCR, NanoWorld AG, Switzerland) were used, having a spring constant of 42 N/m and a resonance frequency of 285 kHz. All the scans (2 x 2 μm^2) were conducted under ambient conditions in tapping mode at 512 pixels per line with a scanning frequency of 0.6 Hz.

6.2.4.4 Impedimetric characterization

The influence of water and ethanol droplets (with or without spores) as well as the effect of gaseous hydrogen peroxide on APTES layers were investigated by means of impedimetric measurements. Therefore, a point-probe station with a precision LCR meter (E4980A, Agilent Technologies, United States) was used with an excitation voltage of 20 mV with a DC (direct current) voltage bias of 0 V with a fixed frequency of 3 kHz. The chips were measured at the end of each step from Figure 6.2.

At least three sensors were used for each experiment. The sensor's signal was normalized with:

$$\text{Normalized impedance}(\%) = \left(\frac{\text{Procedure}}{\text{Blank sensor}}\right) \times (100) \quad \text{(Equation 6.2)}$$

Here, *Blank sensor* denotes the first measurement of the sensor after being cleaned (section 6.2.2.2) and *Procedure*, the sensor's signal after APTES, droplet casting or sterilization, respectively.

6.2.5 Microbiological approaches

6.2.5.1 Bacterial culture, sporulation and spore purification

The strain of *Bacillus atrophaeus* (DSM 675) was purchased from the Leibniz Institute DSMZ – German Collection of Microorganisms and Cell cultures (Germany). All methods were carried out under sterile conditions (laminar flow hood) and the spore suspensions were obtained as mentioned in [10]. The spore suspensions were free of vegetative cells (>99%). To prepare the water- and ethanol-based spore suspensions, an aliquot of 1 ml of the main suspension was centrifuged at 20,000 rpm for 5 min for each suspension. The solvent was changed to water or ethanol and this was done 3 times. After that, the spore concentrations were evaluated by serial dilutions and plating with a final concentration of 10^8 CFU/ml.

6.2.5.2 Microbiological method for the evaluation of the APTES efficiency

The APTES efficiency to immobilize spores was determined by the spore recovery method as stated in [11]. In short, after spore immobilization on APTES-modified surfaces, the spores are detached from the surface using an ultrasonic bath and a surfactant. Then, the recovered spores in the suspension are counted and compared to the total cell concentration from the main suspension (highest possible countable cells). The ratio between them is calculated and showed as percentage of the detached spores for the APTES efficiency: the lower the percentage, the better the attachment of the spores (i.e., more spores remained on the surface after the spore recovery method and less in the suspension).

Interdigitated structures were functionalized with APTES in toluene or ethanol. After that, 10 µl from a water- or ethanol-based spore suspension were pipetted onto the sensor chips and air-dried under sterile conditions. Then, the sensors were immersed in a 10 ml surfactant solution and treated with ultrasonic bath for 10 min. Finally, these suspensions were serially diluted, plated and cultivated at 30 °C. Cleaned sensors (section 6.2.2.2) without APTES were used as a control.

6.2.6 Sterilization process

The sterilization process was performed in a sterilization test rig, previously described in [8]. This test rig mimics the sterilization module of industrial aseptic filling machines. Pressurized air is used as a carrier gas to provide a H_2O_2 gas stream of 10 m^3/h. The air-H_2O_2 mixture is

heated in a vaporizer up to 240 °C. Then, the gaseous hydrogen peroxide stream is divided into four outlet nozzles. The concentration of hydrogen peroxide can be adjusted from 0 to 7.6% v/v.

The Si/SiO_2 substrates and the spore-based biosensors were exposed to a concentration of 7.6% v/v $H2O_2$ for 200 ms at 240 °C.

6.3. Results and discussion

6.3.1 Physical characterization of the APTES layer on Si/SiO_2 substrates after sterilization

6.3.1.1 Contact angle measurements (CA)

Water contact angle measurements (Figure 6.4) were conducted to validate the presence of the APTES layer and to study the effect of the wettability on APTES-modified Si/SiO_2 substrates before and after being sterilized following the air-drying process of water or ethanol droplets. As reference, hydroxylated blank Si/SiO_2 chips and Si/SiO_2 surfaces functionalized with APTES in toluene or ethanol (without any further treatment) were used. After sterilization, the hydroxylated blank Si/SiO_2 chips suffered an increase of its contact angle from nearly 0° to 48° ± 0.5°, indicating the reduction of hydroxyl groups [19]. After the air-drying process of the water droplet on the Si/SiO_2 surface modified with APTES in toluene, the contact angle was increased from 50° ± 0.3° to 53° ± 1°, while the one of its control decreased. A similar, but opposite case from 60° ± 0.1° to 57° ± 1° was found for the Si/SiO_2 surface functionalized with APTES in ethanol for the water droplet and its control. Furthermore, the ethanol droplet showed the same behavior of the controls after sterilization. The initial contact angle of both Si/SiO_2 surfaces functionalized with APTES in toluene and ethanol correspond to literature values [20, 21] from amino-terminated layers. The increase of contact angle after sterilization might be due to the modification of the APTES layer, as a result more alkyl groups are exposed at the surface. However, it also can be the case that hydrogen peroxide catalysts the oxidation of silanes into silanols [22], decreasing their contact angle. Nevertheless, these results assist a successful APTES grafting on Si/SiO_2 substrates and suggest that the sterilization does not significantly affect the

wettability of APTES layers functionalized in ethanol and toluene, which underwent the air-drying process of water and ethanol droplets in comparison to the hydroxylated Si/SiO_2 chip.

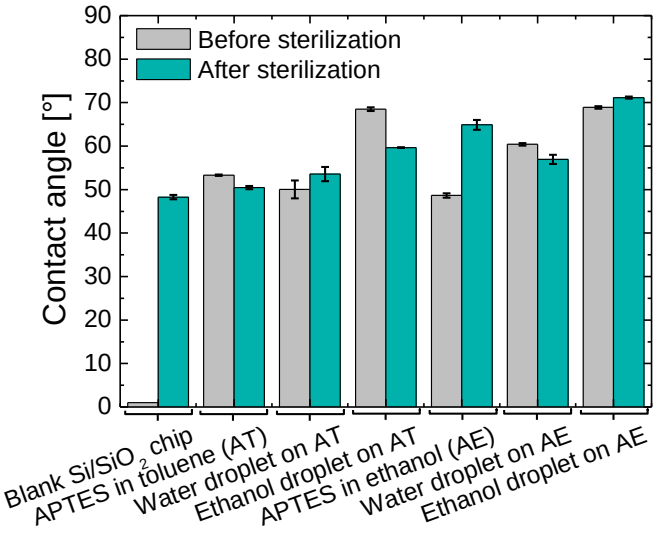

Figure 6.4 Contact angle measurements of functionalized Si/SiO_2 substrates with APTES dissolved in toluene and ethanol and treated with water and ethanol droplets before and after sterilization with gaseous hydrogen peroxide.

6.3.1.2 Ellipsometry

Since morphological changes from the microbiological spores are expected after sterilization, controlling the thickness of the APTES layer is a crucial aspect for the reliability of the sensor's signal after sterilization. For this reason, it was investigated by means of ellipsometry using the same conditions as in the previous section. The results are overviewed in Table 6.1. The thickness of the APTES layer in ethanol was extremely abundant in comparison to that of the APTES layer in toluene. This can be because of the relatively long silanization time in comparison to the short evaporation time of the ethanol since complete evaporation of the solvent was observed. Nevertheless, after water- and ethanol droplets were dried on the Si/SiO_2 substrates modified with APTES in toluene, an increase of the layer thickness was seen, probably due to further polymerization of formed pentacoordinate intermediates produced as a result of hydrolysis of siloxane bonds catalyzed by the amino functionality of APTES [23]. After sterilization, for both cases the thickness of APTES decreased. For the Si/SiO_2 substrates modified with APTES in ethanol, the thickness of its control group was affected by a laminar air flow with a thickness increase of almost 10 nm. However, after sterilization its thickness decreased. In the case of the water droplet, the

thickness increased slightly after the droplet was dried and hardly decreased after being sterilized. On the other hand, the thickness decreased after the ethanol droplet was dried and increased after the sterilization process. These results indicate that the water droplet on Si/SiO_2 surfaces functionalized with APTES in ethanol showed the least thickness layer change before and after being sterilized with H_2O_2 and therefore, it might be suitable to be used in spore-based biosensors during sterilization.

Table 6.1 APTES thickness on Si/SiO_2 substrates.

Thickness (nm)	APTES	Droplet	Sterilization
APTES in toluene (AT)	2.7 ± 0.2	2.6 ± 0.2*	2.2 ± 0.2
Water droplet on AT	2.2 ± 0.3	3.6 ± 0.2	2.8 ± 0.2
Ethanol droplet on AT	1.8 ± 0.3	3.5 ± 0.2	2.4 ± 0.1
APTES in ethanol (AE)	828.9 ± 3.1	841.2 ± 6.0*	835 ± 3.0
Water droplet on AE	775.5 ± 3.7	778.0 ± 5.2	776.0 ± 5.7
Ethanol droplet on AE	771.0 ± 2.3	756.9 ± 3.1	775.9 ± 3.1

*The control groups were exposed to the same conditions as the others without droplets.

6.3.1.3 Atomic force microscopy (AFM)

AFM was used to further characterize the morphology and roughness (R_q) of Si/SiO_2 surfaces functionalized with APTES in toluene and ethanol before and after the sterilization. Characteristic scans of their surface topography are illustrated in Figure 6.5. A decrease of roughness after sterilization for APTES in toluene from 0.46 nm to 0.37 nm could be observed, as well as a domain reduction from APTES agglomeration. Moreover, for APTES in ethanol, a thick layer can be seen as previously shown in section 6.3.1.2. After sterilization, the surface roughness in this case increased from 1.6 nm to 3.7 nm. These results are in good agreement with the previously observed during ellipsometry.

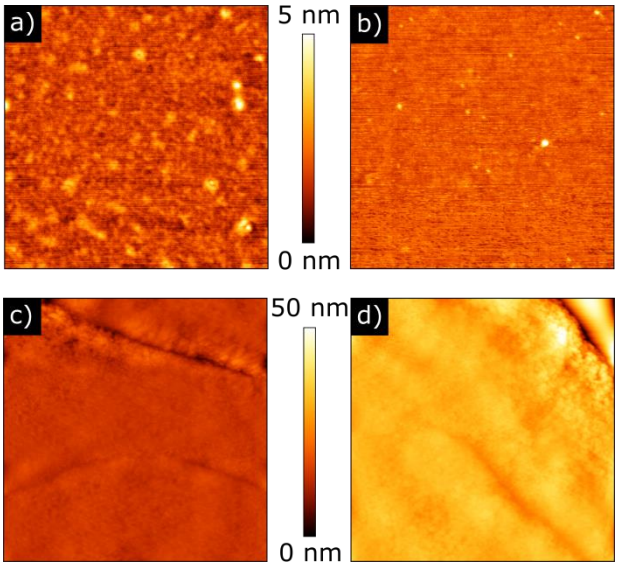

Figure 6.5 AFM 2x2 µm² scans of Si/SiO_2 substrates functionalized with APTES in toluene (a, b) and ethanol (c, d), before (a, c) and after (b, d) sterilization with gaseous hydrogen peroxide.

6.3.2 APTES efficiency for the immobilization of spores on sensors

The reproducible immobilization of spores on the sensor is a critical aspect to assure its reliability. For this reason, the adhesion of the spores on the sensors (in this case, measuring how many spores detach from the sensor surface) was determined (APTES efficiency) as mentioned in section 6.2.5.2. Variations of this method are widely used [5, 24] to recover spores after being immobilized on different surfaces. Therefore, it is a convenient approach to directly quantify the remaining spores on the sensor substrate after spore recovery. The results are summarized in Figure 6.6. Non-functionalized sensors with immobilized spores from a water- or an ethanol-based suspension were used as a reference and the solvents of the suspensions did not affect the spore viability [25].

In the diagram, the blue dotted line describes the original number of spores in the main suspension, i.e. 100% (equal to 5 x 10^6 CFU/ml). The first three bars represent the immobilization of the spores from a water-based suspension with three variations, whereas the second three bars correspond to the three experiments for spore immobilization from an ethanol-based suspension. In general, the immobilization of spores from a water-based suspension was better in comparison to that from ethanol. The best APTES efficiency of 2% ± 1% was obtained for the sensors functionalized with APTES in toluene and spores immobilized from a water-based suspension, followed by the APTES functionalization in

ethanol and the same suspension with an efficiency of 5% ± 1%. For the spores from an ethanol-based suspension immobilized with APTES in toluene and in ethanol, the efficiencies were 17% ± 1% and 15% ± 1%, respectively. In addition, as a reference, the spores stored in an ethanol solution showed less adhesion efficiency (35% ± 5%) in comparison to those of a water solution (22% ± 2%). One of the mechanisms of binding to the positive amino groups of APTES is through the negative N-Acetylmuramic acid (NAM) residues on the spore coat [26, 27]. It can be the case, that the NAMs from the spore coat in the ethanol suspension are hindered, resulting in less binding sites for the APTES molecules. For this reason, a water-based spore suspension may suggest to be more effective for the immobilization of spores on spore-based biosensors than an ethanol-based one.

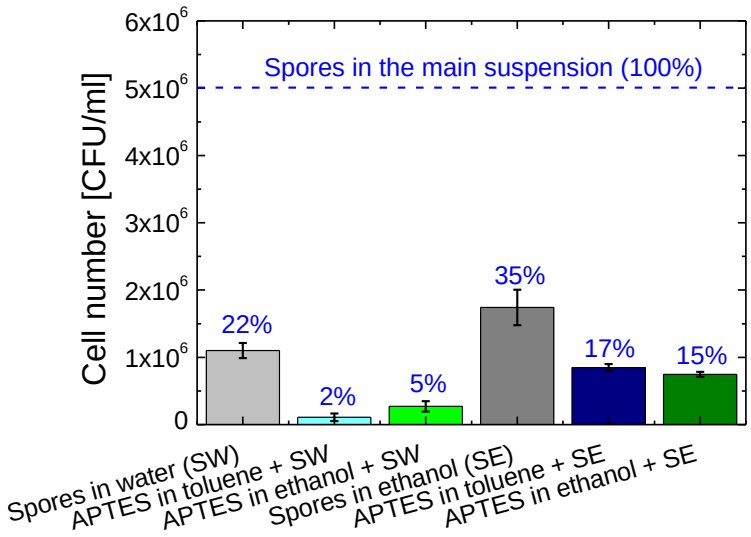

Figure 6.6 APTES efficiency (see section 6.2.5.2) for the individual immobilization of *B. atrophaeus* spores on sensor chips. The first three bars show the attachment of spores from a water suspension on spore-based biosensors modified with APTES in ethanol and in toluene. The second set of the next three bars show a similar case, but from spores from an ethanol suspension. The error bars show the standard deviations of three samples for each group.

6.3.3 Effect of gaseous hydrogen peroxide on APTES-funtionalized spore-based biosensors

The stability of the functionalized sensor after sterilization with H_2O_2 shall be taken into consideration to guarantee its performance. Therefore, a minimal (or absent) impedance change from the APTES layer treated with H_2O_2 is desired. In this case, the sensor's signal

was monitored after each process step from Figure 6.3 by means of impedimetric measurements on spore-based biosensors functionalized with APTES in toluene and ethanol as shown in Figures 6.7 and 6.8, accordingly.

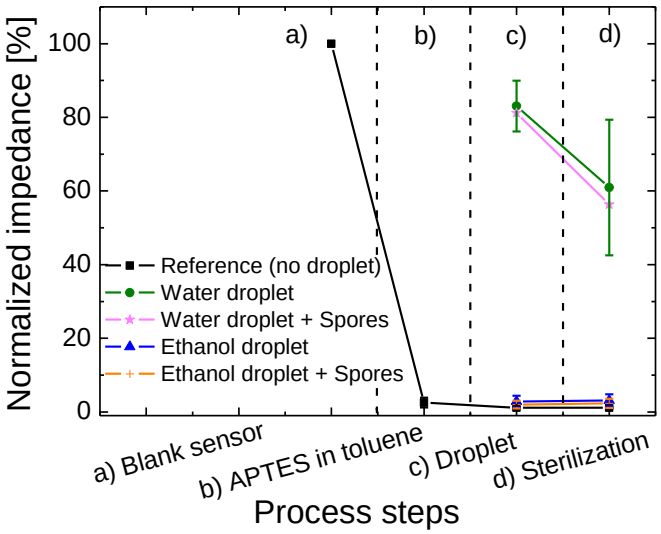

Figure 6.7 Impedimetric measurements of the spore-based biosensor after being functionalized with APTES in toluene. The sensors were measured after each process step as shown in Figure 6.3. First, the sensor was measured after being hydroxylated and taken as reference (Figure 6.7 a). Subsequently, the spore-based biosensor was modified with APTES in toluene (Figure 6.7 b). The effect of different droplets on the modified APTES surface grafted in toluene was studied in Figure 6.7 c); as a reference from this step, the sensors were left air-dried like the others, but without any droplet deposition. At the end, the spore-based biosensors modified with APTES in toluene and with different droplets air-dried (except for the reference) were submitted to the sterilization process with gaseous hydrogen peroxide (Fig.6. 7 d)).

For these experiments, the blank sensor (IDE structures without APTES layer and spores) served as normalized reference value (impedance at 100%). The impedance of the sensor decreased dramatically from 100% (Figure 6.7 a) to 2.5% ± 1% (Figure 6.7 b) after being functionalized with APTES in toluene. However, after a water droplet or an aliquot (water) of spores were air-dried on the sensor's surface, its impedance went nearly (83% ± 6%) to its original value (Figure 6.7 c). In addition, after sterilization a further drop up to 60% ± 18% could be seen (Figure 6.7 d). Moreover, for the ethanol droplet as well as for the aliquot (ethanol) of spores and after sterilization, no significant changes were observed (Figure 6.7 c and d): both of them showed a similar impedance change after sterilization (~ 0.3%).

Previously [11], it was assumed that the amine groups from APTES may increase the electrical conductivity because of its electron-donating nature [28].

Furthermore, it can be the case that because of toluene (nonpolar), extremely reduced amount of water was present during silanization and not all the ethoxy groups of APTES were completely hydrolyzed [29]. Therefore, after water was dried on the surface, the APTES molecules might be further hydrolyzed changing their structure and orientation [30] and decreasing the overall electrical conductivity at the sensor's surface. Then, after sterilization, the APTES layer might be oxidized by hydrogen peroxide, changing again its structure and orientation, resulting as well in a decrease of impedance. As a result, in this case, toluene as a solvent for the silanization of APTES on spore-based biosensors is not advisable for sterilization with gaseous hydrogen peroxide as water deposited on such layer reacts with the sterilant, compromising their reliability. On the other hand, for the ethanol droplet it was not the same situation, probably because of its low surface tension and high evaporation rate in comparison to water. It might not let in enough water within the short drying time to hydrolyze and change the APTES layer. Nevertheless, it could not be distinguished between a pure ethanol solution and spores in an ethanol suspension.

In a second set of experiments, further investigations were performed for the silanization of APTES in ethanol as shown in Figure 6.8. A slight decrease of impedance from 100% to 95% ± 1% can be observed after the surface is functionalized with APTES in ethanol (see change from Figure 6.8 a to b), much less in comparison to that of APTES in toluene from Figure 6.7. When a water droplet and spores from a water suspension were air-dried, the impedance of the sensor decreased by sterilization from 92.5% ± 2% to 89.5% ± 5% and from 87% ± 3% to 85% ± 4%, correspondingly (see Figure 6.8 c and d). However, for the spores suspended in water, this change of the impedance after sterilization was less pronounced in comparison to the droplet of pure water, as well as the one resulting because of the sterilization process, 3% for the water droplet and 2% for the spores in water. Furthermore, the ethanol droplet after being air-dried showed a similar valued compared to the reference (APTES-modified sensor without any further treatment) and decreased after sterilization (91% ± 3%), see Figure 6.8 d). However, for the spores in ethanol, the impedance value is decreased after being immobilized (93% ± 1.5%) and it further slightly decreased after being sterilized (92% ± 2%). The change of impedance after sterilization for water and ethanol-based spore suspensions

for sensors functionalized with APTES in ethanol were more pronounced than the ones prepared in toluene (Figure 6.7), except for the case of water (Figure 6.7 c and d), where it dramatically affected the sensor signal after deposition. However, it also showed the highest standard deviation as well as the highest dynamic impedance change within 24 h, i.e. the impedance nearly went back to its reference value during the deposition step (results not shown). In conclusion, taking into account the experimental results discussed in Figures 6.6 to 6.8, a sensor modified with APTES in ethanol in combination with a water- or ethanol-based suspension would give the best results in terms of monitoring the sterilization effect on spores.

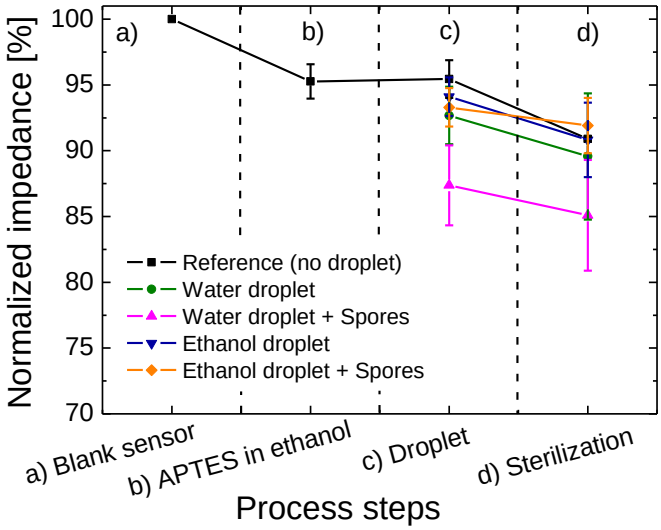

Figure 6.8 Impedimetric measurements of the spore-based biosensor after being functionalized with APTES in ethanol. The sensors were measured after each process step as shown in Figure 6.3. First, the sensor was measured after being hydroxylated and taken as reference (Figure 6.8 a). Subsequently, the spore-based biosensor was modified with APTES in ethanol (Figure 6.8 b). The effect of different droplets on the modified APTES surface grafted in ethanol was studied in Figure 6.8 c); as a reference from this step, the sensors were left air-dried like the others, but without any droplet deposition. At the end, the spore-based biosensors modified with APTES in ethanol and with different droplets air-dried (except for the reference) were submitted to the sterilization process with gaseous hydrogen peroxide (Figure 6.8 d).

6.4 Conclusions

In the present work, the effects of water- and ethanol-based spore suspensions as well as of gaseous hydrogen peroxide on Si/SiO_2 substrates and APTES-functionalized spore-based biosensors were studied. APTES-modified Si/SiO_2 substrates with air-dried droplets of water and ethanol after sterilization were physically characterized by means of contact angle- and ellipsometric measurements. Contact angle measurements demonstrated the successful surface functionalization of APTES prepared in toluene and ethanol and that the wettability of the functionalized Si/SiO_2 substrates is not significantly affected after sterilization with gaseous hydrogen peroxide. In addition, ellipsometry measurements were performed to determine the thickness of the APTES layer after air-drying aliquots of water and ethanol, following sterilization with gaseous hydrogen peroxide. The layer thickness from APTES prepared in ethanol was extremely thick (~800 nm) in comparison to that prepared in toluene (~2 nm). Nevertheless, a water droplet on an APTES layer prepared in ethanol and sterilized showed the best stability in means of marginal changes of the layer thickness. Furthermore, the surface topography as well as the surface roughness (R_q) were studied with AFM. Characteristic domains were seen supporting the successful coupling of APTES. After sterilization, the roughness of the APTES layer developed in toluene decreased. The opposite was for the APTES layer in ethanol being in good agreement as shown in the ellipsometric measurements.

Moreover, electrochemical measurements suggested a higher sensor's signal stability against hydrogen peroxide and water or ethanol aliquots when using ethanol as solvent for APTES instead of toluene. In addition, the spore adhesion on spore-based biosensors was studied via microbiological investigations. It could be observed that a water-based suspension was better for the spore adhesion than an ethanol-based one in means of measuring the efficiency of APTES on APTES-functionalized sensors.

Additional investigations will address the use of this immobilization technique on spore-based biosensors for different hydrogen peroxide concentrations in sterilization processes as well as its application on gas- or cell-based sensors.

Acknowledgements

This project was funded by the Federal Ministry of Education and Research, Germany, Project: "ImpediPack" (Fund. No.: 03FH012I3). The authors are would like to thank Prof. Dr. P. Siegert and Prof. Dr. J. Bongaerts for admittance to the microbiology laboratory to performed microbiological investigations, Prof. Dr. T. Mang for access to the instrument for contact angle measurements, H. Iken for assisting the fabrication of the spore-based biosensors, D. Rolka for the scanning electron microscopy measurements and L. Breuer for technical support during the ellipsometry measurements.

References

[1] I.A. Ansari and A.K. Datta, "An overview of sterilization methods for packaging materials used in aseptic packaging systems", *Food Bioprod. Process.* 81 (1), 57–65 (2003).

[2] L. Hall, J.A. Otter, J. Chewins, and N.L. Wengenack, "Deactivation of the dimorphic fungi *Histoplasma capsulatum*, *Blastomyces dermatitidis* and *Coccidioides immitis* using hydrogen peroxide vapor", *Med. Mycol.* 46 (2), 189–191 (2008).

[3] J.E. Meszaros, K. Antloga, C. Justi, C. Plesnicher, and G. McDonnell, "Area fumigation with hydrogen peroxide vapor", *Appl. Biosaf.* 10 (2), 91–100 (2005).

[4] T. Pottage, C. Richardson, S. Parks, J.T. Walker, and A.M. Bennett, "Evaluation of hydrogen peroxide gaseous disinfection systems to decontaminate viruses", *J. Hosp. Infect.* 74 (1), 55–61 (2010).

[5] K. Pruß, S. Stirtzel, and U. Kulozik, "Influence of the surface temperature of packaging specimens on the inactivation of *Bacillus* spores by means of gaseous H_2O_2", *J. Appl. Microbiol.* 112 (3), 493–501 (2012).

[6] G. McDonnell and A.D. Russell, "Antiseptics and disinfectants: activity, action, and resistance", *Clin. Microbiol. Rev.* 12 (1), 147–179 (1999).

[7] P. Kirchner, B. Li, H. Spelthahn, H. Henkel, A. Schneider, P. Friedrich, J. Kolstad, M. Keusgen, and M.J. Schöning, "Thin-film calorimetric H_2O_2 gas sensor for the validation of germicidal effectivity in aseptic filling processes", *Sens. Actuat. B-Chem.* 154 (2), 257–263 (2011).

[8] N. Näther, L.M. Juárez, R. Emmerich, J. Berger, P. Friedrich, and M.J. Schöning, "Detection of hydrogen peroxide (H_2O_2) at exposed temperatures for industrial processes", *Sensors (MDPI)* 6 (4), 308–317 (2006).

[9] J. Oberländer, M. Mayer, A. Greeff, M. Keusgen, and M.J. Schöning, "Spore-based biosensor to monitor the microbicidal efficacy of gaseous hydrogen peroxide sterilization processes", *Biosens. Bioelectron.* (104), 87–94 (2018).

[10] J. Arreola, M. Mätzkow, M.P. Durán, A. Greeff, M. Keusgen, and M.J. Schöning, "Optimization of the immobilization of bacterial spores on glass substrates with organosilanes", *Phys. Status Solidi A* 213 (6), 1463–1470 (2016).

[11] J. Arreola, J. Oberländer, M. Mätzkow, M. Keusgen, and M.J. Schöning, "Surface functionalization for spore-based biosensors with organosilanes", *Electrochim. Acta* 241, 237–243 (2017).

[12] T.J. Park, K.-B. Lee, S.J. Lee, J.P. Park, Z.-W. Lee, S.-K. Choi, H.-C. Jung, J.-G. Pan, S.Y. Lee, and I.S. Choi, "Micropatterns of spores displaying heterologous proteins", *J. Am. Chem. Soc.* 126 (34), 10512–10513 (2004).

[13] B. Arkles, "Hydrophobicity, hydrophilicity and silanes", *Paint Coating Ind.* 22 (10), 114–125 (2006).

[14] C.M. Halliwell and A.E.G. Cass, "A factorial analysis of silanization conditions for the immobilization of oligonucleotides on glass surfaces", *Anal. Chem.* 73 (11), 2476–2483 (2001).

[15] N. Aissaoui, L. Bergaoui, J. Landoulsi, J.F. Lambert, and S. Boujday, "Silane layers on silicon surfaces: mechanism of interaction, stability, and influence on protein adsorption", *Langmuir* 28 (1), 656–665 (2012).

[16] D.L. Angst and G.W. Simmons, "Moisture absorption characteristics of organosiloxane self-assembled monolayers", *Langmuir* 7 (10), 2236–2242 (1991).

[17] A.V. Krasnoslobodtsev and S.N. Smirnov, "Effect of water on silanization of silica by trimethoxysilanes", *Langmuir* 18 (8), 3181–3184 (2002).

[18] B. Yameen, C. Rodriguez-Emmenegger, C.M. Preuss, O. Pop-Georgievski, E. Verveniotis, V. Trouillet, B. Rezek, and C. Barner-Kowollik, "A facile avenue to conductive polymer brushes via cyclopentadiene-maleimide Diels-Alder ligation", *Chem. Commun.* 49 (77), 8623–8625 (2013).

[19] Q.-Y. Tong, "The role of surface chemistry in bonding of standard silicon wafers", *J. Electrochem. Soc.* 144 (1), 384-389 (1997).

[20] S.E. Asenath and W. Chen, "How to prevent the loss of surface functionality derived from aminosilanes", *Langmuir* 24 (21), 12405–12409 (2008).

[21] J.A. Howarter and J.P. Youngblood, "Optimization of silica silanization by 3-aminopropyltriethoxysilane", *Langmuir* 22 (26), 11142–11147 (2006).

[22] R. Ishimoto, K. Kamata, and N. Mizuno, "Highly selective oxidation of organosilanes to silanols with hydrogen peroxide catalyzed by a lacunary polyoxotungstate", *Angew. Chem. Int. Ed.* 48 (47), 8900–8904 (2009).

[23] S.M. Kanan, W.T.Y. Tze, and C.P. Tripp, "Method to double the surface concentration and control the orientation of adsorbed (3-aminopropyl)dimethylethoxysilane on silica powders and glass slides", *Langmuir* 18 (17), 6623–6627 (2002).

[24] V.K. Rastogi, L. Wallace, L.S. Smith, S.P. Ryan, and B. Martin, "Quantitative method to determine sporicidal decontamination of building surfaces by gaseous fumigants, and issues related to laboratory-scale studies", *Appl. Environ. Microbiol.* 75 (11), 3688–3694 (2009).

[25] A.D. Russell, "Bacterial spores and chemical sporicidal agents", *Clin. Microbiol. Rev.* 3 (2), 99–119 (1990).

[26] D.L. Popham, J. Helin, C.E. Costello, and P. Setlow, "Muramic lactam in peptidoglycan of *Bacillus subtilis* spores is required for spore outgrowth but not for spore dehydration or heat resistance", *Proc. Natl. Acad. Sci. U.S.A.* 93 (26), 15405–15410 (1996).

[27] T.S. Sreeprasad, P. Nguyen, A. Alshogeathri, L. Hibbeler, F. Martinez, N. McNeil, and V. Berry, "Graphene quantum dots interfaced with single bacterial spore for bio-electromechanical devices: a graphene cytobot", *Sci. Rep.* 5, 9138 (1-7) (2015).

[28] M. Song, J.-W. Kang, D.-H. Kim, J.-D. Kwon, S.-G. Park, S. Nam, S. Jo, S. Yoon Ryu, and C. Su Kim, "Self-assembled monolayer as an interfacial modification material for highly efficient and air-stable inverted organic solar cells", *Appl. Phys. Lett.* 102 (14), 143303-143305 (2013).

[29] L.C. Mugica, B. Rodríguez-Molina, S. Ramos, and A. Kozina, "Surface functionalization of silica particles for their efficient fluorescence and stereo selective modification", *Colloids Surf. A Physicochem. Eng. Asp.* 500, 79–87 (2016).

[30] R.G. Acres, A.V. Ellis, J. Alvino, C.E. Lenahan, D.A. Khodakov, G.F. Metha, and G.G. Andersson, "Molecular structure of 3-aminopropyltriethoxysilane layers formed on silanol-terminated silicon surfaces", *J. Phys. Chem. C* 116 (10), 6289–6297 (2012).

7 Combined calorimetric gas- and spore-based biosensor array for online monitoring and sterility assurance of gaseous hydrogen peroxide in aseptic filling machines (*Biosensors & Bioelectronics*, 143 (2019), 111628 (1-8))

Julio Arreola[1,2], Michael Keusgen[2], Torsten Wagner[1,3], Michael J. Schöning[1,3,*]

[1] Institute of Nano- and Biotechnologies, Aachen University of Applied Sciences, Campus Jülich, 52428 Jülich, Germany

[2] Institute of Pharmaceutical Chemistry, Philipps-University Marburg, Marbacher Weg 6-10, 35032 Marburg, Germany

[3] Institute of Complex Systems 8, Research Centre Jülich GmbH, 52425 Jülich, Germany

Published in: *Biosensors & Bioelectronics*, 143 (2019), 111628 (1-8). Reprinted with permission from Elsevier.

Received 18 June 2019; **revised** 09 August 2019; **accepted** 21 August 2019

Keywords: biosensor, sterilization, spore, hydrogen peroxide, aseptic filling machine.

Abstract

A combined calorimetric gas- and spore-based biosensor array is presented in this work to monitor and evaluate the sterilization efficacy of gaseous hydrogen peroxide in aseptic filling machines. H_2O_2 has been successfully measured under industrial conditions. Furthermore, the effect of H_2O_2 on three different spore strains, namely *Bacillus atrophaeus*, *Bacillus subtilis*

and *Geobacillus stearothermophilus*, has been investigated by means of SEM, AFM and impedimetric measurements. In addition, the sterilization efficacy of a spore-based

biosensor and the functioning principle are addressed and discussed: the sensor array is convenient to be used in aseptic food industry to guarantee sterile packages.

7.1 Introduction

Aseptic filling machines are broadly employed in biomedical and food industry to provide sterilized liquid products. In these machines, the entire aseptic processing is performed, including the sterilization of the packing material, filling and sealing of the product. Maintaining sterile aseptic packaging is a crucial aspect to assure the shelf life and safety of the goods. A wide range of sterilization methods is available for this purpose, for instance heat, hydrogen peroxide and UV or plasma radiation [1]. Among them, chemical methods in form of gases are extensively used such as ethylene oxide, formalaldehyde, peracetic acid or gaseous hydrogen peroxide (H_2O_2). Although all of them have been employed to sterilize packaging materials, not all are optimal for aseptic processing; ethylene oxide and formaldehyde are carcinogenic [2]. Peracetic acid is a mixture formed from acetic acid and hydrogen peroxide; upon decomposition, it forms acetic acid and water. Since, its vapor is very pungent and irritating, residuals may cause unwanted flavors in some food products [3]. As a result, H_2O_2 has become a popular choice as a sterilant for aseptic filling machines. H_2O_2 has the best safety profile in comparison to other sterilization gases [4], mainly because it breaks down into water and oxygen, leaving virtually no residues and therefore being eco-friendly. In addition, its strong oxidation properties are capable of killing an extensive amount of microorganisms, for example, viruses, bacteria, spores and fungi [5–8]. The effectiveness of H_2O_2 is primarily affected by its exposure time, temperature and concentration.

Microbiological methods are the standard approach to evaluate the efficacy of sterilization systems with gaseous hydrogen peroxide. Here, the packaging is artificially inoculated with microbiological spores, which are extremely resistant to the sterilization agent. Subsequently, the inoculated packing is exposed to the sterilant and finally incubated for a certain amount of time. After that, the viability of the spores is determined either by counting the surviving spores before and after sterilization (count-reduction test) or by determining the relationship between the number of non-sterile and sterile packages (end-point test) [9]. Although these methods are reliable and widespread, they lack rapid output responses (48-72 h) and they are cumbersome.

Over the last few years, more sophisticated methods have been developed by the integration of sensor technologies to determine, for instance, hydrogen peroxide concentrations or the viability of spores. Gaseous H_2O_2 detection has been broadly reported in literature by means

of electrochemical [10], acoustic [11], conductometric [12], colorimetric [13] or calorimetric measurements [14]. Some of them are not suitable for online- and inline monitoring in aseptic filling machines (electrochemical, colorimetric), because of the lack of portability of the measuring equipment or sophisticated sample preparation (solution-based). Other methods have high response times (>30 s) in comparison to standard industrial H_2O_2 exposure times (<2 s) or may not be able to handle high temperatures (up to 300 °C). Moreover, calorimetric gas sensors have been previously introduced [14–16] to overcome these limitations for applications in aseptic food industry. They incorporate a differential setup of two temperature-sensitive structures: one of them is passivated by an inert polymer layer and functions as a reference, whereas the other one is catalytically activated by manganese oxide (MnO_2). When gaseous H_2O_2 is in contact with the sensor surface, only where the catalyst is located, hydrogen peroxide is split into oxygen and water, and the other part of the sensor remains inert. As a result, an exothermic reaction and therefore an increase of temperature particularly on the active side of the sensor occurs. At the end, the temperature difference can be correlated quantitatively to the H_2O_2 concentration.

However, the measurement of H_2O_2 concentrations alone cannot substitute the need of the microbiological methods by itself. Therefore, it is preferable to incorporate an additional measurement method of the spores' viability. Different methods have been proposed to measure this, such as with optical [17, 18], potentiometric [19], piezoelectric [20] or impedimetric sensors [21]. The determination of the spores' viability generally employs additional unique biomarkers from the spore coat or byproducts from germination, for example, mRNA (messenger ribonucleic acid) [22], dipicolinic acid (DPA) or calcium ions (Ca^{2+}) [23]. Therefore, specific (bio-)chemical transducers must be adapted. Nevertheless, most of these methods are solution-based, having high response times (>20 min) and are not convenient to perform under a dry gaseous environment. Recently, a novel impedimetric sensor was suggested to monitor the microbiological efficacy of gaseous H_2O_2 during sterilization processes [24]. This sensor measures the spore morphology by means of impedance changes in regard to the hydrogen peroxide concentration. It consists in a differential setup of two interdigitated electrode arrangements. On one arrangement, microbiological spores (e.g., *Bacillus atrophaeus*) are immobilized and the other one functions as a reference. The impedance of the spores is measured before and after the sterilization process and the spores' viability can be determined due to the correlation

between the H_2O_2 concentration and the impedance change. However, the principle of this sensor is still under ongoing research.

So far, to the extent of our knowledge, no sensor that can measure at the same time gaseous H_2O_2 concentrations and can additionally evaluate the spores' viability under industrial conditions has been presented. In addition, the effect of H_2O_2 on the morphology of spores has not been either investigated in detail. For these reasons, the purpose of this contribution is to develop a sensor array constructed of a calorimetric gas sensor, which can determine H_2O_2 concentrations together with a spore-based biosensor, which can evaluate the spores' viability, and as a whole is able to evaluate the efficacy of the sterilization process with gaseous H_2O_2 for industrial applications. Furthermore, three different spore strains, namely *Bacillus atrophaeus* DSM 675, *Bacillus subtilis* DSM 402 and *Geobacillus stearothermophilus* DSM 5934 are characterized regarding the effect of H_2O_2 on them by means of impedimetric-, AFM-, SEM- and microbiological measurements.

7.2. Materials and methods

7.2.1 Sensor fabrication: calorimetric gas- and spore-based biosensor array

The fabrication process of the sensor array was introduced in [25]. This is schematically shown in the supplementary information in Figure 7.S1. An adhesion promoter (Ti prime, Microchemicals GmbH, Germany) was spin-coated onto a dehydrated borosilicate glass wafer. Likewise, a positive photoresist (AZ®5214E, Microchemicals GmbH, Germany) was deposited as well. Then, a mask aligner was used to photolithographically pattern the selected design to the photoresist (Süss MicroTec AG, Germany). Subsequently, the wafer was developed and the metals (10 nm titanium and 100 nm platinum) were deposited by means of an e-beam evaporation process. A lift-off process (TechniStrip®Micro D350, Microchemicals GmbH, Germany) was then employed to obtain the final structures.

Moreover, the calorimetric H_2O_2 sensor was fabricated according to previous investigations as shown in [14, 26, 27]. Briefly, the meander structures were passivated with a photoresist (SU-8, Microchemicals GmbH, Germany) to protect Pt from vaporized hydrogen peroxide. Afterwards, on the active side of the sensor, MnO_2 as a catalyst was deposited.

In addition, for the spore-based biosensor, a 10 µl aliquot of the spore suspension (stock solution of at least 10^8 CFU/ml, see section 7.2.2 for further details) was pipetted only onto the active side of the sensor and air-dried under sterile conditions. A final spore concentration on the chip of least 10^6 CFU/ml (colony forming units per milliliter) was obtained; this preparation was done in accordance to industrial requirements [9]. The spore concentration of 10^6 CFU/ml on the chip was assured during all experiments since all cleaning procedures (washing steps) were performed before spore immobilization. Both the schematic (left) and the photograph (right) of the combined sensor array can be observed in Figure 7.1 a).

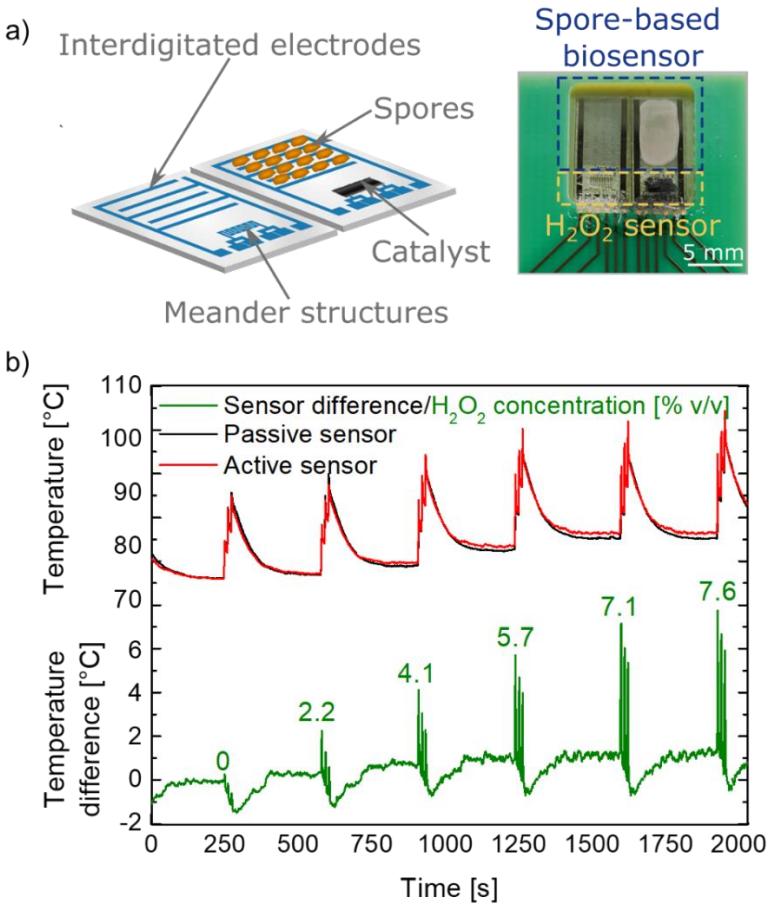

Figure 7.1 a) The sensor array has a differential setup: on one sensor (active) the spores are immobilized on interdigitated electrodes and a catalyst is deposited on the meander structures, the other sensor (passive) serves as a reference. b) calorimetric gas sensor response to different concentrations of gaseous hydrogen peroxide. The upper curves correspond to the temperature of the catallytically active sensor and the passive one. The temperature difference and by this, the actual H_2O_2 concentration is shown in the lower part curve.

7.2.2 Spore production

The spore suspensions were produced according to a modified method of [28] and performed under sterile conditions. The strains of *Bacillus subtilis* DSM 402 and *Geobacillus stearothermphilus* DSM 5934 were kindly provided from Prof. Dr. J. Bongaerts (Aachen University of Applied Sciences). The *Bacillus atrophaeus* DSM 675 strain was purchased from the Leibniz Institute DSMZ – German Collection of Microorganisms and Cell Cultures (Germany). All strains were cultivated with a complex medium consisting of meat extract dry (3 g/l) and peptone (5 g/l) for 24 h at 30 °C for *B. subtilis* and *B. atrophaeus*, and at 55 °C for *G. stearothermophilus*. Afterwards, the sporulation was induced by inoculation of cells on nutrient agar plates enriched with $MnSO_4$ (10 g/l) and incubated for 7 days with the above mentioned temperatures for each microorganism. Then, the spores were collected from the plates with an inoculation loop and deposited into a 15 ml centrifuge tube containing 5 ml of distilled water. The tubes were subsequently mixed by a vortex mixer and centrifuged at 4,000 rpm (A-4-81; Centrifuge 5810R, Eppendorf, Germany) for 20 min at 20 °C. The vegetative cells and debris were removed from the suspension and the spores were washed with distilled water and then centrifuged again. This process was repeated at least eight times, until a spore suspension of at least 99% bacteria/debris-free was reached. Finally, to guarantee the inactivation of any remaining bacteria, the suspension was pasteurized at 80 °C for 20 min. A final concentration of 10^8 CFU/ml was obtained by means of serial dilutions and plating.

7.2.3 Sterilization with vaporized H_2O_2

All sterilization procedures were carried out in a test rig presented in [14, 27] analog to those sterilization modules used in industrial aseptic filling machines. Here, a H_2O_2 gas stream of 10 m^3/h is provided by pressurized air used as a carrier. This air-H_2O_2 combination is heated in a vaporizer up to 240 °C. Hydrogen peroxide concentrations can be set in the range from 0 to 7.6% v/v.

The sensor arrays were submitted to H_2O_2 sterilization for different concentrations, namely, 0% v/v, 2.2% v/v, 4.1% v/v, 5.7% v/v, 7.1% v/v and 7.6% v/v at 240 °C for 2 s. The exposure time, the temperature and the highest H_2O_2 concentration used in this study resemble standard parameters applied in the industry.

7.2.4 Physical and electrical characterizations

7.2.4.1 Calorimetric H_2O_2 sensor

Two passivated platinum meander structures were used as resistance temperature resistors (RTDs): a change of resistance linearly varies with a change of temperature. One meander structure serves as a reference (passive sensor), whereas the other one as a sensing element (active sensor); the passive sensor remains inert to H_2O_2 while on the active sensor, MnO_2 catalyzes H_2O_2. As a result, an increase of temperature occurs on the active sensor and a temperature difference between both sensors can be correlated to the hydrogen peroxide concentration. Furthermore, a water-bath thermostat (Omnicool, LAUDA Scientific GmbH, Germany) was used to temperature-calibrate them from 0 to 80 °C in 10 °C steps. In addition, the four-point probe method was used to measure the resistance of the sensors and it was recorded using a data acquisition card (USB-9219, National Instruments Corpotation, United States) and a built-in LabView program. At least four sensors were used for each hydrogen peroxide concentration and spore strain.

7.2.4.2 Spore-based biosensor

The viability of the spores was measured by means of impedimetric measurements. For this, a precision LCR meter (E4980A, Agilent Technologies, United States) was utilized with a fixed frequency of 3 kHz and an excitation voltage of 20 mV with a direct current voltage bias of 0 V. The direct current bias of 0 V was carefully chosen according to typically used literature values for similar impedance spectroscopy measurements with interdigitated electrodes in combination with microorganisms [29, 30]. Furthermore, the OCP was not measured, since we do not use any external reference electrode or measure in solution during our experiments. Nevertheless, stability investigations of the interdigitated structures have been made showing no effect from gaseous hydrogen peroxide on them or any other described process steps [31]. In addition, to assure a reliable sensor signal, we implement a differential setup, where one sensor serves as a reference and the other as sensing element (e.g., catalytically activated or with spores).

Moreover, to be able to analyze between different sensors, the sensor impedance was normalized by the following equation (Equation 7.1):

$$Normalized\ impedance\ (\%) = \left(\frac{Procedure}{Blank\ sensor}\right) \times 100 \qquad \text{(Equation 7.1)}$$

Blank sensor connotes the measurement of the sensor without spores and *Procedure*, the impedance change after the spores were confined onto the IDEs, and sterilized with different hydrogen peroxide concentrations (see section 7.2.3). At least four sensors were used for each H_2O_2 concentration.

7.2.4.3 Scanning electron microscopy (SEM)

A scanning electron microscope (JSM-7800F, JEOL Ltd., Japan) was employed to study the morphology of the spores after sterilization with H_2O_2. For these measurements, the samples were prepared by sputtering a 10 nm layer of Pt/Pd (80:20) on them.

Moreover, qualitative evaluations were performed by classifying the spores in different types, namely "normal", "deformed" and "flattened". For each hydrogen peroxide concentration, the ratio of the particular spore type was determined by counting them manually; this was performed at least three times. 1551 to 3440 spores were counted and evaluated for each spore strain.

7.2.4.4 Atomic force microscopy (AFM)

A more quantitative investigation (height measurements) to study the morphology of spores after being treated with H_2O_2 was conducted utilizing an atomic force microscope (BioMat Workstation, JPK Instruments, Germany). Here, silicon probes (Arrow NCR, NanoWorld AG, Switzerland) were operated with a force constant of 42 N/m and a resonance frequency of 285 kHz. All the recordings (20 x 20 µm²) were carried out in tapping mode at 512 pixels per line with a scanning frequency of 0.6 Hz under environmental conditions. Moreover, an open-source software (Gwyddion, http://gwyddion.net/) was used to visualize and analyze the height measurement of the spores; this was obtained by measuring the average height of each spore, i.e. no cross-section tool was used, but a mask for the whole spore.

7.3. Results and discussion

7.3.1 Calorimetric H_2O_2 sensor

H_2O_2 concentrations between 0 and 7.6% v/v were determined within 2 s by means of a calorimetric H_2O_2 sensor as shown in Figure 7.1 b). On the upper part of the graph, the temperatures of both active and passive sensors can be observed. Furthermore, their temperature difference and the hydrogen peroxide concentration are shown on the bottom part. Taken 0% v/v H_2O_2 as a reference, no distinguishable temperature difference was observed during the resting phase (no exposure). However, for all other concentrations, as the H_2O_2 concentration rises, a higher exothermic reaction takes place on the active sensor part than the passive one and the temperature difference between them increases. As a result, a sensor sensitivity of 0.97 °C/(% v/v) was obtained. This sensitivity is lower than that found in literature by polyimide sensors (2.06 °C/(% v/v), [32]). The reason for that is due to the fact that polyimide films have a lower thermal conductivity (0.16 W/mK) than borosilicate glass substrates (1.2 W/mk). Thus, it may reduce thermal flow [33] generated on the active sensor and hence increase the temperature difference between sensors, i.e., enhancing the sensitivity. Additionally, three characteristic peaks [32] can be seen along all H_2O_2 concentrations, which correspond to the 2 s response time of the sensor; the precise measurement of H_2O_2 concentrations up to 7.6% v/v (a typical concentration in industrial applications) within 2 s was successfully demonstrated. Further magnification of the peaks and the calibration curve of the sensor can be found in Figure 7.S2 a) and b) from the supplementary section.

7.3.2 Effect of gaseous H_2O_2 on the morphology of spores

7.3.2.1 SEM measurements

Different spore suspensions of *B. subtilis*, *B. atrophaeus* and *G. stearothermophilus* were physically characterized by SEM measurements after exposure to various H_2O_2 concentrations to analyze morphological changes of spores. Several morphology conditions of spores could be differentiated for each strain: depending on the spore status the spores were labeled as "normal", "deformed" or "flattened" as shown in Figure 7.2. The normal and deformed conditions were encountered in a specific ratio, which varies, depending on the

applied H_2O_2 gas concentration. In contrast, the flattened condition was only found after treating the spores with gaseous hydrogen peroxide.

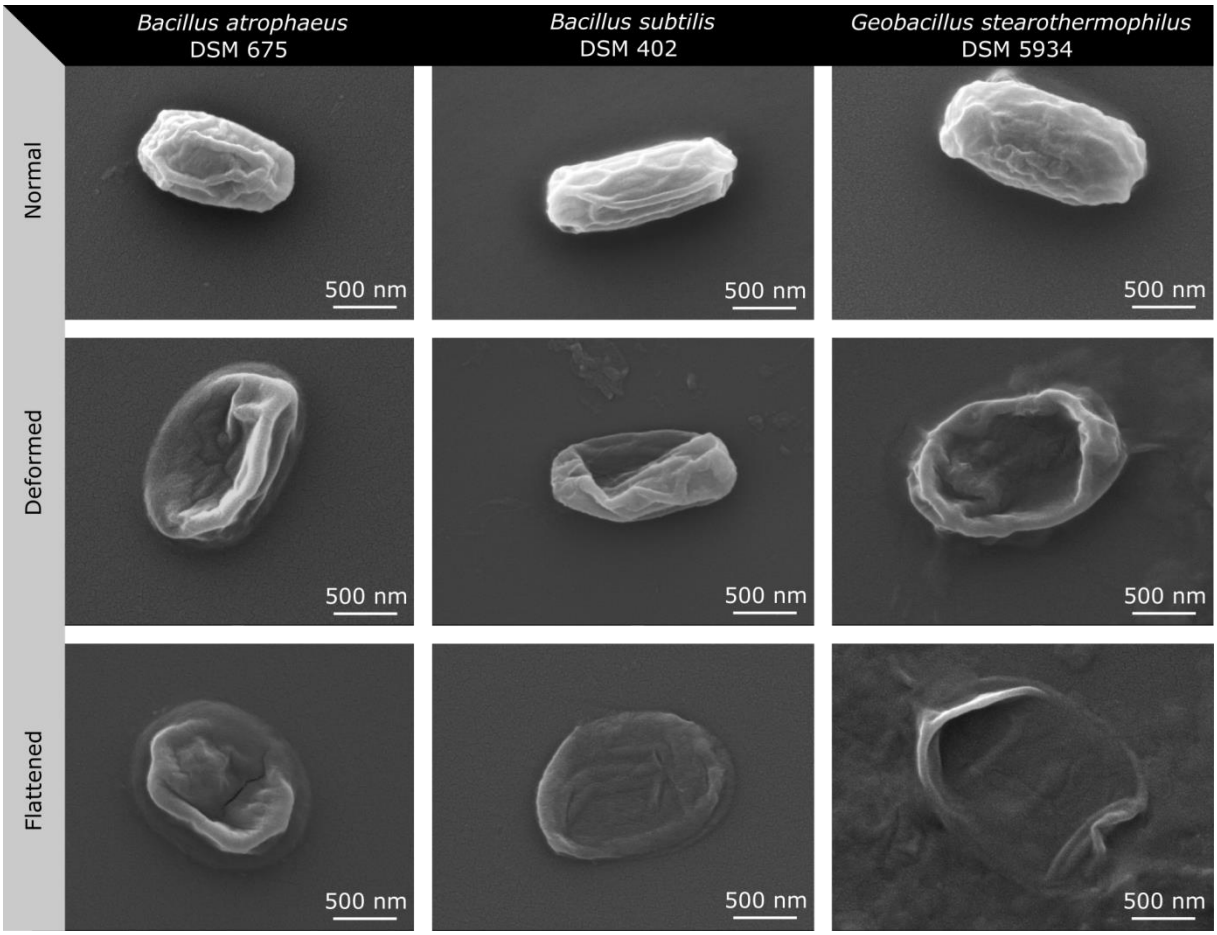

Figure 7.2 SEM pictures of representative morphology types *of Bacillus atrophaeus* DSM 675, *Bacillus subtilis* DSM 402 and *Geobacillus stearothermophilus* DSM 5934 spores commonly encountered as: "normal", "deformed" and "flattened". The flattened type was found only after H_2O_2 sterilization.

The ratio of such conditions was evaluated by SEM in Figure 7.3 a), b) and c), as stated in section 7.2.4.3. For the evaluation of the data between 1551 and 3440 spore samples have been investigated each, to guarantee statistically relevant data. As it can be seen for *B. atrophaeus* (Figure 7.3 a), at the beginning of the sterilization process (0% v/v H_2O_2) 77.76% ± 2.04% were normal spores and 22.23% ± 2.04% deformed spores; no flattened spores were found at this stage. As the H_2O_2 concentration was increased, the amount of normal spores decreased (the only exception was 5.7% v/v H_2O_2), and that of the deformed and flattened spores increased. During the maximum concentration of 7.6% v/v H_2O_2, 38.97% ± 2.49% of normal-, 27.77% ± 3.48% deformed- and 33.25% ± 0.98% flattened spores were

found. Moreover, for *B. subtilis* (Figure 7.3 b), without H_2O_2 exposure the flattened spore type was practically absent with a value of 0.97% ± 0.41%, following by 30.94% ± 5.59% of deformed and 68.07% ± 5.57% of normal spores. For concentrations higher than 5.7% v/v H_2O_2 no significant further decrease of the flattened spores was observed. However, a

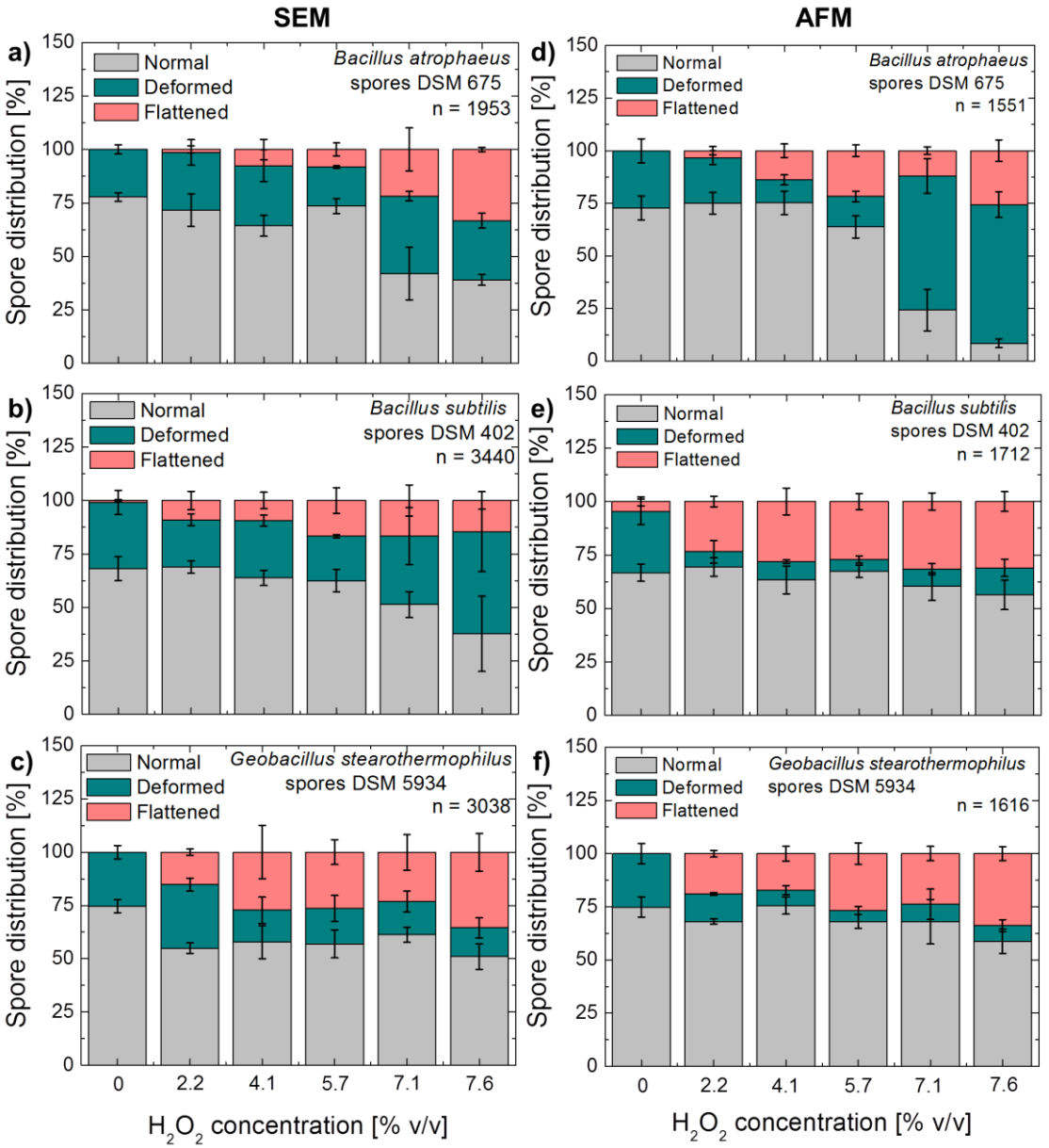

Figure 7.3 Comparison of SEM- (a, b and c) vs. AFM measurements (d, e and f) regarding the distribution of different spore conditions ("normal", "deformed", "flattened") from *Bacillus atrophaeus* DSM 675 (top), *Bacillus subtilis* DSM 402 (middle) and *Geobacillus stearothermophilus* DSM 5934 (bottom) after being treated with gaseous hydrogen peroxide. For each presented graph "n" spores were investigated for all shown concentrations.

decrease of the normal spores as well as an increase of the deformed spores can be seen for the last two concentrations of 7.1% v/v and 7.6% v/v H_2O_2. As an example, the distributions at 7.6% v/v for normal, deformed and flattened spores were 47.46% ± 5.98%, 36.97% ± 0.74% and 15.56% ± 5.23%, accordingly. Furthermore, in the case of *G. stearothermophilus* (Figure 7.3 c), it can be noted that the proportion of the spore types along the H_2O_2 concentrations changed significantly after the first dosage (2.2% v/v H_2O_2), where the presence of normal spores decreased and the deformed- and flattened spores dramatically increased. Further concentrations from 4.1% v/v H_2O_2 onwards did not notably influence the spore condition distribution, except for the last concentration of 7.6% v/v, where the flattened spores increased and the deformed- and normal spores decreased with final values of 35.50% ± 8.86%, 13.52% ± 4.63% and 50.97% ± 5.93%, respectively.

Besides the morphology change of spores due to hydrogen peroxide, other parameters may also intervene in the structure modification of the spores such as the sample preparation (sputtering of metal on spores) or vacuum during the SEM measurement. For this reason, the spores were further evaluated by means of AFM.

7.3.2.2 AFM measurements

The effect of hydrogen peroxide on different spores was additionally quantitatively evaluated by means of AFM. Firstly, the height of each spore category ("normal", "deformed" and "flattened") was determined (Table 7.1), even though the spore size values vary depending on the preparation and measurement techniques of the spores [34]. To each value 520 spores have been investigated, in our case, under normal conditions, *G. stearothermophilus* possesses the highest height of all of them. Meanwhile *B. atrophaeus* and *B. subtilis* retain similar values. During the deformed condition, *B. subtilis* and *G. stearothermophilus* share similar heights, whereas *B. atrophaeus* displays the lowest height in this form. Lastly, similar heights of all spores can be seen in the flattened case. It is also worthy to note that those height values do not significantly change along H_2O_2 concentrations, but the ratio of the different spore conditions does. For example, a normal spore encountered at 0% v/v H_2O_2 has a comparable height value as a normal spore encountered at 7.6% v/v H_2O_2; the same is also true for the other spore conditions.

Table 7.1 Height measurements (nm) of *B. atrophaeus*, *B. subtilis* and *G. stearothermophilus* spores (to each value in the table 520 spores have been investigated).

Spore condition	*B. atrophaeus*	*B. subtilis*	*G. stearothermophilus*
"Normal"	530.05 ± 120.31	540.35 ± 96.97	671.19 ± 119.15
"Deformed"	375.00 ± 85.30	437.00 ± 83.09	441.36 ± 122.98
"Flattened"	241.36 ± 68.38	239.67 ± 77.68	242.57 ± 81.49

Moreover, to corroborate the SEMs measurements from the last section, the spores were treated with the same conditions as before: they were exposed to different hydrogen peroxide concentrations. Later, they were qualitatively (spore distribution) and quantitatively (spore height) assessed. From Figure 7.3 d), e) and f) similar results can be observed after sterilization with H_2O_2. Without hydrogen peroxide, both SEM and AFM are in a good agreement, probably suggesting no additional effect from the SEM measurements to the morphology of the spores at this stage. Furthermore, from the H_2O_2 concentration of 2.2% v/v onwards, differences are appreciable; particularly, this has been found for the last two concentrations (7.1% v/v and 7.6% v/v H_2O_2) of *B. subtilis and B. atrophaeus*, where the amount of normal and deformed spores deviates from than that of the SEM. Nonetheless, both characterization methods show similar tendency.

Besides the different conditions, the respective averaged spore height of all three types of factors (average of all conditions weighted by the distribution of different spore conditions from Figure 7.3 d), e) and f)) was determined (Figure 7.4) and evaluated (Figure 7.5 a) for each H_2O_2 concentration. As it can be seen for *B. atrophaeus*, at the beginning of the sterilization test series (0% v/v H_2O_2) the average height of all spore categories was 463.4 nm ± 129.05 nm. During the maximum concentration of 7.6% v/v H_2O_2, the average spore height was 288.99 nm ± 134.96 nm. Moreover, for *B. subtilis* after 2.2% v/v H_2O_2 concentration, no further significant decrease of the average height of the spores was observed. At the end of the sterilization process, the average height was 409.68 nm ± 162.66 nm. As comparison, for the 0% v/v H_2O_2 concentration, the spores' height was 460.29 nm ± 168.35 nm. Furthermore, for

G. stearothermophilus no significant average height change was observed; it was nearly constant for all H_2O_2 concentrations.

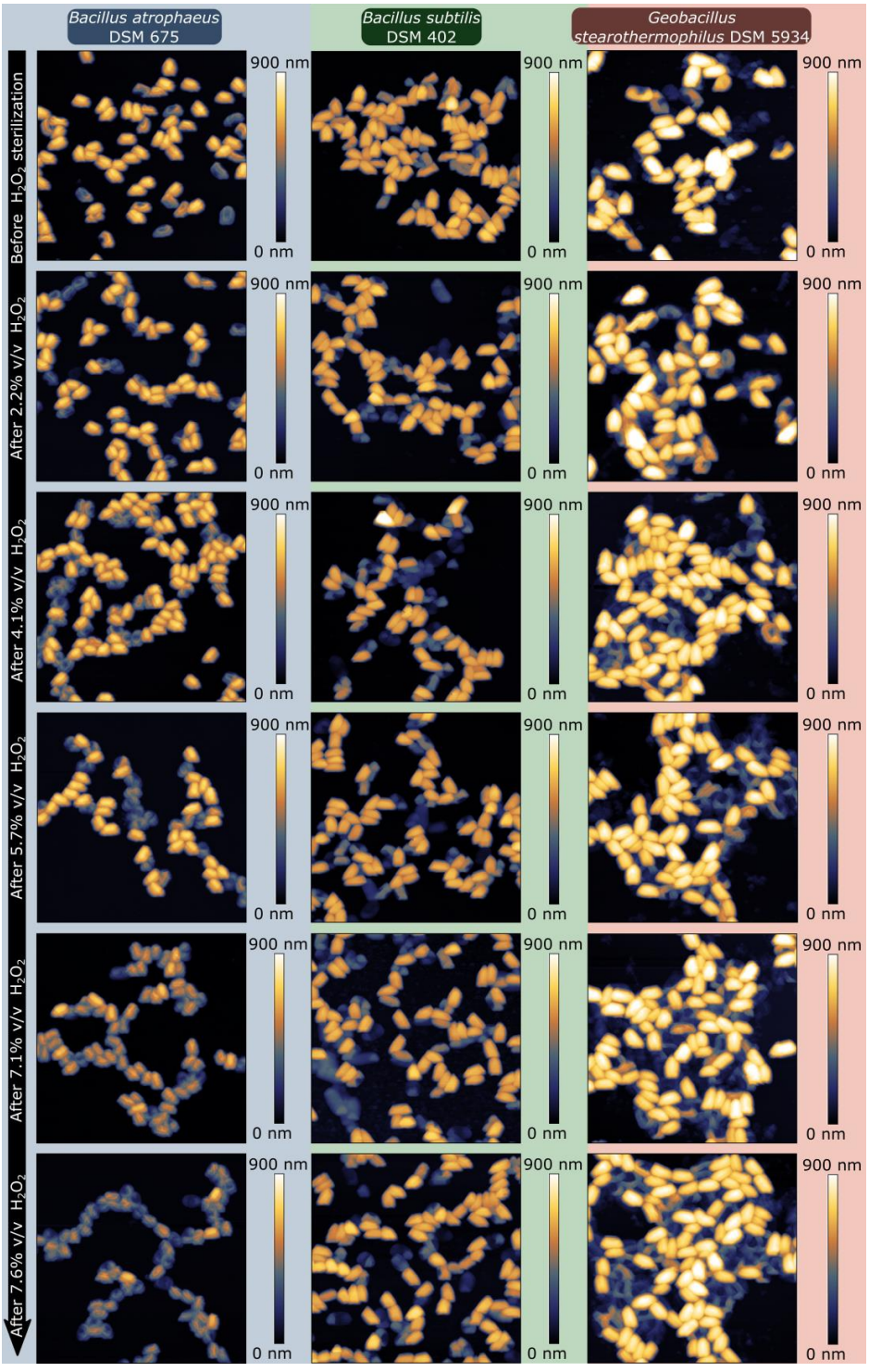

Figure 7.4 AFM measurements (20 x 20 µm²) of *Bacillus atrophaeus* DSM 675 (left), *Bacillus subtilis* DSM 402 (middle) and *Geobacillus stearothermophilus* DSM 5934 (right) spores sterilized with different concentrations of H_2O_2 (0% v/v to 7.6% v/v from top to bottom).

In summary, H_2O_2 influences in a different manner each spore strain. The decreases of height and of the spore conditions of *B. atrophaeus* spores have a relatively linear relationship to the increase of H_2O_2 concentration. In addition, the height of spores of *B. subtilis* after being exposed to the minimal concentration (in our case 2.2% v/v H_2O_2) remains practically constant, whereas the normal and deformed spores linearly decrease, but the flattened spores prevail in a steady behavior. For *G. stearothermophilus*, the spores' height is fairly maintained during all hydrogen peroxide concentrations. Moreover, after the first exposure to H_2O_2, the normal proportion of spores decreased and the deformed spores notably increased. From this step on until the penultimate concentration (7.1% v/v H_2O_2), the spores' height as well as the different spore types stayed at a constant state.

The relationship between H_2O_2 concentration and the spore morphology (different spore conditions and spore height) is a decisive parameter to shed light on further development on this novel type of spore-based biosensors applied in industrial processes. For example, from the AFM- and SEM measurements, it has been realized that not all spore strains may be optimal candidates for a spore-based biosensor used to assure a proper functioning of aseptic machines, since the spore coat sensitivity to gaseous hydrogen peroxide of each varies.

So far, the impact of H_2O_2 on spores by means of morphological changes has been investigated. One step further is to examine the relationship between these morphological- and sensor signal changes (impedance) from spore-based biosensors (see section 7.3.3).

7.3.3 Spore-based biosensor

The different spore types, namely *B. atrophaeus*, *B. subtilis* and *G. stearothermophilus* (see section 7.2.2), were simultaneously characterized by means of impedimetric measurements. Fig. 7.5 b) depicts the respective normalized sensor signal at different stages of the measurement process, including a reference step (blank sensor), the electrical properties of the spores after immobilization onto the sensor surface (spores) and the effect of different concentrations of H_2O_2 peroxide (2.2-7.6% v/v) on the spores, measured at the same time with the H_2O_2 calorimetric sensor from section 7.3.1. As it is noticeable from the graph, after immobilizing the spores on the sensor surface, *G. stearothermophilus* has the highest sensor signal change (impedance) to 79.84% ± 2.5% from the starting value of 100% compared to the other *Bacillus* species, particularly 96.12% ± 0.8% for *B. subtilis* and 94.03% ± 1.31% for *B.*

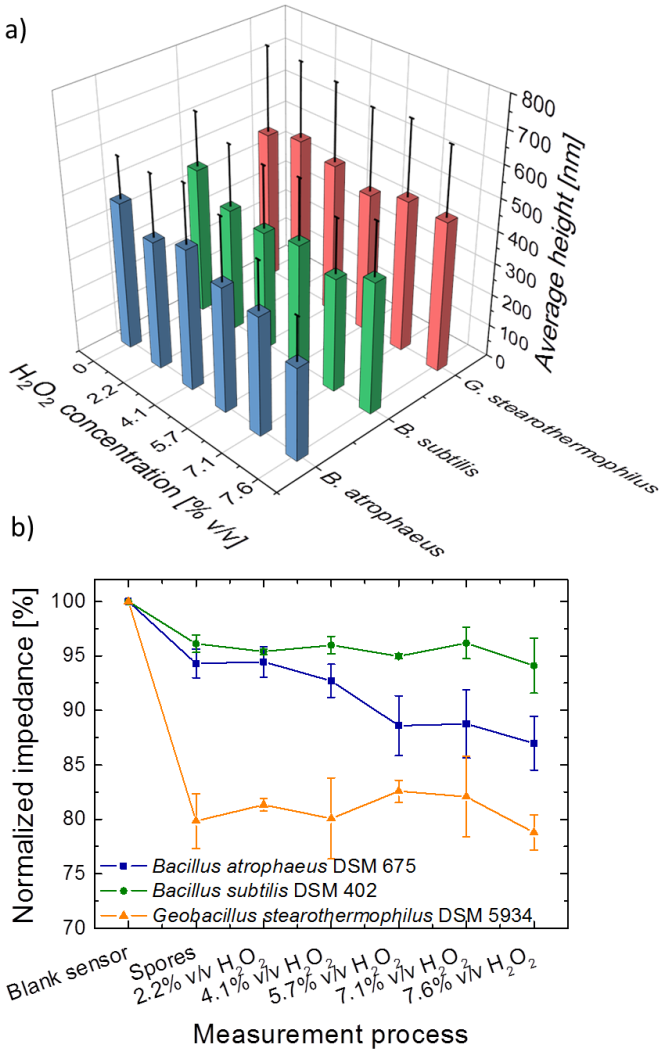

Figure 7.5 a) Averaged spore height measurements of *Bacillus atrophaeus* DSM 675, *Bacillus subtilis* DSM 402 and *Geobacillus stearothermophilus* DSM 5934 spores for different concentrations of hydrogen peroxide; b) signal response (impedance) of spore-based biosensors. The sensors were measured at different stages (at least four sensors were used for each step). In the first stage, the sensors were measured after being cleaned. In the second step, *Bacillus atrophaeus* DSM 675, *Bacillus subtilis* DSM 402 and *Geobacillus stearothermophilus* DSM 5934 spores were immobilized on them. Subsequently, in the following stages, the spore-bases biosensors were submitted to several concentrations of gaseous hydrogen peroxide.

atrophaeus. Furthermore, most of them do not show a linear behavior to the increment of H_2O_2 concentrations (except for *B. atrophaeus*). *B. subtilis* and *G. stearothermophilus* exhibit an irregular flat performance; however, for all the cases the impedance change at the highest concentration (7.6% v/v) could underline a measurable impedance change for typical

concentrations applied in industrial processes. The highest impedance change at this concentration for *B. atrophaeus* was 7.05%, followed by *B. subtilis* with 2.02% and finally, *G. stearothermophilus* with 1.05%. In case of *B. atrophaeus* as a test organism, the spore-based biosensor is able to distinguish between all investigated concentrations. For *B. subtilis* and *G. stearothermophilus* this is still true but limited only to the highest hydrogen peroxide concentration (7.6% v/v).

Moreover, it has been suggested in literature [24] that the change of impedance after sterilization with gaseous H_2O_2 can be related to a morphological change of the spores. This correlation of the morphological change has been similarly reported for other sterilization techniques, such as spores treated with metal-oxide nanoparticles [35], surfactants [36] or plasma treatment [37]. However, the opposite has been discussed in literature as well: no morphological change after a sterilization process, for example, by treating the spores with electrical discharges [38]. In our case, as reviewed in the previous section, H_2O_2 indeed induced a morphology change on all investigated spores. Therefore, the impedance change from the spore-based biosensor is likely to occur due to the transition to different spores conditions. As the spores change from the deformed to flattened condition, they may start leaking cell constituents, making the sensor surface more conductive and thus reducing its overall impedance [24]. As a result, the morphology change of the spores is suitable as a physical parameter to determine the spores' viability.

7.4. Conclusions

In this work, a combined sensor array consisting of a calorimetric gas- and a spore-based biosensor for online monitoring of sterilization processes with gaseous H_2O_2 under industrial conditions was introduced for the first time. H_2O_2 concentrations up to 7.6% v/v were determined with a sensor sensitivity of 0.97 °C/(% v/v). Furthermore, the effect of H_2O_2 on different spore strains, namely *Bacillus atrophaeus* DSM 675, *Bacillus subtilis* DSM 402 and *Geobacillus stearothermophilus* DSM 5934, were meticulously investigated by means of SEM-, AFM- and impedimetric measurements. Every spore strain was differently affected by H_2O_2. Three spores categories were identified during the sterilization process and eventually transited from one to the next condition: "normal", "deformed" and "flattened". The average spores' height of *B. atrophaeus* showed a fairly linear correlation to the H_2O_2

concentration. Meanwhile, *B. subtilis* spores showed a rapid decrement of their height after 2.2 % v/v H_2O_2, whereas *G. stearothermophilus* showed a steady height along all H_2O_2 concentrations. In addition, the efficacy of a sterilization process with gaseous H_2O_2 was carried out with a spore-based biosensor. Sensors fabricated with *B. atrophaeus* were able to successfully distinguish between all investigated H_2O_2 concentrations. Spores from *B. subtilis*, and *G. stearothermophilus* were still able to evaluate qualitatively the sterilization process but limited to the H_2O_2 concentration of 7.6% v/v. Nevertheless, it was shown as well that the sensor's signal is likely due to the morphology change of the spores; specifically, the transition to the different spores' conditions and this parameter is convenient to determine the viability of the spores.

The presented combined sensor array consisting of a gaseous hydrogen peroxide sensor that benefits from a quick response time (2 s) and a spore-based biosensor, which enables measuring impedance changes due to morphological variation of spore size, opens unique approaches regarding evaluation and monitoring of sterilization processes with H_2O_2 in aseptic food industry. Hydrogen peroxide concentrations can be precisely measured within industrial operation conditions. This provides several advantages such as online- and inline monitoring, ease of portability (miniaturized system) and no further sample preparation is needed. Additionally, the efficacy of the sterilization process can be effectively determined by the embedded spore-based biosensor. This work demonstrated that *Bacillus atrophaeus* spores can be used for quantitative determination and the other investigated strains (*B. subtilis and G. stearothermophilus*) showed restricted correlation between morphological- and impedance changes while being exposed to hydrogen peroxide. The synergy of the two sensor types as one combined sensor array allows a considerably more specific multi-parameter experience in aseptic filling machines in comparison to isolated microbiological state-of-the-art- or hydrogen peroxide methods.

Further investigations will focus on the increase of the sensor's sensitivity of the calorimetric gas- and spore-based biosensors by employing substrates with lower thermal coefficients (e.g., polyimide films) or optimizing the spore number and immobilization techniques on the biosensor array.

Acknowledgements

The authors are thankful to Prof. Dr. P. Siegert and Prof. Dr. J. Bongaerts for access to the microbiology laboratory for microbiological research, H. Iken and J. Oberländer for support during the fabrication of the sensor array and D. Rolka for the SEM measurements. The financial funds were provided by the Federal Ministry of Education and Research, Germany, Project: "SteriSens" (Fund. No.: 03FH057PX5).

References

[1] I.A. Ansari and A.K. Datta, "An overview of sterilization methods for packaging materials used in aseptic packaging systems", *Food Bioprod. Process.* 81 (1), 57–65 (2003).

[2] S. Koda, S. Kumagai, and H. Ohara, "Environmental monitoring and assessment of short-term exposures to hazardous chemicals of a sterilization process in hospital working environments", *Acta Med. Okayama* 53 (5), 217–223 (1999).

[3] R.T. Toledo, "Overview of sterilization methods for aseptic packaging materials", in *Food and Packaging Interactions: Developed from a Symposium Sponsored by the Division of Agricultural and Food Chemistry at the 193rd Meeting of the American Chemical Society, Denver, Colorado, April 5-10, 1987*, American Chemical Society, Washington, DC, USA 1988, 94-105.

[4] M.D. Johnston, S. Lawson, and J.A. Otter, "Evaluation of hydrogen peroxide vapour as a method for the decontamination of surfaces contaminated with *Clostridium botulinum* spores", *J. Microbiol. Meth.* 60 (3), 403–411 (2005).

[5] R.A. Heckert, M. Best, L.T. Jordan, G.C. Dulac, D.L. Eddington, and W.G. Sterrit, "Efficacy of vaporized H_2O_2 against exotic animal viruses", *Appl. Environ. Microb.* 63 (10), 3916–3918 (1997).

[6] N. Kitancharoen, A. Yamamoto, and K. Hatai, "Fungicidal effect of hydrogen peroxide on fungal infection of rainbow trout eggs", *Mycoscience* 38 (4), 375–378 (1997).

[7] J.A. Otter and G.L. French, "Survival of nosocomial bacteria and spores on surfaces and inactivation by hydrogen peroxide vapor", *J. Clin. Microbiol.* 47 (1), 205–207 (2009).

[8] P. Swartling and B. Lindgren, "The sterilizing effect against *Bacillus subtilis* spores of hydrogen peroxide at different temperatures and concentrations", *J. Dairy Res.* 35 (03), 423–428 (1968).

[9] G. Cerny, "Testing of aseptic machines for efficiency of sterilization of packaging materials by means of hydrogen peroxide", *Packag. Technol. Sci.* 5 (2), 77–81 (1992).

[10] J. Kulys, "Flow-through amperometric sensor for hydrogen peroxide monitoring in gaseous media", *Sensor Actuat. B-Chem.* 9 (2), 143–147 (1992).

[11] S. Liu, H. Sun, R. Nagarajan, J. Kumar, Z. Gu, J. Cho, and P. Kurup, "Dynamic chemical vapor sensing with nanofibrous film based surface acoustic wave sensors", *Sensor Actuat. A-Phys.* 167 (1), 8–13 (2011).

[12] A.L. Verma, S. Saxena, G.S.S. Saini, V. Gaur, and V.K. Jain, "Hydrogen peroxide vapor sensor using metal-phthalocyanine functionalized carbon nanotubes", *Thin Solid Films* 519 (22), 8144–8148 (2011).

[13] M. Xu, B.R. Bunes, and L. Zang, "Paper-based vapor detection of hydrogen peroxide: colorimetric sensing with tunable interface", *ACS Appl. Mater. Inter.* 3 (3), 642–647 (2011).

[14] P. Kirchner, B. Li, H. Spelthahn, H. Henkel, A. Schneider, P. Friedrich, J. Kolstad, M. Keusgen, and M.J. Schöning, "Thin-film calorimetric H_2O_2 gas sensor for the validation of germicidal effectivity in aseptic filling processes", *Sensor Actuat. B-Chem.* 154 (2), 257–263 (2011).

[15] N. Näther, H. Henkel, A. Schneider, and M.J. Schöning, "Investigation of different catalytically active and passive materials for realizing a hydrogen peroxide gas sensor", *Phys. Status Solidi A* 206 (3), 449–454 (2009).

[16] J. Oberländer, P. Kirchner, H.-G. Boyen, and M.J. Schöning, "Detection of hydrogen peroxide vapor by use of manganese(IV) oxide as catalyst for calorimetric gas sensors", *Phys. Status Solidi A* 211 (6), 1372–1376 (2014).

[17] D. L. Rosen, *Bacterial spore detection and quantification methods* 1997 (Patent, 5876960).

[18] M. B. Tabacco and L. C. Taylor, *Optical sensors for rapid, sensitive detection and quantitation of bacterial spores* 2000 (Patent, 6498041 B1).

[19] Y. Zhou, B. Yu, and K. Levon, "Potentiometric sensor for dipicolinic acid", *Biosens. Bioelectron.* 20 (9), 1851–1855 (2005).

[20] G.A. Campbell and R. Mutharasan, "Piezoelectric-excited millimeter-sized cantilever (PEMC) sensors detect *Bacillus anthracis* at 300 spores/mL", *Biosens. Bioelectron.* 21 (9), 1684–1692 (2006).

[21] M. Labib, A.S. Zamay, O.S. Kolovskaya, I.T. Reshetneva, G.S. Zamay, R.J. Kibbee, S.A. Sattar, T.N. Zamay, and M.V. Berezovski, "Aptamer-based viability impedimetric sensor for bacteria", *Anal. Chem.* 84 (21), 8966–8969 (2012).

[22] A.J. Baeumner, B. Leonard, J. McElwee, and R.A. Montagna, "A rapid biosensor for viable *B. anthracis* spores", *Anal. Bioanal. Chem.* 380 (1), 15–23 (2004).

[23] N. Tehri, N. Kumar, H.V. Raghu, and A. Vashishth, "Biomarkers of bacterial spore germination", *Ann. Microbiol.* 68 (9), 513–523 (2018).

[24] J. Oberländer, M. Mayer, A. Greeff, M. Keusgen, and M.J. Schöning, "Spore-based biosensor to monitor the microbicidal efficacy of gaseous hydrogen peroxide sterilization processes", *Biosens. Bioelectron.* 104, 87–94 (2018).

[25] J. Arreola, M. Keusgen, and M.J. Schöning, "Toward an immobilization method for spore-based biosensors in oxidative environment", *Electrochim. Acta* (302), 394–401 (2019).

[26] P. Kirchner, J. Oberländer, H.-P. Suso, G. Rysstad, M. Keusgen, and M.J. Schöning, "Monitoring the microbicidal effectiveness of gaseous hydrogen peroxide in sterilization processes by means of a calorimetric gas sensor", *Food Control* 31 (2), 530–538 (2013).

[27] N. Näther, L.M. Juárez, R. Emmerich, J. Berger, P. Friedrich, and M.J. Schöning, "Detection of hydrogen peroxide (H_2O_2) at exposed temperatures for industrial processes", *Sensors (MDPI)* 6 (4), 308–317 (2006).

[28] J. Arreola, M. Mätzkow, M.P. Durán, A. Greeff, M. Keusgen, and M.J. Schöning, "Optimization of the immobilization of bacterial spores on glass substrates with organosilanes", *Phys. Status Solidi A* 213 (6), 1463–1470 (2016).

[29] M. Mallén-Alberdi, N. Vigués, J. Mas, C. Fernández-Sánchez, and A. Baldi, "Impedance spectral fingerprint of *E. coli* cells on interdigitated electrodes: a new approach for label free and selective detection", *Sens. Biosensing Res.* 7, 100–106 (2016).

[30] G. Rosati, A. Cunego, F. Fracchetti, A. Del Casale, M. Scaramuzza, A. de Toni, S. Torriani, and A. Paccagnella, "Inkjet printed interdigitated biosensor for easy and rapid detection of bacteriophage contamination: a preliminary study for milk processing control applications", *Chemosens.* 7 (1), 8 (1-13) (2019).

[31] J. Oberländer, A. Bromm, L. Wendeler, H. Iken, M.P. Durán, A. Greeff, P. Kirchner, M. Keusgen, and M.J. Schöning, "Towards a biosensor to monitor the sterilization efficiency of aseptic filling machines", *Phys. Status Solidi A* 212 (6), 1299–1305 (2015).

[32] P. Kirchner, J. Oberländer, H.-P. Suso, G. Rysstad, M. Keusgen, and M.J. Schöning, "Towards a wireless sensor system for real-time H_2O_2 monitoring in aseptic food processes", *Phys. Status Solidi A* 210 (5), 877–883 (2013).

[33] M.C. Wheeler, J.E. Tiffany, R.M. Walton, R.E. Cavicchi, and S. Semancik, "Chemical crosstalk between heated gas microsensor elements operating in close proximity", *Sensor Actuat. B-Chem.* 77 (1-2), 167–176 (2001).

[34] M. Carrera, R.O. Zandomeni, J. Fitzgibbon, and J.-L. Sagripanti, "Difference between the spore sizes of *Bacillus anthracis* and other *Bacillus* species", *J. Appl. Microbiol.* 102 (2), 303–312 (2007).

[35] P.K. Stoimenov, R.L. Klinger, G.L. Marchin, and K.J. Klabunde, "Metal oxide nanoparticles as bactericidal agents", *Langmuir* 18 (17), 6679–6686 (2002).

[36] P.A. Pinzon-Arango, G. Scholl, R. Nagarajan, C.M. Mello, and T.A. Camesano, "Atomic force microscopy study of germination and killing of *Bacillus atrophaeus* spores", *J. Mol. Recognit.* 22 (5), 373–379 (2009).

[37] O. Tarasenko, S. Nourbakhsh, S.P. Kuo, A. Bakhtina, P. Alusta, D. Kudasheva, M. Cowman, and K. Levon, "Scanning electron and atomic force microscopy to study plasma torch effects on *B. cereus* spores", *IEEE Plasma Sci.* 34 (4), 1281–1289 (2006).

[38] C. Lamarche, C. Da Silva, G. Demol, E. Dague, M.-P. Rols, and F. Pillet, "Electrical discharges in water induce spores' DNA damage", *PLOS ONE* 13 (8), e0201448 (1-15) (2018).

Supplementary information

7. S1 Sensor fabrication: calorimetric gas- and spore-based biosensor array

The fabrication process of the sensor array was introduced in [1] and is shortly summarized in Figure 7.S1.

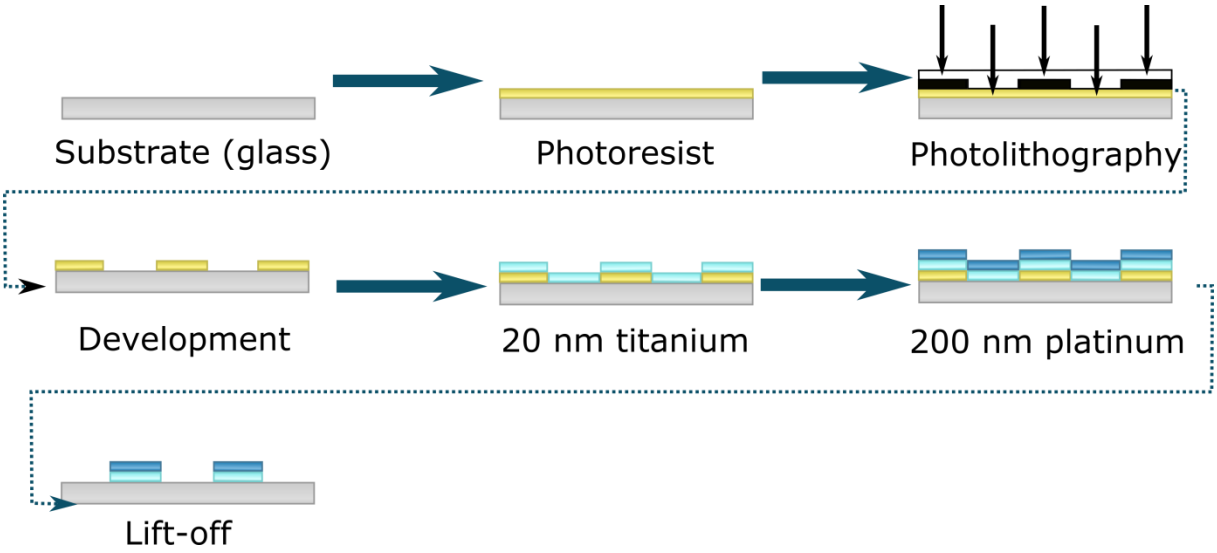

Figure 7.S1 Fabrication process of the calorimetric gas- and spore-based biosensor array. An adhesion promoter and a photoresist are spin-coated onto a glass substrate. Then, the desired design is patterned by photolitography. After that, the structures are developed to remove the remaining photoresist and 20 nm of Ti and 200 nm of Pt are deposited by evaporation, respectively. At the end, the final structures are obtained by a lift-off process.

7.S1.1 H_2O_2 response time and calibration curve

The response time of the calorimetric H_2O_2 sensor as well as its calibration curve for H_2O_2 concentrations from 0% v/v to 7.6% v/v are shown in Figure 7.S2 a) and b), respectively.

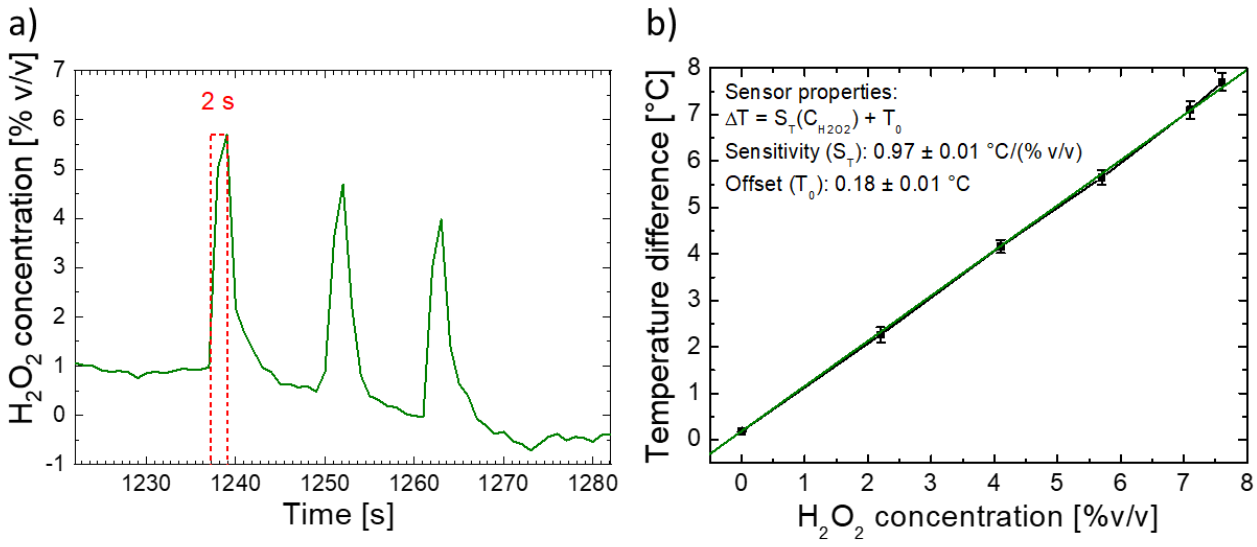

Figure 7.S2 a) Response time (2 s) from the calorimetric H_2O_2 sensor, exemplarily depicted at 5.7% v/v; b) calibration curve of the calorimetric gas sensor.

References

[1] J. Arreola, M. Keusgen, and M.J. Schöning, "Toward an immobilization method for spore-based biosensors in oxidative environment", *Electrochim. Acta* (302), 394–401 (2019).

8 Conclusions and remarks

Throughout this thesis, several aspects were examined regarding the functionalization of sensor substrates for the immobilization of bacterial spores. Here, a systematic approach to establish an immobilization strategy resistant against harsh conditions (high temperature, oxidizing environment) for spore-based biosensors in aseptic processing was presented. In addition, a sensor array capable of simultaneously measuring hydrogen peroxide concentrations as well as the spores' viability to evaluate the efficacy of sterilization processes was introduced.

The global aseptic market was evaluated to be about 39.5 billion USD in 2017 with a forecast of 79.5 billion USD by 2024 [1]. Lots of liquid food products are packaged every day utilizing aseptic filling machines. For instance, these machines can dispense approximately 12,000 ready-packaged products per hour (e.g., Pure-Pak® Aseptic Filling Line E-PS120A). However, a validation of such machines has to be performed to assure contamination-free products. The cutting-edge methods to validate such machines are by means of microbiological tests, where endospores (shortly spores) are used as probes because of their high resistance against several sterilants (e.g., gaseous hydrogen peroxide). The main disadvantage of the aforementioned tests is time: it takes at least 36-48 hours to obtain the results, i.e., the products cannot be delivered to customers without the validation certificate. Just in this example, in 36 hours, 432,000 products would be on hold for dispatchment; if more machines are evaluated, this number would linearly grow and at the end, the cost (only for waiting for the results) would be considerably high. For this reason, the development of new sensor technologies is very valuable to overcome this challenge. Therefore, the main focus of this thesis was on the further development of a spore-based biosensor; this sensor can determine the viability of spores after being sterilized with hydrogen peroxide (see sections 1.4 and 2.1). However, the immobilization strategy as well as its implementation on sensing elements and a more detailed investigation regarding its operating principle were missing.

Firstly, the immobilization strategy was selected according to the sensor application: it is needed that the immobilization layer attaching the spores onto the sensor surface is strong against an oxidative environment and heat (gaseous hydrogen peroxide). For this reason, organosilanes were chosen as discussed in section 1.5. One of the first steps to functionalize

the spore-based biosensor was hydroxylation (creation of OH groups at the sensor surface); this was performed by treating the sensor surface with an O_2 plasma. However, the sensor signal was not stable anymore (it changed over time). Therefore, this effect was meticulously studied in chapter 3.

At the beginning, the spore-based biosensors used Si/SiO_2 as a substrate material, where the SiO_2 surface represents a good approximation for a glass surface in general. Therefore, analogous to them, EIS chips were chosen to study the effect of O_2 plasma radiation on them because of their availability and sufficient amount of published literature. Here, physical (contact angle measurements) and electrochemical characterizations (C-V- and ConCap measurements) were performed on EIS structures to study the nature of the sensor signal change after being treated with O_2 plasma, namely by measuring the wettability of the sensor surface and the sensor signal. Two different effects were found: hydroxylation at the sensor surface and trapped charges in the Si/SiO_2 interface. The contact angle measurements provided a rapid tool to diagnose the surface wettability of the sensor, i.e., if hydroxyl groups are present at the surface (the more hydrophilic, the more OH groups), whereas the C-V- and ConCap measurements provided evidence of this effect in the Si/SiO_2 interface. Further steps were realized to achieve a relatively high hydroxylated (~6°) surface and to reset the effect of the O_2 plasma on the EIS chips by an annealing process. This resetting was probably possible since trapped charges might be generated by the O_2 plasma and by applying an annealing process, they might be released, improving the oxide quality of the sensor. Considering that the implementation of sensor technologies is growing at a rapid speed, the functionalization of such sensors to immobilize cells or biomolecules would also be needed. Furthermore, O_2 plasma is not only used for hydroxylation, but also to clean chip surfaces. As a result, the aforementioned established method opens the possibility for further employing of O_2 plasma on Si/SiO_2 structures without compromising their reliability.

In addition, in chapter 4, an immobilization strategy was optimized to localize spores on glass substrates with organosilanes. Specifically, three different organosilanes (APTES, GPTMS and PFDTES) were grafted on glass substrates for the immobilization of spores; glass was used as a model system for spore-based biosensors. Characterizations were performed by microbiological experiments, contact angle measurements and AFM. Numerous silanization (process of organosilane grafting) parameters were optimized for such immobilization such

as the nature of the solvent, concentration of the silane, silanization time, curing time and temperature. Additionally, the organosilanes were resistant to a buffer solution (e.g., Ringer solution), surfactants and sonication. At the end, the spores were successfully immobilized with APTES and GPTMS, whereas PFTDES was applied to hinder the attachment of the spores.

Abundant immobilization strategies have been introduced in literature regarding immobilization of microorganisms and biomolecules with organosilanes. However, the silanization process is hard to control because it happens automatically, i.e., the silane molecules assemble themselves on the surface autonomously. Therefore, depending on the application, the silanization process has to be optimized specifically for each case. This part of the thesis provides a systematic and robust immobilization protocol with organosilanes for spores on glass surfaces, where APTES has been chosen as the organosilane suitable for spore-based biosensors since it shows the best immobilization efficiency; this was later investigated in chapter 5.

In Chapter 5, the functionalization of spore-based biosensors was performed with APTES. In addition, the immobilization of spores was studied on different substrate materials for biosensors (SiO_2, Pt and a glass substrate with transducer elements made out of platinum). Characterization investigations were performed by contact angle-, AFM-, SEM-, microbiological- and impedimetric measurements. In this case, APTES on SiO_2 was the best combination for the immobilization of spores. Furthermore, impedimetric measurements showed a resistive behavior of the APTES at low frequencies (200 Hz-10 kHz) and a decrease of the sensor impedance. This section of the thesis contributes with a reproducible sensor functionalization with APTES as well as insights on the substrate material to be chosen for spore immobilization.

Moreover, in chapter 6, the APTES functionalization was further optimized to withstand gaseous hydrogen peroxide and the nature of the spore suspension was analyzed on sensors. Particularly, APTES-functionalized spore-based biosensors and Si/SiO_2 substrates were studied to investigate the effects of water- and ethanol-based spore suspensions and gaseous hydrogen peroxide. Furthermore, the substrates were characterized by contact angle-, ellipsometric-, AFM- and impedimetric measurements. The layer thickness from APTES prepared in ethanol was extremely thick (~800 nm) in comparison to that of toluene

(~2 nm). Despite of this, a water droplet on an APTES surface prepared in ethanol and sterilized showed the best stability against gaseous hydrogen peroxide. A higher stability of the sensor signal against hydrogen peroxide can be reached by using ethanol as a solvent for APTES instead of toluene. In addition, nowadays, with the increasing demand of sensor methods in aseptic processing, more robust immobilization strategies are needed that can withstand harsh conditions (e.g., oxidative environment). Here, for the first time, a protocol for the immobilization of spores without affecting the sensor signal (stability) and being resistant to gaseous hydrogen peroxide was established.

In the last part of this thesis (chapter 7), a sensor array consisting of a calorimetric gas- and a spore-based biosensor for online monitoring of sterilization processes with gaseous H_2O_2 under industrial conditions was introduced. In addition, the effect of hydrogen peroxide on different spore strains was investigated. Characterizations were carried out by means of impedimetric-, AFM-, SEM-, and microbiological measurements. H_2O_2 concentrations up to 7.6% v/v within 2 s were determined with a sensor sensitivity of 0.97 °C/(% v/v). *Bacillus atrophaeus* spores were able to successfully evaluate (by change of morphology) all investigated H_2O_2 concentrations, whereas *Bacillus subtilis*- and *Geobacillus stearothermophilus* spores were able to favorably evaluate the concentration of 7.6 % H_2O_2 v/v. As it could be seen from this study, each spore strain possesses its own response by means of morphological changes to gaseous hydrogen peroxide and should be optimized accordingly to its own sterilization conditions. Nevertheless, this sensor arrangement opens unique approaches regarding evaluation and monitoring of sterilization processes with H_2O_2 in aseptic food industry. The synergy of the two sensor types as one combined sensor array enables a considerably more specific multiparameter experience in aseptic filling machines in comparison to isolated microbiological state-of-the-art- or hydrogen peroxide methods.

In Figure 8.1 the main investigations of this thesis are summarized. In short, it starts with the optimization of a method to obtain a hydroxylated surface and a stable sensor signal (chapter 3), which served as a basis for the immobilization of spores with organosilanes (chapter 4). Furthermore, this method was implemented for different sensor substrates (SiO_2, Pt and glass substrates with Pt structures) and the influence of APTES immobilization on the sensor signal was characterized by impedimetric measurements (chapter 5). In chapter 6, the APTES

protocol was further optimized to withstand an oxidative environment (e.g., H_2O_2) and different spore suspensions were characterized. Finally, in chapter 7, a sensor array consisting of a calorimetric gas sensor and a spore-based biosensor was developed to monitor gaseous hydrogen peroxide concentrations and to determine the viability of spores simultaneously.

Chapter	Investigation	
3	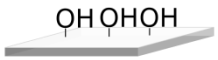 Hydroxylation	Optimization of a method to obtain a hydroxylated surface and a stable sensor signal
4	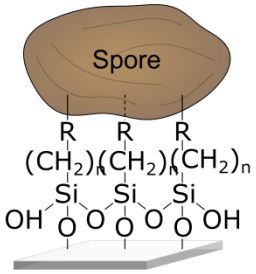 Spore immobilization	Establishment of a method to immobilize spores by means of organosilanes
5	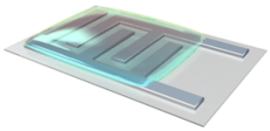	Implementation of APTES on sensor substrates and sensor response characterization
6	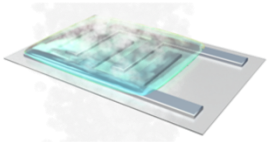	Optimization of APTES to withstand gaseous hydrogen peroxide and spore suspension characterization
7	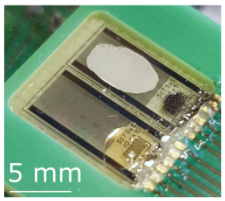	Development of a sensor array to simultaneously monitor gaseous H_2O_2 and spores' viability

Figure 8.1 Main investigations of the presented thesis.

Concerning the immobilization of spores, in most standardized tests, they can be immobilized on spore strips, spore discs, plastic rods or glass bulbs [2]. However, none of these methods deal with chemical immobilization, since the spores have to be recovered after the test for further analysis. Furthermore, several chemical immobilization methods for spores have been presented in literature as it was shown in chapter 1. Still, most of them are

not convenient for the use in aseptic processing. In Table 8.1, different methods to immobilize spores are compared with regard to their possible suitability in aseptic food industry: here, user-friendly means the difficulty of the spore immobilization, type is the nature of the immobilization (physical or chemical), heat and H_2O_2 stability stand if they are stable to high temperatures (>240 °C) and to gaseous hydrogen peroxide; standardized means if the immobilization is already regulated by a standardized institute. As it can be seen from the table, the spore strips and disk foils excell in most of the comparable parameters. However, the type of immobilization plays an important role in sensor applications. In addition, gel entrapment and biospecific binding system are less suitable immobilization techniques because of their lack of stability against heat and H_2O_2. Finally, APTES immobilization (via electrostatic interactions) is relatively time-consuming, but with optimized parameters can withstand both heat and H_2O_2.

Table 8.1 Comparison of immobilization of spores and their possible application in aseptic food industry.

Spore immobilization	User-friendly	Type of immobilization	Heat stability	H_2O_2 stability	Standardized
Spore strips	++	Physical	+	+	Yes
Spore discs	++	Physical	++	+	Yes
Gel entrapment	+	Chemical	-	-	No
Biospecific binding system	-	Chemical	-	-	No
APTES	*	Chemical	++	++	No

Note: ++ very good, + good, * fair, - bad.

Moreover, in terms of sensor-based methods to monitor (low) H_2O_2 concentrations, some are indeed available on the market. For instance, Dräger Polytron® 7000 (from Drägerwerk AG & Co. KgaA) can electrochemically measure H_2O_2 concentrations from 0.1 up to 7,000 ppm, or the PI2114 gas concentration analyzer (from Picarro, Inc.) can detect H_2O_2 concentrations

from 3 up to 100 ppm. However, both devices are not adapted for in-line monitoring. In addition, the measured H_2O_2 concentrations in aseptic filling machines can reach up to 10% H_2O_2 v/v (1×10^5 ppm) that is about 100 times higher above the detection limit of these sensors. As a result, non-sensor-based methods are commonly used to measure H_2O_2 concentrations in aseptic filling machines by disposable colorimetric techniques, which, however, can only give a qualitative "yes/no" answer and no quantitative correlation. For this reason, extensive work has been done in previous years to develop a H_2O_2 sensor for aseptic filling machines [3–6] as described in chapter 1. This sensor is tailored specifically for this purpose. However, microbiological tests are still needed to validate such machines.

The typical standardized procedures to evaluate aseptic filling machines using gaseous hydrogen peroxide as sterilizer were introduced in Chapter 1 (count-reduction test and end-point test). In this case, the packaging material is contaminated with spores that are strong against the sterilization process. Subsequently, the contaminated package is exposed to the sterilant and finally incubated for a certain amount of time. After that, the viability of the spores is determined either by counting the surviving spores before and after sterilization (count-reduction test) or by determining the relationship between the number of non-sterile and sterile packages (end-point test). In general, commercially available sensor-based methods to impedimetrically diagnose bacterial growth can also be used. For example, BacTrac®4300 (from SY-LAB Geräte GmbH) is a device that performs impedance analysis in a microbial culture process. In this case, the nutrient media and the liquified product are incubated in a measuring cell and the impedance change of the fluid is monitoring by means of pin electrodes. Its principle is based on metabolic products created when microorganisms grow, changing the impedance of the medium. Additionally, Rapid Automated Bacterial Impedance Technique (RABIT) (from Don Whitley Scientific Limited) is another device for impedimetric measurements of bacterial growth. Similarly, as with the BacTrac®4300, the impedance of the medium can be also measured, but another method that detects the metabolic CO_2 production is combined, having more flexibility for detecting microorganisms that do not produce highly charged molecules. Despite of this, both of them are, however, not suitable for online monitoring the spore viability in aseptic filling machines mainly because of the size and sample preparation. Thus, this was the motivation for the development of a new kind of spore-based biosensor to measure the viability of spores, which was recently introduced also in previous works [7, 8]. While the impedance change of such

sensor was in correlation with the increase of H_2O_2 concentration, its operating principle was still on ongoing research. The assumption was that morphological changes of the spores during H_2O_2 sterilization were responsible for the sensor signal; several hints (SEM measurements) were provided pointing in that direction. This was further investigated (as shown in chapter 7), where more evidence was given and indeed, gaseous H_2O_2 changed the structure of the spores, and this could be also correlated to the impedance change of the sensor. Various morphology conditions of spores were able to be characterized for each strain: depending on the spore status the spores were labeled as "normal", "deformed" or "flattened". The normal and deformed conditions were encountered in a specific ratio, which changes, depending on the applied H_2O_2 gas concentration. In contrast, the flattened condition was only found after treating the spores with gaseous hydrogen peroxide. However, not all spore strains (*B. subtilis* and *G. stearothermophilus*) followed the same behavior. This may increase the importance of *B. atrophaeus* in the development of spore-based biosensors for aseptic processing.

Due to the previous works already mentioned, the possibility of combining a calorimetric gas sensor together with a spore-based biosensor was realized. And as previously discussed, besides of offering simultaneous online parameters such as H_2O_2 concentration or spore status, this sensor array may open new possibilities in regard to standardized regulations, since the microbiological aspect is also covered. In Table 8.2, the discussed sensors are summarized and assessed in terms of their suitability for aseptic processing.

In this work, several protocols were established for the immobilization of spores on spore-based biosensors. Specially, an immobilization layer strong against sterilization conditions (high temperatures and gaseous hydrogen peroxide) was optimized by means of organosilanes. Furthermore, a combined calorimetric gas sensor/spore-based biosensor was developed to simultaneously monitor H_2O_2 concentrations and the viability of spores.

Future work might consolidate the further optimization of the APTES layer to facilitate the silanization process (e.g., using gas-phase silanization instead of liquid-phase silanization), as well as decreasing the size of the interdigitated electrodes to also increase the sensitivity of the spore-based biosensor. In addition, the sensor array could be also upgraded by integrating other sensor structures to monitor, for instance, humidity or gas flow. In another case, the sensor array as well as the spore strains (*B. atrophaeus*, *B. subtilis* and *G.*

stearothermophilus) can be also investigated for other sterilization methods such as radiation

Table 8.2 Comparison of commercially available sensor methods with previously developed calorimetric gas- and spore-based biosensors.

Sensor method	Operating principle	Sensing parameter	Suitable for aseptic processing
Dräger Polytron® 7000	Electrochemical	H_2O_2	No
PI2114	Optical	H_2O_2	No
Calorimetric-gas sensor (CGS)	Calorimetric	H_2O_2	Yes
BacTrac®4300	Impedimetric	Culture medium impedance	No
RABIT	Impedimetric	Culture medium impedance	No
Spore-based biosensor (SBB)	Impedimetric	Spores' impedance	Yes
Sensor array (CGS + SBB)	Calorimetric and impedimetric	H_2O_2 and spores' impedance	Yes

or pressure with saturated steam (autoclave). Further spore-based biosensors could be developed by functionalizing the spore surface. As it can be seen in Chapter 7, the impedance of the spores is measured and it can be correlated to the viability of spores. However, their impedance also depends on the electrical properties of the spore coat. Thus, by modifying the spore coat in such a way (e.g., with amino-charged groups) that more electrical charge carriers can flow along the spore surface, the conductivity of the spores may increase and with this, the capabilities of the impedimetric sensor may be further extended (e.g., sensitivity). Out of the scope of aseptic processing, spore-based biosensors may also be used as a model to further investigate essential parameters such as "live" or "dead" microorganisms, since the spores are in a dormant state and their status is normally known until they find the right conditions to outgrow.

Moreover, due to the extraordinary properties of spores to withstand harsh conditions and to have an "unlimited" shelf-life (i.e., they can be dormant for long time till needed), the

popularity of spore-based biosensors may increase and become a state-of-the-art method to be utilized in challenging environments. For instance, in medicine, on-site sterilization methods may be applied to the medical equipment needed and at the same time, the sterility efficacy could be evaluated by means of spore-based biosensors. In addition, in pharmacy, for drug-delivery systems, photo-functionalized spore-based biosensors may be used. In this case, the spore coat could be functionalized with photo-sensitive materials (similar like contrast agents used in medicine) for tracking them inside the body. As the spores reached the desired destination, they could be light-activated to germinate and by this, they may release a specific pharmaceutical compound. Furthermore, in astrobiology, spore-based biosensors might enable the search of favorable conditions for the growth of microorganisms and plants in different planets (e.g., Mars), i.e., the spore-based biosensor could be used as an indicator of deadly or non-deadly atmosphere/conditions. Nonetheless, further committed research in the area of spore-based biosensors and functionalization of spores may be advisable, on the one hand, to get an upgrade on the actual microbiological state-of-the-art methods, and on the other, to additionally explore new scientific fields.

References

[1] Zion Market Research, https://www.zionmarketresearch.com/report/aseptic-packaging-market, downloaded at 12.11.2019.

[2] D. Serp, U. von Stockar, and I.W. Marison, "Immobilized bacterial spores for use as bioindicators in the validation of thermal sterilization processes", *J. Food Protect.* 65 (7), 1134–1141 (2002).

[3] F. Vahidpour, J. Oberländer, and M.J. Schöning, "Flexible calorimetric gas sensors for detection of a broad concentration range of gaseous hydrogen peroxide: a step forward to online monitoring of food-package sterilization processes", *Phys. Status Solidi A* 215 (15), 1800044 (1–7) (2018).

[4] P. Kirchner, J. Oberländer, P. Friedrich, J. Berger, G. Rysstad, M. Keusgen, and M.J. Schöning, "Realization of a calorimetric gas sensor on polyimide foil for applications in aseptic food industry", *Sens. Actuators, B* 170, 60–66 (2012).

[5] P. Kirchner, B. Li, H. Spelthahn, H. Henkel, A. Schneider, P. Friedrich, J. Kolstad, M. Keusgen, and M.J. Schöning, "Thin-film calorimetric H_2O_2 gas sensor for the validation of germicidal effectivity in aseptic filling processes", *Sensor Actuat. B-Chem.* 154 (2), 257–263 (2011).

[6] N. Näther, L.M. Juárez, R. Emmerich, J. Berger, P. Friedrich, and M.J. Schöning, "Detection of hydrogen peroxide (H_2O_2) at exposed temperatures for industrial processes", *Sensors (MDPI)* 6 (4), 308–317 (2006).

[7] J. Oberländer, M. Mayer, A. Greeff, M. Keusgen, and M.J. Schöning, "Spore-based biosensor to monitor the microbicidal efficacy of gaseous hydrogen peroxide sterilization processes", *Biosens. Bioelectron.* 104, 87–94 (2018).

[8] J. Oberländer, A. Bromm, L. Wendeler, H. Iken, M.P. Durán, A. Greeff, P. Kirchner, M. Keusgen, and M.J. Schöning, "Towards a biosensor to monitor the sterilization efficiency of aseptic filling machines", *Phys. Status Solidi A* 212 (6), 1299–1305 (2015).

Zusammenfassung

Im Rahmen dieser Arbeit wurden verschiedene Verfahren bezüglich der Funktionalisierung von Sensorsubstraten für die Immobilisierung von bakteriellen Sporen untersucht. Es wurde ein systematischer Ansatz für die Entwicklung einer Immobilisierungstrategie für Sporen-basierte Biosensoren in aseptischen Prozessen, welche bei hohen Temperaturen oder oxidativer Atmosphäre resistent sind, vorgestellt. Außerdem wurde ein Sensor-Array präsentiert, das Wasserstoffperoxidkonzentrationen sowie die Lebensfähigkeit der Sporen simultan messen kann. Die Zusammenfassung der vorgestellten Kapitel ist nachfolgend aufgelistet.

Kapitel 3: Effekt des O_2-Plasmas auf die Eigenschaften von Elektrolyt-Isolator-Halbleiter-Strukturen

- ✓ Die Funktionalisierung (Hydroxylierung) mit O_2-Plasma auf EIS-Chips wurde mittels elektrochemischer Charakterisierung (C-V- and ConCap-Messungen) und Kontaktwinkelmessungen untersucht.
- ✓ Das O_2-Plasma verursachte eine Verschiebung im Flachband-Potential des EIS-Sensors. Dies lässt sich anhand von Strahlungsschäden durch das Plasma und „trapped charges" am Si/SiO_2-Interface erklären.
- ✓ Es wurde erfolgreich ein Temperprozess angewendet, um diesen Effekt des O_2-Plasmas auf die EIS-Sensoren zurückzusetzen.
- ✓ Es konnte eine stabile (ohne Beeinfluss des O_2-Plasmas) und hydroxylierte Si/SiO_2-Oberfläche mit einer gleichzeitigen Optimierung der Wärmebehandlung (300 °C für 10 min) realisiert werden.

Kapitel 4: Optimierung der Immobilisierung von bakteriellen Sporen auf Glassubstraten mit Organosilanen

- ✓ Drei verschiedene Organosilane, nämlich APTES, GPTMS und PFDTES, wurden für die Immobilisierung von Sporen auf Glassubstrate untersucht. Glas wurde als Modellsystem für die Sporen-basierten Biosensoren benutzt. Die Charakterisierungen wurden mittels mikrobiologischer Experimente, Kontaktwinkel-Untersuchungen und AFM durchgeführt.

- ✓ Zahlreiche Silanisierungparameter wurden für eine solche Immobilisierung optimiert, wie z.B. die Zusammensetzung des Lösungsmittels, die Silankonzentration, die Silanisierungszeit, die Aushärtungszeit und die Temperatur. Die resultierenden Organosilane waren resistent gegenüber Pufferlösung (z.B. Ringer-Lösung), Tensidlösungen und Ultraschallbehandlung.
- ✓ Die Sporen wurden erfolgreich mit APTES und GPTMS immobilisiert. Gleichzeitig wurde das Protokoll für PFTDES optimiert, um die Kopplung von Sporen zu verhindern.

Kapitel 5: Oberflächenfunktionalisierung für sporenbasierte Biosensoren mit Organosilanen

- ✓ Sporenbasierte Biosensoren wurden mit APTES funktionalisiert. Des Weiteren wurde die Immobilisierung von Sporen auf unterschiedlichen Trägermaterialien für Biosensoren (SiO_2, Pt und Glassubstrate mit Pt-Strukturen) untersucht. Die Charakterisierungen wurden mit Kontaktwinkel-, AFM-, REM- und mikrobiologischen Messungen durchgeführt. APTES auf SiO_2 war die beste Kombination für die Immobilisierung der Sporen.
- ✓ Impedimetrische Messungen zeigten ein resistives Verhalten des APTES bei niedrigen Frequenzen (200 Hz-10 kHz).

Kapitel 6: Entwicklung einer Immobilisierungsmethode für sporenbasierte Biosensoren in einer oxidativen Atmosphäre

- ✓ APTES-funktionalisierte, sporenbasierte Biosensoren mit Si/SiO_2-Substraten wurden untersucht, um die Effekte von Wasser- und Ethanol-basierten Sporensuspensionen und Wasserstoffperoxid zu analysieren. Ferner wurden die Substrate mittels Kontaktwinkel-, ellipsometrischen, AFM- und impedimetischen Messungen charakterisiert.
- ✓ Die Abscheidung von APTES-Schichten in Ethanol resultierte in sehr dicken Schichten (~800 nm) im Vergleich zu Toluol als Lösungsmittel (~ 2 nm). Gleichzeitig zeigte die APTES-Oberfläche, die in Ethanol vorbereitet und darüber hinaus sterilisiert wurde, die beste Stabilität gegenüber gasförmigem Wasserstoffperoxid.

- ✓ Eine ebenfalls höhere Sensorsignalstabilität gegenüber Wasserstoffperoxid kann erreicht werden, wenn Ethanol als Lösungsmittel für die Abscheidung von APTES benutzt wird (statt Toluol).

Kapitel 7: Kalorimetrisches Gas- und sporenbasiertes Biosensor-Array für die Online-Überwachung und Sterilitätssicherung mittels gasförmigem Wasserstoffperoxid in aseptischen Auffüllanlagen

- ✓ Es wurde ein Sensor-Array, bestehend aus einem kalorimetrischen Gas-Sensor und einem sporenbasierten Biosensor, für die Online-Überwachung von Sterilisationsprozessen mit gasförmigem H_2O_2 eingeführt und unter industriellen Bedingungen getestet. Außerdem wurde der Effekt von H_2O_2 auf verschiedene Sporenstämme untersucht. Charakterisierungen wurden anhand von impedimetrischen, AFM-, SEM- und mikrobiologischen Messungen durchgeführt.
- ✓ Es konnten H_2O_2-Konzentrationen von bis zu 7,6% v/v innerhalb von 2 s mit einer Sensitivität von 0,97 °C/(% v/v) erfasst werden.
- ✓ *Bacillus atrophaeus*-Sporen konnten mit allen untersuchten H_2O_2-Konzentrationen erfolgreich evaluiert werden, während *Bacillus subtilis*- and *Geobacillus stearothermophilus*-Sporen nur eine quantitative Abhängigkeit des Sensorsignals bei einer Konzentration von 7,6 % H_2O_2 v/v zeigten.

List of publications

Publications in peer-reviewed journals

[1] **J. Arreola**, M. Mätzkow, M.P. Durán, A. Greeff, M. Keusgen, and M.J. Schöning, "Optimization of the immobilization of bacterial spores on glass substrates with organosilanes", *Physica Status Solidi A* 213 (6), 1463–1470 (2016).

[2] **J. Arreola**, M. Keusgen, and M.J. Schöning, "Effect of O_2 plasma on properties of electrolyte-insulator-semiconductor structures", *Physica Status Solidi A* 214 (9), 1700025 (1-6) (2017).

[3] **J. Arreola**, J. Oberländer, M. Mätzkow, M. Keusgen, and M.J. Schöning, "Surface functionalization for spore-based biosensors with organosilanes", *Electrochimica Acta* 241, 237–243 (2017).

[4] **J. Arreola**, M. Keusgen, and M.J. Schöning, "Toward an immobilization method for spore-based biosensors in oxidative environment", *Electrochimica Acta* (302), 394–401 (2019).

[5] **J. Arreola**, M. Keusgen, T. Wagner, and M.J. Schöning, "Combined calorimetric gas- and spore-based biosensor array for online monitoring and sterility assurance of gaseous hydrogen peroxide in aseptic filling machines", *Biosensors & Bioelectronics*, 143 (2019), 111628 (1-8).

Proceedings

[1] **J. Arreola**, J. Oberländer, M. Keusgen, and M.J. Schöning, "Viability analysis of spore-based biosensors in sterilization processes", *Proceedings* (MDPI) 1 (8), 789 (2017).

[2] J. Oberländer, **J. Arreola**, C. Hansen, A. Greeff, M. Mayer, M. Keusgen, and M.J. Schöning, "Impedimetric biosensor to enable fast evaluation of gaseous sterilization processes", *Proceedings* (MDPI) 1 (4), 435 (2017).

[3] **J. Arreola**, J. Oberländer, F. Vahidpour, M. Keusgen and M. J. Schöning, "Validation of sterilization methods by means of gas sensors and spore-based biosensors", *IMCS 2018* (DOI 10.5162/IMCS2018/DH1.3).

Oral and poster presentations

[1] **J. Arreola**, C. Probst, M.J. Schöning, D. Kohlheyer, "Temperature control in microfluidics for single-cell analysis: Characterization and development of thin-film sensors", Engineering of Functional Interfaces, Jülich, Germany (14.-15.07.2014).

[2] **J. Arreola**, M. Mätzkow, M. Palomar Durán, A. Greeff, M. Keusgen, M.J. Schöning, "Immobilization of bacterial spores on biosensor substrates with organosilanes", Engineering of Functional Interfaces, Hannover, Germany (06.-07.07.2015).

[3] J. Oberländer, **J. Arreola**, A. Bromm, L. Wendeler, H. Iken, M. Palomar Durán, A. Greeff, M. Bäcker, M. Keusgen, and M.J. Schöning, "Überwachung von Sterilisationsprozessen in der Lebensmittelindustrie mittels einer Biosensor-Lösung", 9. Deutsches Biosensor Symposium (DBS) 2015, München, Germany (11.-13.03.2015).

[4] **J. Arreola**, J. Oberländer, T. Bronder, S. Dantism, T. Kerschgens, M. Mätzkow, M. Keusgen, M.J. Schöning, "Study of the effect of hydroxylation for surface functionalization on biosensor chips", Engineering of Functional Interfaces, Wildau, Germany (03.-05.07.2016).

[5] **J. Arreola**, J. Oberländer, M. Mätzkow, M. Keusgen, M.J. Schöning, "Surface functionalization for spore-based biosensors with organosilanes", Electrochemical Micro & Nanosystem Technologies, Brussels, Belgium (16.-19.08-2016).

[5] **J. Arreola**, J. Oberländer, M. Keusgen, M.J. Schöning, "Study of functionalized spore-based biosensors in sterilization processes", Kurt-Schwabe Symposium, Mittweida, Germany (04.-07.09.2016).

[6] J. Oberländer, **J. Arreola**, C. Hansen, A. Greeff, M. Mayer, M. Keusgen, and M.J. Schöning, Functionalized spore-based biosensor to evaluate gaseous sterilization processes, 1st European Biosensor Symposium 2017, Potsdam, Germany (20.-23.03.2017).

[7] **J. Arreola**, J. Oberländer, M. Keusgen, M.J. Schöning, "Towards an immobilization strategy for spore-based biosensors in harsh conditions", Engineering of Functional Interfaces, Marburg, Germany (28.-29.08.2017).

[8] **J. Arreola**, J. Oberländer, M. Keusgen, M.J. Schöning, "Viability analysis of spore-based biosensors in sterilization processes", 5th International Symposium on Sensor Science, Barcelona, Spain (27.-29.09.2017).

[9] J. Oberländer, **J. Arreola**, C. Hansen, A. Greeff, M. Mayer, M. Keusgen, and M.J. Schöning, "Impedimetric biosensor to enable fast evaluation of gaseous sterilization processes", Eurosensors 2017, Paris, France (03.-06.09.2017).

[10] **J. Arreola**, M. Keusgen, M.J. Schöning, "Effect of oxidative environment on functionalized spore-based biosensors", Engineering of Functional Interfaces, Lutherstadt Wittenberg, Germany (01.-03.07.2018).

[11] **J. Arreola**, J. Oberländer, F. Vahidpour, M. Keusgen and M.J. Schöning, "Validation of sterilization methods by means of gas sensors and spore-based biosensors", 17th International Meeting on Chemical Sensors - IMCS 2018, Vienna, Austria (15.-19.07.2018).

[12] **J. Arreola**, M. Keusgen, M.J. Schöning, "Spore-based biosensors as a rapid method for sterilization evaluation in aseptic filling machines", 2nd European Biosensor Symposium 2019, Florence, Italy (18.-21.02.2019).

[13] **J. Arreola**, M. Keusgen, M.J. Schöning, "Implementation of a biosensor array as a biological indicator in food industry", Engineering of Functional Interfaces, Leuven, Belgium (07.-09.07.2019)

Acknowledgments

This thesis would not be possible without the help and advice of many people. First, I would like to thank Prof. Dr. Schöning for his guidance and dedication, but mostly for allowing me to start on this Ph.D. project. Further thankfulness goes to Prof. Dr. Keusgen for supervising and giving me also the opportunity to enroll on this journey.

In addition, I would like to express my gratitude to Prof. Dr. Bongaerts and Prof. Dr. Siegert, who provided the working environment regarding the microbiological investigations.

Prof. Dr. Poghossian for his fruitful discussion is appreciated as well as my colleagues and friends of the Institute of Nano- and Biotechnologies for their support and technical assistance during my stay in the institute.

Last, but not least, I would like to thank my family and close friends for their encouragement and assistance in this period of time. Special thanks go to my parents that enabled me to do my studies abroad.

Curriculum Vitae

Vorname: Julio César

Nachname: Arreola Becerra

Geburtsdatum: 13. September 1989

Geburtsort: Monterrey, Mexiko

Staatsangehörigkeit: Deutsch

Ausbildung

2014-Jetzt	**Promotionsstudium**
	Philipps-Universität Marburg und FH Aachen, Deutschland
2012-2014	**M.Sc. in Biomedical Engineering**
	FH Aachen, Deutschland
2006-2011	**B.Eng. in Mechatronics**
	Universidad Autónoma de Nuevo León, Mexiko
2004-2006	**Abitur**
	Preparatoria 7 Oriente, Mexiko
2001-2004	**Sekundarbildung**
	Escuela Secundaria Técnica 56 - 80 Aniversario de la constitución mexicana, Mexiko
1996-2001	**Grundschule**
	Ford 54 Prof. Plinio D. Ordoñez, Mexiko